NTNU – Trondheim
Norwegian University of
Science and Technology

FDTD simulations of novel gain media

Hans Olaf Hågenvik

Nanotechnology
Submission date: June 2014
Supervisor: Johannes Skaar, IET

Norwegian University of Science and Technology
Department of Electronics and Telecommunications

Problem description

Isotropic metamaterials can in principle be designed to have any refractive index. The real part can be positive (positive refraction), or it can be negative (negative refraction). Provided we allow the medium to be active (involving pumping), the imaginary part can have either sign as well. Due to the possibility of instabilities, such gain media must be analyzed using Laplace-Fourier theory, in which the usual Fourier transform in time is replaced by the Laplace transform, and the Fourier transform in space is retained. By suitable deformation of the two-dimensional integration surface, one rigorously establishes well-known behaviors of gain media, in addition to confirming more controversial or novel results. In particular, the theory predicts the existence of simultaneously positive and negative refracting media. In this master proposal, the candidate will consider this theory in detail, and try to verify it independently by solving the Maxwell equations in the time-domain using FDTD simulations.

Abstract

Fourier-Laplace analysis of gain media predicts the existence of novel types of media. In particular it predicts the existence of media refracting positively and negatively at the same time, so-called simultaneous refraction. This effect is analytically derived through deformation of the inverse Fourier-Laplace integration surface. The requirements, and possible problems, of such media are discussed. It is argued that this is a two-dimensional effect, meaning side waves must be present for the effect to occur. For a medium to be simultaneous refracting it must have gain, and it is discussed how this gain can be minimized.

A Finite Difference Time Domain (FDTD) method for dispersive Lorentz media was implemented in MATLAB. The program solves Maxwell's equations numerically in the time domain, where the real physics happens. If the Fourier-Laplace theory predicts novel optical properties for a given $\epsilon(\omega)$ and $\mu(\omega)$, the program can thus be used to simulate the actual response from a medium with permittivity and permeability $\epsilon(\omega)$ and $\mu(\omega)$. It can therefore be used to independently verify the results obtained using Fourier-Laplace theory.

The FDTD program was used to simulate various types of novel media. Simulation results showing evanescent gain and non-magnetic negative refraction are presented. For media with large gain the program fails after some time, due to amplified, artificial reflections caused by numerical errors. The reflections were found to originate from the numerical precision of MATLAB.

Gain media may involve instabilities. There are two types of instabilities, convective and absolute. A *convective instability* is convected away. An *absolute instability* grows with time, even at a fixed point in space. The deformation theory is used to explain the occurrence of such instabilities, in particular in infinite or semi-infinite media.

Wave propagation in passive media is usually considered in the so called monochromatic and plane wave limits, meaning only a single frequency ω_1 and plane wave component K_x is present. Physically these limits can never fully be reached. The monochromatic limit is approached by turning on a single frequency oscillation at $t = 0$, and waiting a sufficiently long time $t \to \infty$. The plane wave limit is approximated by letting the source width σ being infinitely large, $\sigma \to \infty$. The Fourier-Laplace theory is used to show that these limits do not necessarily exist in gain media, as instabilities may lead to diverging fields. Even for media where the monochromatic limit exists, it may for certain gain media take a very long time for the transients to die out. This fact is studied with the help of frequency domain and time domain simulations, and is the main reason why simultaneous refraction appears impossible to simulate with FDTD or realized experimentally, at least with the proposed types of media.

Sammendrag

Fourier-Laplace analyse av gainmedier forutsier nye typer medier. Spesielt forutsier det at det finnes medier som bryter lys både positivt og negativt på en gang, såkalt samtidig brytning. Denne effekten utledes analytisk ved å deformere den inverse Fourier-Laplace integrasjonsoverflaten. Krav til, og mulige problemer med slike medier diskuteres. Det argumenteres for at dette er en todimensjonal effekt, som betyr at sidebølger må være til stede for at effekten skal kunne oppstå. For at et medium skal kunne være samtidig brytende må det ha gain (forsterkning), og det diskuteres hvordan denne gainen kan minimeres.

En metode basert på endelige differanser i tidsdomenet (FDTD) for dispersive Lorentzmedier ble implementert i MATLAB. Programmet løser Maxwells likninger numerisk i tidsdomenet, hvor den egentlige fysikken finner sted. Dersom Fourier-Laplaceteorien forutsier nye typer optisk respons for en gitt $\epsilon(\omega)$ og $\mu(\omega)$ kan programmet brukes til å simulere den faktiske responsen fra et medium med permittivitet og permeabilitet $\epsilon(\omega)$ og $\mu(\omega)$. Det kan derfor brukes til å uavhengig verifisere resultatene som finnes gjennom Fourier-Laplaceteorien.

FDTD-programmet ble brukt til å simulere ulike typer medier. Simuleringsresultater som viser evanescent gain og ikke-magnetisk negativ brytning presenteres. For medier med stor gain mislykkes programmet, på grunn av forsterkede, kunstige refleksjoner, som skyldes numeriske feil. Refleksjonene blir funnet til å skyldes den numeriske oppløsningen i MATLAB.

Gainmedier kan innebære ustabiliteter. Det finnes to typer ustabiliteter, konvektive og absolutte. En *konvektiv ustabilitet* ledes bort. En *absolutt ustabilitet* vokser med tiden, selv for et gitt punkt i rommet. Deformasjonsteorien brukes til å forklare når slike ustabiliteter vil oppstå, spesielt for uendelige eller semi-uendelige medier.

Bølgeforplantning i passive medier undersøkes normalt i de såkalte monokromatiske- og planbølgegrensene, som betyr at bare én frekvens ω_1 og én planbølgekomponent K_x er til stede. Fysisk kan disse grensene aldri oppnås. Den monokromatiske grensen tilnærmes ved å skru på en enkelfrekvensoscillasjon ved tiden $t = 0$ og vente en tilstrekkelig lang tid $t \to \infty$. Planbølgegrensa tilnærmes ved å la bredden på kilden bli uendelig stor, $\sigma \to \infty$. Fourier-Laplaceteorien brukes til å vise at disse to grensene ikke nødvendigvis eksisterer i gainmedier, ettersom ustabiliteter kan føre til divergerende felt. Selv for medier hvor den monokromatiske grensen eksisterer vil det for enkelte gainmedier ta en veldig lang tid for transientene å dø ut. Dette fenomenet studeres ved hjelp av simuleringer i tids- og frekvensdomenene, og er hovedgrunnen til at samtidig brytning virker umulig å simulere med FDTD, eller realiseres eksperimentelt, i det minste for de foreslåtte medietypene.

Preface

This master thesis is a continuation of a preparatory project done the fall 2013, titled *Simultaneous refraction in active metamaterials*. In this preparatory work a FDTD simulation program was implemented in MATLAB. The aim of the project was to understand the phenomenon of simultaneous refraction, and use the implemented FDTD program to simulate the effect. The originally suggested simultaneous refractive medium had a very large gain, and we ran into several challenges related to simulations of strong gain media.

This thesis seeks to explain the origin of these challenges, and provide suggestions on how to overcome them. The preparatory project indicated that an effort should be made to find possible simultaneous refracting media with a minimal amount of gain at all frequencies. An extensive amount of time was thus spent thinking about this. It was also an underlying goal to finish the attached paper, which both the preparatory project and this thesis are based upon. The main emphasis of this report therefore focus on elaborating the findings in this paper.

The past year has taught me that even though something is shown theoretically to be possible, does not necessarily mean it is easy to realize. The fact that media exhibiting both a positive and negative refractive index at the same time may exist is quite sensational, and it has been very interesting to be involved in the early investigation of this phenomenon. Unfortunately simulations have still not been able to reveal the effect of simultaneous refraction. Reasonable explanations for why this is the case were found, and we have therefore by no means any reason for doubting that the effect in fact is possible to obtain. As we have seen, gain media may have very interesting properties. Understanding the challenges related to simulating them may therefore turn out to become useful later on. The implemented program has also been used to simulate a range of novel media, and can be used to analyze other interesting phenomena also in the years ahead.

I must thank my supervisor Johannes Skaar for excellent guidance throughout my work with this thesis. The discussions during our weekly meetings has really been an inspiration to me. He has always been available for answering my questions, and really has the ability to explain complicated things in a simple way. I must also thank Ph.D.-student Christopher Dirdal for some informative discussions on some of the topics discussed in this thesis. I am really looking forward to working with the two of you in the coming years. Thanks to Markus Malema for suggesting FDTD simulations using Luebbers' PLRC-method. Finally, I would like to thank my family and friends for always being there for me, life would be dull to live alone.

Hans Olaf Hågenvik

Contents

1 Introduction

Optical technologies play an important role in today's society. Fiber optics and wireless technologies dominate the way we communicate. These technologies make use of electromagnetic radiation below the visible frequency range. Examples of applications at optical frequencies are microscopes, lenses, eyeglasses and cameras. To enable further development of these technologies it is crucial to understand, and know how to control the optical properties of materials. The optical properties of a material will in general depend on the frequency of light, a phenomenon called dispersion. In a prism with dispersive refractive index the different frequencies will be refracted at slightly different angles. If we shine white light at such a prism the different color components will thus be separated.

Recent development within microprocessing- and structuring techniques has made it possible to design materials with desired optical properties, in particular properties that cannot be found in nature. Such artificially designed materials are called *metamaterials*. One such novel property is the phenomenon of negative refraction. The idea of negative refraction was first proposed by Veselago [1] in 1968. He claimed that for a material with negative permittivity and permeability, ϵ and μ, the refractive index would also be negative. Pendry showed in 2000 [2] that a slab of a medium with refractive index $n = -1$ would function as a perfect lens, going beyond the diffraction limit. In 2006 [3] he further showed that if ϵ and μ can be controlled at will, it is possible to design a cloaking devices, i.e. a container where light is bend around it, and effectively makes it invisible. Metamaterials can also be used to increase efficiency of antennas, and obtaining a magnetic response even at very high frequencies. To obtain desired responses such as negative refraction, some metamaterials make use of material resonances. A resonant response is often associated with high losses, which is an extensive problem in current metamaterial realizations. To overcome these losses it has been suggested to make use of active media, i.e. media with gain.

In an unpublished paper Hågenvik, Malema and Skaar use Fourier-Laplace theory to analyze gain media. The media are assumed to be infinite or semi-infinite, meaning fields never reach the end of the media. One may argue that this situation is unphysical, as infinitely large media don't exist. However, for a finite medium the theory will still predict the response for the duration before the light reaches the outer boundaries of the medium. It also helps us understand the optical response given solely by the medium's properties - all effects related to interactions with surrounding media have been ruled out. The mentioned paper is attached in appendix A.

Infinite or semi-infinite gain media may involve instabilities, as the waves may travel infinitely far, picking up gain as they propagate. The theory is used to understand when these instabilities will be *convective*, meaning they are convected away, and when they will be *absolute*, meaning the fields grow with time even at a fixed point in space. The theory is also used to predict the existence of novel types of media. In particular it predicts isotropic media exhibiting simultaneous refraction, meaning that they refract positively and negatively at the same time. It is shown that for this to be possible the medium must have gain. A discussion on what is required from such a medium, and suggestions for optimal realizations are presented in this thesis.

When light goes from one material to another it is refracted at some angle, as shown in Figure 1a. This is because light travels at different speed in different materials. If a specific metamaterial is used, the refraction may happen at a negative angle, which implies that the light inside the metamaterial travels towards the boundary, as shown in Figure 1b. By simultaneous refraction it is meant that both this peculiar effect, and the regular positive refraction happen at the same time. A principle sketch is given in Figure 1c. The possible existence of this effect is derived by deformation of the inverse Fourier-Laplace integration surface.

Optical phenomena are often considered in the so called monochromatic and plane wave limits, meaning the signal is assumed to contain a single frequency ω_1, and a single plane wave component K_x. Physically these limits can never be reached. The source will always have a finite width, so other k_x than K_x will be excited to some extent. The source is turned on at some time $t = 0$, and other frequencies than ω_1 must be present to describe this onset. The monochromatic limit is approximated by turning on a single frequency oscillation at $t = 0$, and waiting a sufficiently long time $t \to \infty$. The plane wave limit is approached by letting the source width σ be infinitely large. It is shown in the attached paper that for gain media these two limits do not commute in general. If the monochromatic limit is taken first, the plane wave limit cannot necessarily be taken, and visa versa. This is because there may be instabilities associated with waves traveling infinite distances, and for infinitely long times in gain media. In a physical situation the order of the limits $t \to \infty$ and $\sigma \to \infty$ will explain how the optical response

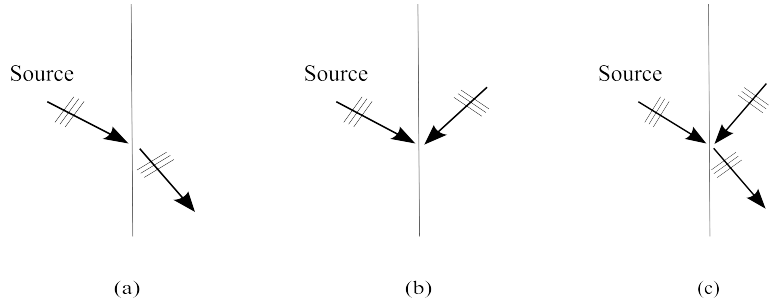

Figure 1: A principle sketch of (a) positive refraction, (b) negative refraction and (c) simultaneous refraction. The source produce an incident wave, which is refracted differently in the three cases. The response in (a) is the type of refraction we see in every day life. To obtain the response (b) or (c) novel media, *metamaterials*, must be used.

will be in the limits $t \ll \sigma/c$ and $t \gg \sigma/c$ when σ and t both gets very large. Even in gain media where the monochromatic limit can be reached, it may require very long experiment durations before the transients ("unwanted" k_x and ω) die out. This is because the transient frequencies may grow faster than the observation frequency ω_1 as the wave propagates. For gain media the transient phase may thus be a lot longer than for conventional, passive media. If there are instabilities involved, the transients will in fact never die out.

To visualize simultaneous refraction a time domain (FDTD)-method was implemented in MATLAB. The analytic derivation of simultaneous refraction is done in the Fourier-Laplace transform domain, but the real physics happens in the time domain. The simulations are therefore done in the time domain, as an independent verification of the theory. It turns out a significant amount of gain is required to obtain simultaneous refraction, where the large gain must be just adjacent to the observation frequency. Unfortunately, for media with large gain the validity of the simulations collapses after even short durations. This is due to numerical errors being amplified, before the monochromatic response may be observed. The implemented FDTD program was used to simulate the time domain response of several (passive and active) negative refracting media. It was also used to show the presence of evanescent gain, and to investigate various phenomena related to instabilities in gain media.

1.1 Scope of report

The report is structured as follows: Section 2 introduces some concepts from complex analysis which frequently occur in this report. Section 3 covers some background theory about the optical parameters of materials, ϵ and μ, and a short introduction to metamaterials is given. Assumptions about the media which will be analyzed, and two different source configurations used to investigate these media are presented in Section 4, before the Fourier-Laplace theory from the attached paper is presented in Section 5.

Section 6 describes how the transient phase may be very long for certain gain media. A method for how to determine whether the monochromatic limit at a given point is reached or not is presented. Section 7 discuss the instabilities associated with infinite gain media. Simulation results of some of the discussed phenomena are presented in Section 12.5.

If the fields grow very large, amplified artificial reflections inside the medium will destroy the validity of FDTD simulations. A discussion on the origin of these reflections is given in Section 11. A short review of the development of the FDTD method, and derivations of the expressions used in the simulation program are given in Section 9. Section 10 explains how this method was implemented in MATLAB, for instance how the simulation parameters were chosen, and how the boundary conditions were set. In Section 12 the FDTD program is used to simulate different negative refracting media. Simulation results showing evanescent gain are presented. Media with zeros in the upper half plane were also simulated.

Finally, Section 13 sums up, and concludes the findings in this thesis. In Section 14 some suggestions on what could be done next are made. The author's results are contained in Secs. 6-8 6-8 and 10-14 10-14, in addition to parts of 4.3 and 5.3. The remaining part of the thesis describes background work.

2 Complex analysis

2.1 Fourier and Laplace transforms

The excitation in time starts at time $t = 0$, so all fields are equal to 0 for $t < 0$. Since we are looking at media with gain, the fields can possibly grow with time. A Laplace transformation decomposes a signal starting at $t = 0$ in exponentials with possibly complex arguments,

$$E(x, z, \omega) = \int_0^\infty E(x, z, t) e^{i\omega t} \mathrm{d}t, \tag{1}$$

where the standard transformation variable s has been substituted with $-i\omega$. For the Laplace transform to exist we must require that the signal does not grow faster than as an exponential with time, so it will be assumed that

$$|E(x, z, t)| < E_0 e^{\gamma t}. \tag{2}$$

This requires $\operatorname{Im}\omega > \gamma$ (i.e. $\operatorname{Re} s > \gamma$).

In reality the width of the source cannot be infinitely large, so the signal will also contain different plane wave components. This decomposition can be done using the Fourier transform

$$E(k_x, z, \omega) = \int_{-\infty}^\infty E(x, z, \omega) e^{-ik_x x} \mathrm{d}x \tag{3}$$

where all the k_x's are real. By comparing Equation (1) and (3) it can be seen that the Laplace transform is just a Fourier transform with a possibly complex argument[1]. The sign of the transformation variables are opposite for the transformation in space and time. This convention is chosen because this gives a wave propagating in the positive x-direction for positive k_x and $\operatorname{Re}\omega$. The inverse Fourier transform is taken by performing a similar integral as the forward transform, but where the sign in the exponent has switched, and a factor of $1/(2\pi)$ is added. The convenience of the substitution of the Laplace transformation variable now becomes apparent, as the inverse Laplace transform becomes an inverse Fourier transform taken along the line $\operatorname{Im}\omega = \gamma$. The actual electric field in the time and spatial domain is thus given by

$$E(x, z, t) = \frac{1}{(2\pi)^2} \int_{i\gamma-\infty}^{i\gamma+\infty} \int_{-\infty}^\infty E(k_x, z, \omega) e^{i(k_x x - \omega t)} \mathrm{d}k_x \mathrm{d}\omega. \tag{4}$$

2.2 Analytic function

A function $f(z)$ is said to be *analytic in a domain* D if $f(z)$ is defined and differentiable at all points of D. The function $f(z)$ is said to be analytic at a point $z = z_0$ in D if $f(z)$ is analytic in a neighborhood of z_0.

Also, by an **analytic function** we mean a function that is analytic in *some* domain.

2.3 Cauchy's integral theorem

If $f(z)$ is analytic in a simply connected domain D, *then for every simple closed path C in D,*

$$\oint_C f(z) \mathrm{d}z = 0 \tag{5}$$

It can be shown that the implication goes both ways, so if $f(z)$ is continuous in a domain D, and if $\oint_C f(z)\mathrm{d}z = 0$ for every closed path in the domain D, then $f(z)$ is analytic in D.

It is easy to extract from (5) that if $f(z)$ is analytic in a domain D, the integration path from a point A to point B in D is path independent. This means that integration paths can be deformed in domains where $f(z)$ is analytic.

[1] In the Laplace transform the integral is taken from $t = 0$ to ∞, but since the electric field is 0 for $t < 0$ it wouldn't make any difference to change the lower limit to $-\infty$

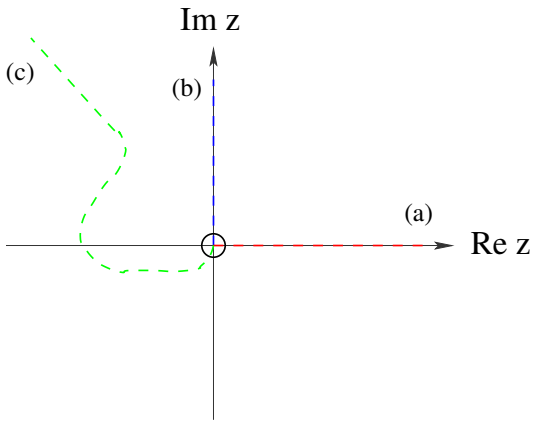

Figure 2: Three possible branch cuts from the branch point of $w = \sqrt{z}$: (a) Along the real axis towards $+\infty$, (b) along the imaginary axis towards $+i\infty$ and (c) along an arbitrary path towards infinity.

2.4 The residue theorem

If $f(z)$ is analytic in a domain except at a finite number of points, an integral around a closed path C can be calculated using the residue theorem

$$\oint_C f(z)\mathrm{d}z = 2\pi i \sum_{j=1}^{k} \mathrm{Res}_{z=z_j} f(z) \tag{6}$$

where C is a closed, counterclockwise path, and z_j are the non-analytic points of $f(z)$ inside C. When f has a simple pole at z_1 we can write $f(z) = \frac{g(z)}{z-z_1}$, where $g(z)$ is analytic in a neighborhood around z_1. Then $\mathrm{Res}_{z=z_1} f(z) = g(z_1)$.

2.5 Square root of complex numbers

The square root of a complex number $z = w^2$ can take the two possible values $\pm w$. For positive numbers the square root is defined to be the positive value, but such a definition is not possible to make for a complex number. By writing a complex number in polar form $z = re^{i\phi}$, the square roots are given by $w = \sqrt{z} = \pm\sqrt{r}e^{i\frac{\phi}{2}}$. First look at the positive root, and let ϕ go from 0 to 2π. One then gets $z(r,0) = z(r,2\pi) = r$, but $w(r,0) = \sqrt{r}$ and $w(r,2\pi) = -\sqrt{r}$. A phase shift of 2π in the argument of the square root will shift the sign of the square root. The same things happens if the negative root considered. This is valid for any r, which means that the square root is discontinuous, and therefore non-analytic along a line from $r = 0$ to ∞. The square root is said to have a *branch point* in $z = 0$, and a *branch cut* goes from the branch point along the real axis to $+\infty$.

The angle ϕ where the sign for the square root flips can be defined to be somewhere else than for $\phi = 0$. For instance if $\phi = \frac{\pi}{2}$, let the sign for w be chosen such that $w(r, \frac{\pi}{2}) = +\sqrt{r}e^{i\frac{\pi}{4}}$. When ϕ goes from $\frac{\pi}{2}$ to $\frac{\pi}{2} + 2\pi$ the value of w goes from $w(r, \frac{\pi}{2}) = +\sqrt{r}e^{i\frac{\pi}{4}}$ through a bunch of complex numbers, and ends up at $w(r, \frac{\pi}{2} + 2\pi) = -\sqrt{r}e^{i\frac{\pi}{4}}$. The branch cut now goes from $z = 0$ to $+i\infty$.

In general the angle where the sign flips can be chosen as a function of r, but no matter how this path is defined there will go a branch cut, where the square root is non-analytic, from $z = 0$ through some path out to ∞. Three such branch cuts are shown in Figure 2.

If z_1 is a point close to the branch cut, and z_2 a point just on the other side of the cut, one will have $f(z_1) = -f(z_2)$. The root $\sqrt{z - z_0}$ will have a branch point in $z = z_0$, and a branch cut from $z = z_0$ to ∞.

3 Background

3.1 Maxwell's equations

Maxwell's equations for a source free medium are given by [4, p. 332]

$$\nabla \times \mathbf{H} = \frac{\partial \mathbf{D}}{\partial t} \tag{7a}$$

$$\nabla \times \mathbf{E} = -\frac{\partial \mathbf{B}}{\partial t} \tag{7b}$$

$$\nabla \cdot \mathbf{D} = 0 \tag{7c}$$

$$\nabla \cdot \mathbf{B} = 0. \tag{7d}$$

The electric flux density $\mathbf{D}$ and electric field $\mathbf{E}$ are related through the material dependent electric property $\mathbf{P}$ (polarization density). $\mathbf{B}$ and $\mathbf{H}$ are similarly related through the magnetization density $\mathbf{M}$:

$$\mathbf{D} = \epsilon_0 \mathbf{E} + \mathbf{P} \tag{8a}$$

$$\mathbf{B} = \mu_0 \mathbf{H} + \mu_0 \mathbf{M}. \tag{8b}$$

For a linear medium the polarization and magnetization densities at the time t are linearly dependent on the electric and magnetic fields at all previous times $\tau < t$. Such a property is mathematically described by a convolution:

$$\mathbf{D}(t) = \epsilon_0 \mathbf{E}(t) + \epsilon_0 \int_0^t \chi_{\mathrm{e}}(t-\tau)\mathbf{E}(\tau)\mathrm{d}\tau \tag{9a}$$

$$\mathbf{B}(t) = \mu_0 \mathbf{H}(t) + \mu_0 \int_0^t \chi_{\mathrm{m}}(t-\tau)\mathbf{H}(\tau)\mathrm{d}\tau. \tag{9b}$$

Here $\chi_{\mathrm{e,m}}$ are called the electric and magnetic susceptibilities, and ϵ_0 and μ_0 are the permittivity and permeability of vacuum, respectively. The integrals are taken from $\tau = 0$ instead of $\tau = -\infty$ because the source is turned on at $t = 0$, so all fields are zero for $t < 0$ due to causality. The arguments of the two functions in a convolution can be interchanged, so the integrals in (9a) can be written $\int_0^t \chi_{\mathrm{e}}(\tau)\mathbf{E}(t-\tau)\mathrm{d}\tau$, and similarly for (9b). The susceptibilities $\chi(\tau)$ thus describe how the polarization/magnetization at time t depends on what the electric/magnetic field was τ ago.

It can be convenient to solve Maxwell's equations in the frequency and wavenumber domains. In the transformation domains the convolution becomes a product, which is a lot easier to deal with than the possibly complicated integral. For the components $\mathbf{E}(k_x, z, \omega)e^{ik_x x - i\omega t}$ the x and t dependency is only in the exponent. The derivatives with respect to x and t are thus equivalent to multiplying with ik_x and $-i\omega$. The Laplace transforms $\mathbf{D}(\omega)$ and $\mathbf{E}(\omega)$ (and $\mathbf{B}(\omega)$ and $\mathbf{H}(\omega)$) are related through

$$\mathbf{D}(\omega) = \epsilon_0(1 + \chi_{\mathrm{e}}(\omega))\mathbf{E}(\omega) = \epsilon_0 \epsilon(\omega)\mathbf{E}(\omega) \tag{10a}$$

$$\mathbf{B}(\omega) = \mu_0(1 + \chi_{\mathrm{m}}(\omega))\mathbf{H}(\omega) = \mu_0 \mu(\omega)\mathbf{H}(\omega) \tag{10b}$$

where the functions $\epsilon(\omega) = 1 + \chi_{\mathrm{e}}(\omega)$ and $\mu(\omega) = 1 + \chi_{\mathrm{m}}(\omega)$ have been introduced. These functions are called the **relative permittivity and permeability functions**, and describes the material dependent electric and magnetic properties of a medium. The electric and magnetic properties are in general frequency dependent, and theoretical models are therefore usually made for the frequency dependent susceptibilities $\chi(\omega)$. For example the susceptibility may be given by the Lorentz oscillator model [5, p. 176]:

$$\chi(\omega) = \frac{F\omega_0^2}{\omega_0^2 - \omega^2 - i\Gamma\omega} \tag{11}$$

which describes a resonant dielectric medium. Here F is the strength of the response, ω_0 is the resonance frequency, and Γ is the damping rate, which also describes the bandwidth of the resonant frequency response.

The same variable has here been used for the time dependent and frequency dependent versions of the functions ($\mathbf{E}(t)$ and $\mathbf{E}(\omega)$ etc). This will be done throughout the report, but it should be apparent from the argument of the functions, and the context, whether it is the time or frequency dependent function which is being evaluated. If $\chi(\omega)$ is known, $\chi(t)$ is found by taking the inverse Laplace transform:

$$\chi(t) = \frac{1}{2\pi}\int_{i\gamma-\infty}^{i\gamma+\infty} \chi(\omega)e^{-i\omega t}\mathrm{d}\omega \tag{12}$$

where γ must be chosen such that $\chi(\omega)$ is analytic for $\mathrm{Im}\,\omega > \gamma$.

For homogeneous media, it can be shown that the Fourier-Laplace transformed solutions of Maxwell's equations must fulfill the Helmholtz equation

$$(\frac{\mathrm{d}^2}{\mathrm{d}z^2} - k_x^2 + \epsilon(\omega)\mu(\omega)\frac{\omega^2}{c^2})\mathbf{E}(k_x, z, \omega) = 0 \tag{13}$$

where $\epsilon(\omega)$ and $\mu(\omega)$ are the relative permittivity and permeability of the material in the frequency domain, and c is the speed of light in vacuum.

3.2 Refractive index

The refractive index is defined as

$$n(\omega) = \sqrt{\epsilon(\omega)\mu(\omega)} = n'(\omega) + in''(\omega) \tag{14}$$

and will in general be a complex number depending on frequency. $n(\omega)$ is given by a square root, so the correct sign must be determined. As mentioned in Section 2.5 the square root of a complex number has two possible solutions. However, only one of the solutions to (14) is physical, as will be explained in Section 4.1.

The real part of the refractive index at a frequency reflects how the phase velocity at the given frequency compares to the speed of light in vacuum, c. The imaginary part indicates how much the wave attenuates or is amplified as it propagates in the medium.

3.3 Negative refraction

The electron gas in a metal approximately behaves as a plasma, where the permittivity function can be written in the form

$$\epsilon(\omega) = 1 - \frac{\omega_\mathrm{p}^2}{\omega^2}, \tag{15}$$

where $\omega_\mathrm{p} = \sqrt{Ne^2/m\epsilon_0}$ is called the plasma frequency. N is here the electron density of the metal, and m and e the mass and charge of the electron, respectively. For $\omega < \omega_\mathrm{p}$ the electric permittivity becomes negative. The plasma model assumes no loss; in reality the electrons will be damped by the metal lattice. In a more realistic model where damping is included, still $\mathrm{Re}\,\epsilon(\omega) < 0$ below ω_p, but now $\mathrm{Im}\,\epsilon(\omega) \neq 0$ because of the damping.

It is also possible to achieve $\mathrm{Re}\,\mu(\omega) < 0$. For instance if $\mu(\omega) = 1 + \chi(\omega)$, where $\chi(\omega)$ is given by the Lorentz model (11), we will get $\mathrm{Re}\,\mu(\omega) < 0$ for $\omega \gtrsim \omega_0$, provided $F > 1$. Such a response can be approximated by the split-ring resonator medium suggested by Pendry [6]. It is shown in the following that for a passive medium with $\epsilon(\omega_1) < 0$ and $\mu(\omega_1) < 0$ at the same frequency ω_1, also the refractive index will become negative at this frequency, $n(\omega_1) < 0$.

Plane wave solutions, in the form $\mathbf{E} = \mathbf{E_0}e^{i\mathbf{k}\cdot\mathbf{r}-i\omega t}$ and $\mathbf{H} = \mathbf{H_0}e^{i\mathbf{k}\cdot\mathbf{r}-i\omega t}$, will satisfy Maxwell's equations. We can without loss of generality assume that $\mathbf{E_0}$ and $\mathbf{H_0}$ are real. Inserting this into the curl Equations (7a)-(7b) gives

$$\mathbf{k}\times\mathbf{E_0} = \omega\mu\mathbf{H_0} \tag{16a}$$

$$\mathbf{k}\times\mathbf{H_0} = -\omega\epsilon\mathbf{E_0}. \tag{16b}$$

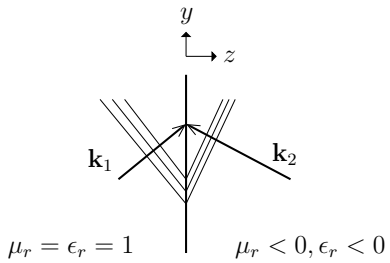

Figure 3: The normal component of k_{2z} is negative for a negative refracting medium. The wave is refracted at a negative angle, and has a phase velocity backwards towards the boundary. This figure is taken from [7].

Since ϵ and μ are negative, the vectors $(\mathbf{E}, \mathbf{H}, \mathbf{k})$ form a left-handed set. Media with negative ϵ and μ are therefore referred to as left-handed media. The energy flow in the medium is described by the Poynting vector

$$\mathbf{S} = \frac{1}{2}\mathbf{E_0} \times \mathbf{H_0}, \tag{17}$$

so $\mathbf{S}$ and $\mathbf{k}$ are antiparallel in a medium with negative ϵ and μ.

Further consider the situation described by Figure 3, with vacuum to the left and the medium with negative ϵ and μ to the right of the boundary, with a monochromatic plane wave incident to the boundary. The polarization $\mathbf{E} = E\hat{y}$ and $\mathbf{H} = H_x\hat{x} + H_z\hat{z}$ is assumed. Since there is no source or "energy drain" at the boundary, the normal component of $\mathbf{S}$ must be continuous. Since $\mathbf{S}$ and $\mathbf{k}$ are antiparallel in the medium with negative ϵ and μ, the normal component of $\mathbf{k_2}$ thus points towards the boundary. The tangential components of the electric and magnetic fields must be continuous, from the boundary conditions. To achieve this, the phase of $\mathbf{E}$ and $\mathbf{H}$ must match at the boundary, so also the tangential component of $\mathbf{k_2}$ must be continuous, i.e. $k_{2x} = k_{1x}$. The monochromatic plane wave in the left-handed medium will thus be refracted negatively, and have a phase velocity towards the boundary as shown in Figure 3. This phenomenon is known as negative refraction.

That the wave is refracted at a negative angle can also be seen from Snells law, $n_1 \sin(\theta_1) = n_2 \sin(\theta_2)$. So if $n_1 > 0$ and $n_2 < 0$ the angles θ_1 and θ_2 will have opposite signs.

3.4 Non-magnetic negative refraction

In 2005 Chen, Fisher and Wise [8] predicted the existence of right-handed negative refracting media, i.e. media with positive $\mathrm{Re}\,\epsilon$ and $\mathrm{Re}\,\mu$, but $\mathrm{Re}\,n < 0$. Such a medium will later in the report be referred to as a CFW-medium. ϵ and μ can be written in complex form:

$$\epsilon = |\epsilon| e^{i\theta_\mathrm{e}} \tag{18a}$$

$$\mu = |\mu| e^{i\theta_\mathrm{m}} \tag{18b}$$

which gives the refractive index as

$$n = \sqrt{\epsilon\mu} = \pm\sqrt{|\epsilon||\mu|}e^{i(\theta_\mathrm{e}+\theta_\mathrm{m})/2} \tag{19}$$

where the sign of n is yet to be determined.

At infinitely large frequencies the electric and magnetic response must disappear, as the charges in the media can't move infinitely fast. This means $|\epsilon| \to 1$, $|\mu| \to 1$, $\theta_\mathrm{e} \to 0$ and $\theta_\mathrm{m} \to 0$ as $\omega \to \infty$. To satisfy $n(\omega) \to 1$ as $\omega \to \infty$ the positive sign must therefore be chosen. For the functions $\epsilon(\omega)$ and $\mu(\omega)$ to be analytic, $|\epsilon|$,$|\mu|$, θ_e and θ_m must be continuous with frequency [9]. For a frequency with $(\theta_\mathrm{e} + \theta_\mathrm{m})/2 \approx \pi$ the refractive index thus becomes negative, independent of ϵ and μ's separate properties.

According to the arguments above it should be possible to achieve negative refraction where all the necessary phase comes from the electrical property ϵ, i.e. $\mu = 1$ and ϵ with $\theta_\mathrm{e} = 2\pi$. Weak magnetic

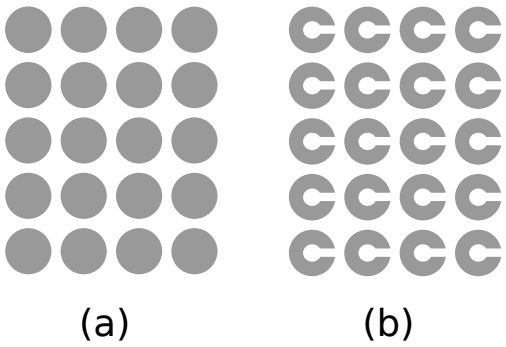

Figure 4: Examples of metamaterials: (a) Cross section of parallel metal wires, for obtaining $\mathrm{Re}\,\epsilon < 0$ and (b) Split ring resonators, for obtaining $\mathrm{Re}\,\mu < 0$, at desired frequencies

response at optical frequencies is one problem with achieving negative refraction in left-handed, passive media, so non-magnetic negative refractive media are very interesting.

One way of obtaining a right-handed, non-magnetic medium is to use a permittivity function which is a sum of a passive and active Lorentz. Such a medium must be constantly pumped with energy. An advantage with using gain media, is that they may be able to overcome the absorption problem of passive left-handed media.

Simulation results show that the right-handed, non-magnetic CFW-medium in fact exhibits negative refraction [10]. It has been suggested that such a medium can be experimentally designed using Bose-Einstein condensates [11].

3.5 Metamaterials

Negative ϵ and μ at the same frequency do not occur in materials found in nature. Negative refractive index media must thus be constructed artificially. Such artificially constructed materials, designed to have specific optical properties, are called metamaterials[2]. Metamaterials are composite materials, where the size of the structures are smaller than the wavelength of the light. The idea is that for electromagnetic waves with wavelengths a lot larger than the feature size of the structures the waves will "see" effective parameters ϵ and μ, rather than the bulk parameters for each of the materials used. To obtain negative refraction at optical frequencies nano structures must thus be used. The rapid development of microprocessing techniques the last years has made it possible to produce such small structures.

Negative ϵ at a desired frequency can for instance be obtained by an array of parallel metal rods. This will simulate a plasma, where the average electron density will depend on the diameter and density of the rods. The plasma frequency $\omega_\mathrm{p} = \sqrt{Ne^2/m\epsilon_0}$ can in this way be tuned as desired. A cross section of such a metal array is shown in Figure 4a.

Similarly will an array of split metal rings, as shown in Figure 4b, make it possible to obtain $\mu < 0$. The circuit equivalent for the split ring will be a RLC-circuit, where R is the internal resistance of the ring, L is the self-inductance of the ring, and C the capacitance from the gap. An oscillating magnetic field through the ring will induce a current, and the RLC-circuit equations can be used to show that the magnetic response μ of this medium in fact is approximated by a Lorentz function. The parameters for this Lorentz function can be tuned through the structure size and density of the split rings. Using split rings to achieve a tunable magnetic response was first suggested in [6].

[2]One meaning of the greek word meta is "beyond", and these materials goes beyond what is found in nature

4 Setup and assumptions

The media in the following analysis are assumed to be linear, time-shift invariant, isotropic and homogeneous, and without spatial dispersion. For simplicity the light only propagates in two dimensions (x and z-direction), with the electric field polarized in the y-direction. The media can in general be active, which means that the fields are allowed to grow with time. It is however assumed that the fields do not grow faster than an exponential function, with exponential growth rate γ:

$$|E(x,z,t)| \leq E_0 e^{\gamma t}. \tag{20}$$

This criterion is not very strict, as there is no upper allowed limit set on γ. When equation (20) is fulfilled the Laplace transform exists for $\operatorname{Im}\omega > \gamma$. In reality the active media will be restricted by gain saturation, which will make the optical response non-linear. This problem is dealt with by assuming that the excitation is sufficiently weak, so that the magnitude of the fields always are below the saturation limit.

To investigate the electromagnetic properties of media where $\epsilon(\omega)$ and $\mu(\omega)$ are known, the wave equation (13) will be solved in two different situations. In the first situation a medium with known $\epsilon(\omega)$ and $\mu(\omega)$ fills the entire space, and the (infinitely thin) source is located in the plane $z = 0$. The second situation is the standard Fresnel case, where two media with known $\epsilon(\omega)$ and $\mu(\omega)$ are located on each side of the plane $z = 0$. The source is located at some $z < 0$, producing an incident wave propagating towards the boundary. The transmission and reflectance coefficients will be given by the Fresnel equations [9].

4.1 Surface current excitation

The situation where a medium with known $\epsilon(\omega)$ and $\mu(\omega)$ fills the entire space, with a surface current source in the plane $z = 0$, as shown in Figure 5, will now be considered. The electric field can be written as an inverse Laplace and Fourier transform with respect to time and space, as described by (4) in Section 2.1. The transversal component of the magnetic field is given by $-i\omega\mu H_x(k_x,z,\omega) = dE(k_x,z,\omega)/dz$. Using this, and (13) we get

$$E(k_x,z,\omega) = A(k_x,\omega)e^{ik_z z} + B(k_x,\omega)e^{-ik_z z} \tag{21a}$$

$$H_x(k_x,z,\omega) = -\frac{k_z}{\omega\mu}[A(k_x,\omega)e^{ik_z z} - B(k_x,\omega)e^{-ik_z z}] \tag{21b}$$

for $z < 0$, and

$$E(k_x,z,\omega) = C(k_x,\omega)e^{ik_z z} + D(k_x,\omega)e^{-ik_z z} \tag{22a}$$

$$H_x(k_x,z,\omega) = -\frac{k_z}{\omega\mu}[C(k_x,\omega)e^{ik_z z} - D(k_x,\omega)e^{-ik_z z}] \tag{22b}$$

for $z > 0$. Here

$$k_z^2 = \epsilon\mu\frac{\omega^2}{c^2} - k_x^2, \tag{23}$$

which means k_z is given by one of the square roots

$$k_z = \pm\sqrt{\epsilon\mu\frac{\omega^2}{c^2} - k_x^2}. \tag{24}$$

The functions $A(k_x,\omega), B(k_x,\omega), C(k_x,\omega)$ and $D(k_x,\omega)$ are related through the boundary conditions, which again will depend on the source. If a surface current is used to generate the propagating wave, the electric field will be continuous across the source plane, while $H(k_x,0^+,\omega) - H(k_x,0^-,\omega) = J(k_x,\omega)$, where $J(k_x,\omega)$ is the (Laplace-Fourier transformed) surface current source. Since $E(k_x,z,\omega)$ is continuous across the boundary the symmetry of the situation gives that $A = D$ and $B = C$. Inserting this in $H_x(k_x,0^+,\omega) - H_x(k_x,0^-,\omega) = J(k_x,\omega)$ gives

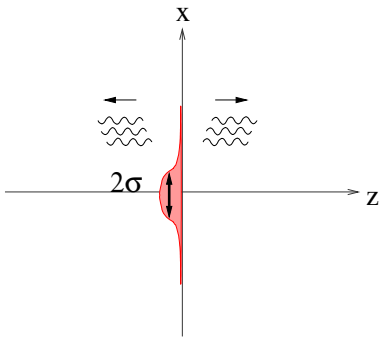

Figure 5: A current source in the plane $z = 0$. The entire space is filled with a medium with known ϵ and μ

$$\frac{2k_z}{\omega\mu}(A - B) = J(k_x, \omega). \tag{25}$$

Since the argument of the square root in general is a complex number it is not straightforward to determine which sign should be chosen for k_z (see Section 2.5 for details). It seems that the scientific community now has agreed upon that the sign should be chosen such that

$$\begin{aligned} &k_z(k_x, \omega) \text{ is analytic for } \operatorname{Im}\omega > \gamma, \text{ and} \\ &k_z(k_x, \omega) \to +\omega/c \text{ as } \omega \to \infty \text{ in the region } \operatorname{Im}\omega > \gamma. \end{aligned} \tag{26}$$

The last criterion makes intuitively sense: For infinitely large frequencies the electrons in the material will not be able to move fast enough for the media to have any electromagnetic response, so for $\omega \to \infty$ the wave should propagate as if it was traveling in vacuum. The first criterion reaches back to Sommerfeld and Brillouin [12] for passive media, and has later been modified to be valid also for active media in general [9]. It is shown in the attached paper (appendix A) that (26), along with the principle of causality, leads to $A(k_x, \omega) = D(k_x, \omega) = 0$.

Since $A = D = 0$ from causality (25) gives us $B = C = -\frac{\omega\mu}{2k_z}J(k_x, \omega)$. Equations (21) and (22) then become

$$E(k_x, z, \omega) = -\frac{\omega\mu}{2k_z}J(k_x, \omega)e^{-ik_z z} \tag{27a}$$

$$H_x(k_x, z, \omega) = -\frac{1}{2}J(k_x, \omega)e^{-ik_z z} \tag{27b}$$

for $z < 0$, and

$$E(k_x, z, \omega) = -\frac{\omega\mu}{2k_z}J(k_x, \omega)e^{ik_z z} \tag{28a}$$

$$H_x(k_x, z, \omega) = \frac{1}{2}J(k_x, \omega)e^{ik_z z} \tag{28b}$$

for $z > 0$.

The inverse Fourier-Laplace transform becomes

$$E(x, |z|, t) = \frac{1}{(2\pi)^2}\int_{i\gamma-\infty}^{i\gamma+\infty}\int_{-\infty}^{\infty} -\frac{\omega\mu}{2k_z}J(k_x, \omega)e^{i(k_x x + k_z|z| - \omega t)}\mathrm{d}k_x\mathrm{d}\omega \tag{29}$$

where k_z is given by (24). The electric field only depends on $|z|$, from the symmetry of the situation.

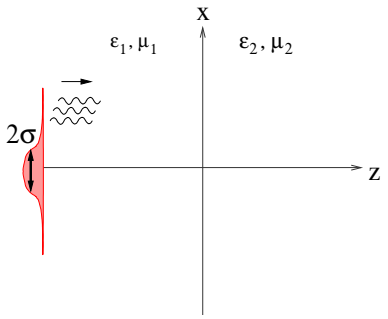

Figure 6: An incident wave at a boundary between two materials with different optical properties. The source is located at some $z < 0$.

4.2 Incident wave at a boundary

We now consider the situation where two different media are located at each side of the plane $z = 0$. The source is located somewhere to the left ($z < 0$) producing an incident wave propagating towards the boundary, as shown in Figure 6. The causality argument from the paper in appendix A can be used to show that $D(k_x, \omega) = 0$, but now $A(k_x, \omega) \neq 0$ since part of the incident wave is reflected from the boundary. In this case there are no charges or currents in the plane $z = 0$. Both the electric and magnetic fields must therefore be continuous across the boundary, i.e. $E(k_x, 0^+, \omega) = E(k_x, 0^-, \omega)$ and $H_x(k_x, 0^+, \omega) = H_x(k_x, 0^-, \omega)$. This gives the reflection and transmission coefficients

$$\frac{B}{A} = \frac{\mu_2 k_{1z} - \mu_1 k_{2z}}{\mu_2 k_{1z} + \mu_1 k_{2z}} \tag{30a}$$

$$\frac{C}{A} = \frac{2\mu_2 k_{1z}}{\mu_2 k_{1z} + \mu_1 k_{2z}} \tag{30b}$$

where $k_{iz}^2 = \epsilon_i \mu_i \omega^2/c^2 - k_x^2$ ($i = 1, 2$, and refers to the media to the left and right of $z = 0$). Equations (30) are known as the Fresnel equations.

For the wave propagating into the area $z > 0$ the Fourier-Laplace transform becomes

$$E(x, z, t) = \frac{1}{(2\pi)^2} \int_{i\gamma-\infty}^{i\gamma+\infty} \int_{-\infty}^{\infty} A(k_x, \omega) \frac{2\mu_2 k_{1z}}{\mu_2 k_{1z} + \mu_1 k_{2z}} e^{i(k_x x + k_{2z} z - \omega t)} \mathrm{d}k_x \mathrm{d}\omega, \tag{31}$$

where k_{iz} ($i = 1, 2$) is given by (24).

4.3 The source

In the current source situation the propagating wave is generated by a surface current $J(k_x, \omega)$ in the plane $z = 0$. For the case with a boundary the incident wave is described by the amplitude function $A(k_x, \omega)$, which for instance could originate from a similar current source in a plane somewhere to the left of the boundary. In both situations the excitation is assumed to be in the form $u(x)v(t)$, which will have a Laplace-Fourier transform in the form $U(k_x)V(\omega)$. Here the functions $u(x)$ and $v(t)$

$$u(x) = \exp\left(-x^2/2\sigma^2\right) \exp\left(iK_x x\right) \tag{32a}$$

$$v(t) = H(t) \exp\left(-i\omega_1 t\right) \tag{32b}$$

will be chosen, where $H(t)$ is the unit step function. The Fourier and Laplace transforms are

$$U(k_x) = \sqrt{2\pi}\sigma \exp\left[-\sigma^2 (k_x - K_x)^2/2\right], \tag{33a}$$

$$V(\omega) = \frac{i}{\omega - \omega_1}, \tag{33b}$$

respectively. The excitation (32) is expressed in complex form, so the actual electric field will be the real part of the final solution $E(x, z, t)$.

For $\sigma \to \infty$, $U(k_x) \to 2\pi\delta(k_x - K_x)$, which means that the excitation only produces waves propagating with wave number K_x in the x-direction. However, in practice an infinitely large source does not exist. In the more realistic situation with a large, but finite σ, the excitation will mainly contain the wave number K_x in the x-direction, but also small contributions from all other k_x will be present. If $K_x = 0$ and σ is large, a plane-like wave propagates in the z-direction.

Inserting $J(k_x, \omega) = U(k_x)V(\omega)$ in (29) gives (for $z > 0$)

$$E(x, z, t) = \frac{1}{(2\pi)^2} \int_{i\gamma-\infty}^{i\gamma+\infty} \int_{-\infty}^{\infty} -\frac{\omega\mu}{2k_z} e^{ik_x x + ikzz - i\omega t} \mathrm{d}k_x \mathrm{d}\omega. \tag{34}$$

Similarly, inserting $A(k_x, \omega) = U(k_x)V(\omega)$ in (31) gives

$$E(x, z, t) = \frac{1}{(2\pi)^2} \int_{i\gamma-\infty}^{i\gamma+\infty} \int_{-\infty}^{\infty} \frac{2\mu_2 k_{1z}}{\mu_2 k_{1z} + \mu_1 k_{2z}} e^{i(k_x x + k_{2z} z - \omega t)} \mathrm{d}k_x \mathrm{d}\omega. \tag{35}$$

It is important to remember that these results are only valid for $\operatorname{Im}\omega > \gamma$, and real k_x. The possibility of moving the inverse Laplace transform down to the real axis is discussed in Section 5.

5 Deformation of integration paths

The inverse Laplace transform (Equation 4) is taken along the line $\mathrm{Im}\,\omega = \gamma$, which means that the time domain solution is a sum of functions exponentially growing with t. We must choose γ large enough that the integrand is analytic for $\mathrm{Im}\,\omega > \gamma$. For an analytic function integration paths can be deformed. If the integrand is analytic in the entire upper half-plane $\mathrm{Im}\,\omega > 0$ one can therefore set $\gamma = 0$. The inverse Laplace transform then turns into an inverse Fourier transform, and the time domain electric field is a sum of functions oscillating at real frequencies. For this to be the case, the argument of the square root in Equation 24 must not be equal to 0 for any ω in the upper frequency plane, i.e. there is no ω with $\mathrm{Im}\,\omega > 0$ for which $k_x = \pm\epsilon\mu\frac{\omega^2}{c^2}$ for any k_x along the real k_x-axis. This is the case for all passive media.

In the paper (appendix A) it is shown that for some media it is possible to deform the integration path down to $\mathrm{Im}\,\omega = 0$, at the expense of deforming the integration path in the complex k_x-plane. The electric field will then be expressed as a sum of functions oscillating at real frequencies, but where the inverse Fourier transform with respect to k_x could contain complex k_x, i.e. exponentially increasing waves in the x-direction. The formalities of this path deformation method are presented in the following section. In this section systems with a finite source width σ are considered. Provided the inverse Laplace transform can be deformed down to the real ω-axis, the fields will not grow with time at a fixed point in space, and the monochromatic limit can thus be approximated by waiting a sufficiently long time. Possible instabilities associated with approximating the plane wave limit, by letting the source width σ go to ∞, are discussed in Section 7.

5.1 Towards real frequencies

First the situation where $\sqrt{\epsilon\mu}$ is zero-free, and has no branch points or branch cuts in the upper half-plane $\mathrm{Im}\,\omega > 0$ is considered. The original integration paths in the complex ω and k_x-planes are shown in Figure 7a-b. The ω integration path can be interpreted as a subsequent sum of small integration segments. We now consider the possibility of moving the part of the integration path at the frequency marked with a circle in Figure 7a down to the real axis. The branch points, which will make k_z non-analytic, are given by $k_x = \pm\sqrt{\epsilon\mu}\omega/c$. For the frequencies in D_ω the corresponding branch points in the k_x-plane are located in the shaded areas, D_{k_z}, in 7b. It is argued in the paper that k_z is analytic along the real k_x-axis for $\mathrm{Im}\,\omega > \gamma$. The branch cuts must therefore avoid the real axis, and are taken as vertical lines to infinity (as shown in Figure 7b).

The idea now is to avoid the k_x values which gives branch points for ω in D_ω, so the integration path in the k_x-domain is deformed as shown in Figure 7c. Fubini's theorem allows the order of integration to be switched. For each k_x in the path in Figure 8b, k_z will be analytic in the entire domain D_ω. The ω integration path can therefore be deformed down to the real axis in this domain, as shown in Figure 8a.

Performing the same procedure for a neighboring piece in the ω path gives the situation in Figure 9a-b, where the deformation of the k_x-path in general will be different for the two ω-segments. This will result in two domains next to each other where the ω-integration is taken along the real axis, but with a vertical path up an down right between the domains.

To get rid of these vertical paths one must require that there exists a common integration path in the k_x-domain for ω along the "up and down"-path. If this is the case the integral up will have the same magnitude but opposite sign of the integral down, and they sum up to 0. A sufficient condition is that $\sqrt{\epsilon\mu}$ is analytic and zero-free for $\mathrm{Im}\,\omega > 0$: Consider the trajectories of k_z's branch points $k_x = \pm\sqrt{\epsilon\mu}\omega/c$, as $\mathrm{Im}\,\omega$ is reduced from γ to 0. For two values of $\mathrm{Re}\,\omega$ approaching each other, these two trajectories will become arbitrarily close to each other. We have also required that $\epsilon\mu$ is zero-free for $\mathrm{Im}\,\omega > 0$. While even order zeros give analytic square root, they induce another problem: At the zero the two branch points in the k_x-domain coincide, so the integration curve get "stuck".

The same method is repeated over again until the integration path goes along the real ω-axis. The inverse Fourier-Laplace transform is then given by

$$E(x,z,t) = \frac{1}{(2\pi)^2}\int_{-\infty}^{\infty}\int_{\kappa(\omega)} E(k_x,z,\omega)e^{ik_x x - i\omega t}\mathrm{d}k_x\mathrm{d}\omega \tag{36}$$

where the ω integration is taken along the real ω-axis, and the integration path $\kappa(\omega)$ in the k_x-plane in general depends on ω and the properties of the medium.

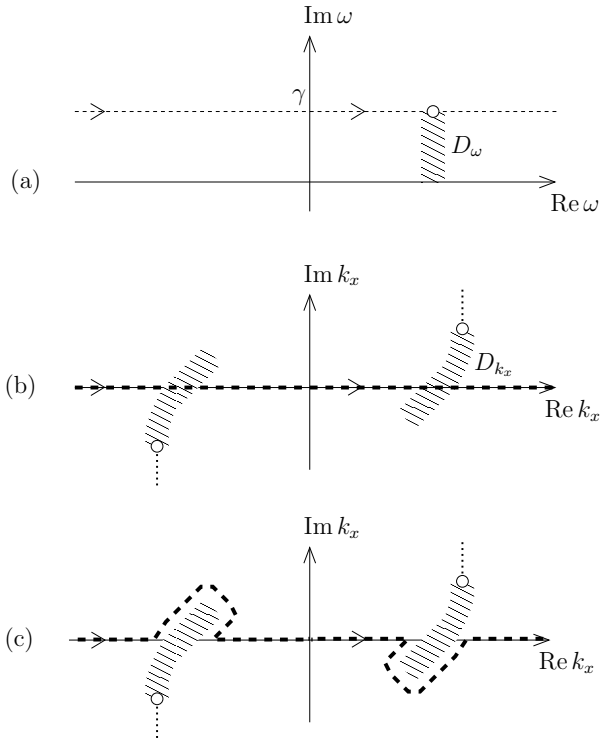

Figure 7: The dashed lines correspond to the integration paths in (4): (a) ω-domain; (b) k_x-domain; and (c) deformed path in the k_x-domain for the ω indicated by a circle in (a). The domain D_{k_x} corresponds to the set of values $k_x = \pm\sqrt{\epsilon\mu}\omega/c$ for $\omega \in D_\omega$. The open circles in the k_x-plane correspond to the open circle in the ω-plane. The dotted vertical lines indicate branch cuts for $k_z(k_x, \omega)$ for the particular ω as indicated by the open circle. It is shown in the paper (appendix A) that $k_z(k_x, \omega)$ is analytic wrt. k_x, for $\operatorname{Im}\omega = \gamma$ and real k_x; thus the branch cuts must avoid the real k_x-axis. In the figure we take them to be vertical, starting at the circles.

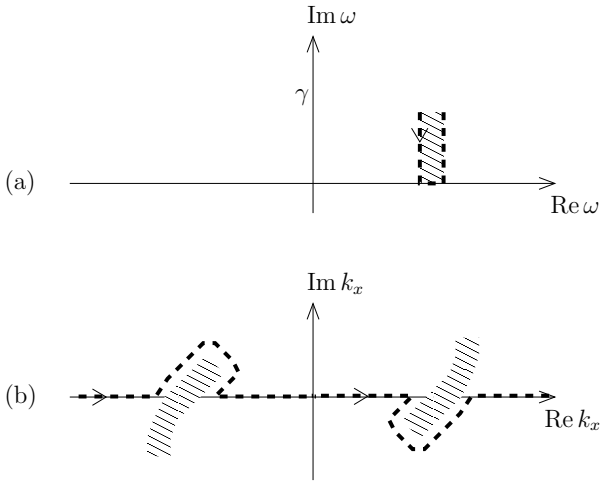

Figure 8: Deformation in the ω-domain. For each k_x in the path in (b), the integration path in D_ω can be deformed (a).

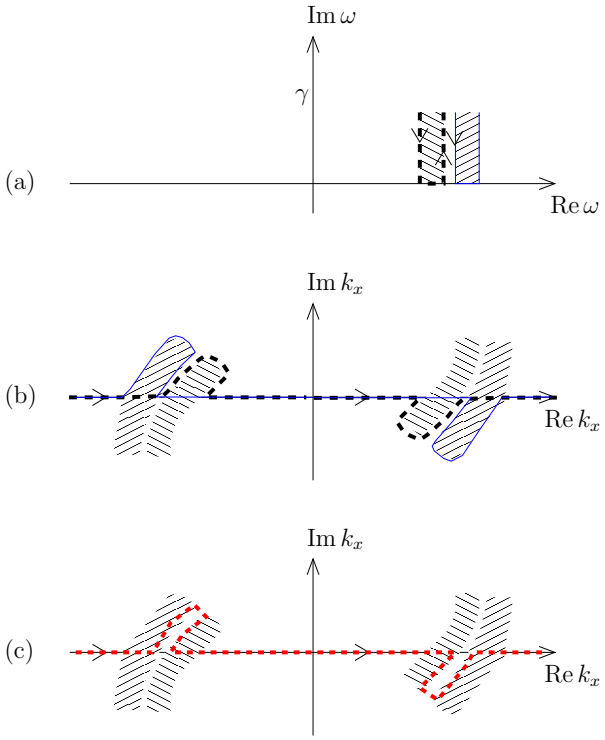

Figure 9: Deformation of two neighboring pieces of the ω-integration curve (dashed black and solid blue) (a) and the associated k_x-integration curves (b). For ω-values along the vertical integration curves between the neighboring domains in (a), one can use a common k_x-integration curve (c).

5.2 Non-analytic $\sqrt{\epsilon\mu}$

Now the more complicated situation where $\sqrt{\epsilon\mu}$ is not analytic or zero-free for $\mathrm{Im}\,\omega > 0$ is considered. For concreteness it is assumed that $\epsilon\mu$ has a single zero in the upper half-plane. $\sqrt{\epsilon\mu}$ will then have a branch cut, which is taken vertical from the zero to $-i\infty$ [3]. Since $\sqrt{\epsilon\mu}$ is analytic everywhere except at the branch cut the procedure described in the previous section can be used to deform the ω integration path to go along the real axis, but with vertical detours around the zeros of $\epsilon\mu$, as shown in Figure 10a. It is not possible to get rid of these paths, as a common integration curve does not exist. For the ω's to the left of the zero, the trajectories of $k_x = \pm\sqrt{\epsilon\mu}$ when $\mathrm{Im}\,\omega$ is reduced from γ to 0 are shown in Figure 10c. Figure 10d shows the trajectories for the ω's to the right of the zero. Since the two k_x-integration paths are different, the the integration up and down in Figure 10a generally do not cancel. The inverse Laplace transform will thus contain exponential terms with complex frequencies $\exp(-i\omega t)$ with $\mathrm{Im}\,\omega > 0$. This means that the field will diverge in time, even at a fixed point in space. Media where $\sqrt{\epsilon\mu}$ is non-analytic and/or has zeros for $\mathrm{Im}\,\omega > 0$ will thus have an absolute instability.

[3] The branch cut cannot be taken towards $+i\infty$, as k_z is required to be analytic for $\mathrm{Im}\,\omega > \gamma$

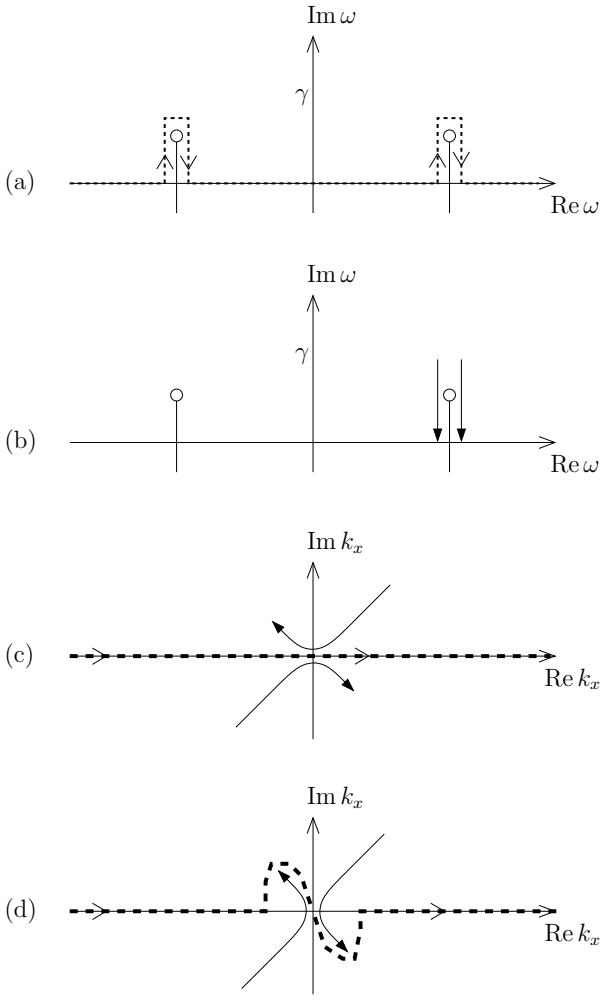

Figure 10: Deformed integration paths (dashed) when $\sqrt{\epsilon\mu}$ has branch cuts in the upper half-plane. The branch points of $\sqrt{\epsilon\mu}$ are shown by open circles in (a); the cuts go vertically towards $-i\infty$. As $\mathrm{Im}\,\omega$ is reduced from γ to zero along the left and right arrows in (b), the corresponding trajectories of $k_x = \pm\sqrt{\epsilon\mu}\omega/c$ are shown by solid lines in (c) and (d), respectively.

5.3 Simultaneous refraction

The deformation theory described above will now be used to predict the existence of media exhibiting simultaneous refraction, i.e. which refracts light positively and negatively at the same time.

Consider a medium where the branch points move as in Figure 11b when $\operatorname{Im}\omega$ is reduced towards 0 at the observation frequency ω_1. The branch cuts can be deformed as shown in Figure 11c, and the k_x integration must follow a zig-zag path to avoid the branch cuts. In the area where the branch cuts are parallel to the real k_x-axis they are taken to be infinitely close to the axis, which allows also the integration path to be infinitely close to the axis. For a large σ the source will produce a plane-like wave, with $U(k_x)$ small for $k_x \neq K_x$, provided $|\operatorname{Re} k_x - K_x| > |\operatorname{Im} k_x|$ along the integration path. As described in Section 2.5 the square root has opposite sign on the two sides of a branch cut. For small K_x, i.e. K_x among the k_x in the zigzag-path, both signs for k_z will survive the k_x-integration[4]. This means that a medium where the branch point trajectories are as in Figure 11b will refract both positively and negatively at the same time. This is what is meant by *simultaneous refraction*.

Consider the situation described in Section 4.1, with a current source at $z = 0$. As will be shown in Section 6.1, for the excitation in time (32b), only the carrier frequency ω_1 will be present after a sufficiently long experiment duration[5]. Inserting (28a) in (36), using that $J(k_x, \omega) = U(k_x)V(\omega)$ (where $U(k_x)$ and $V(\omega)$ are given by (33)), we get for the single frequency component ω_1 where $\kappa(\omega_1)$ is as in Figure 11c:

$$\begin{aligned} 2\pi\frac{E(x,z,\omega_1)}{V(\omega_1)} &= \left(\int_{-\infty}^{-k_\mathrm{b}} + \int_{k_\mathrm{b}}^{\infty}\right) - \frac{\mu\omega}{2k_z}U(k_x)e^{ik_z z + ik_x x}\mathrm{d}k_x \\ &+ \int_{-k_\mathrm{b}}^{k_\mathrm{b}} -\frac{\mu\omega}{2k_z}U(k_x)\left(2e^{ik_z z} + e^{-ik_z z}\right)e^{ik_x x}\mathrm{d}k_x + \int_{\text{vertical detours}} -\frac{\mu\omega}{2k_z}U(k_x)e^{ik_z z + ik_x x}\mathrm{d}k_x. \end{aligned} \tag{37}$$

Here k_b is the real part of the branch point in the first quadrant. In the second integral k_z is the value along the upper integration path in the zigzag area. Note that the second term is positive, since the integration is taken in the opposite direction, but k_z in the fraction has also switched sign.

The equivalent of (37) in the Fresnel situation is

$$\begin{aligned} 2\pi\frac{E(x,z,\omega_1)}{V(\omega_1)} &= \left(\int_{-\infty}^{-k_\mathrm{b}} + \int_{k_\mathrm{b}}^{\infty}\right) U(k_x)\frac{2\mu_2 k_{1z}e^{ik_{2z}z}}{\mu_2 k_{1z} + \mu_1 k_{2z}}e^{ik_x x}\mathrm{d}k_x \\ &+ \int_{-k_\mathrm{b}}^{k_\mathrm{b}} U(k_x)\left(\frac{4\mu_2 k_{1z}e^{ik_{2z}z}}{\mu_2 k_{1z} + \mu_1 k_{2z}} - \frac{2\mu_2 k_{1z}e^{-ik_{2z}z}}{\mu_2 k_{1z} - \mu_1 k_{2z}}\right)e^{ik_x x}\mathrm{d}k_x \\ &+ \int_{\text{vertical detours}} U(k_x)\frac{2\mu_2 k_{1z}e^{ik_{2z}z}}{\mu_2 k_{1z} + \mu_1 k_{2z}}e^{ik_x x}\mathrm{d}k_x. \end{aligned} \tag{38}$$

where the transmission coefficients (30b) has been included. It is crucial to remember that the integrand in (38) must be analytic as $\operatorname{Im}\omega$ is reduced from γ to 0. To maintain analyticity the denominators in the transmission coefficients must not equal zero in the upper half-plane, which is an additional requirement to choosing the correct sign for k_z. This must be kept in mind when searching for possibly simultaneous refracting media.

The second integrals in Equation (37) and (38) show that both signs for k_z are present for the plane wave components k_x along the zigzag path in Figure 11c. If the branch points are sufficiently close to the real axis the integrals around the vertical detours may become negligible. For a sufficiently large source width ($\sigma \to \infty$) only the plane wave component K_x is present. For large times, when only the frequency component ω_1 is present, the electric field in the current source situation is given by

$$E(x,z,t) = -\frac{\mu(\omega_1)\omega_1}{2K_z}(2e^{iK_z z} + e^{-iK_z z})e^{iK_x x - i\omega_1 t}, \tag{39}$$

[4]Since branch cuts separate the three horizontal parts of the zigzag-pattern, and a square root has opposite sign on each side of a branch cut.

[5]Provided the inverse Laplace transform path can be deformed down to the real ω-axis, so there are no absolute instabilities present, meaning the fields do not grow in time at a fixed point in space.

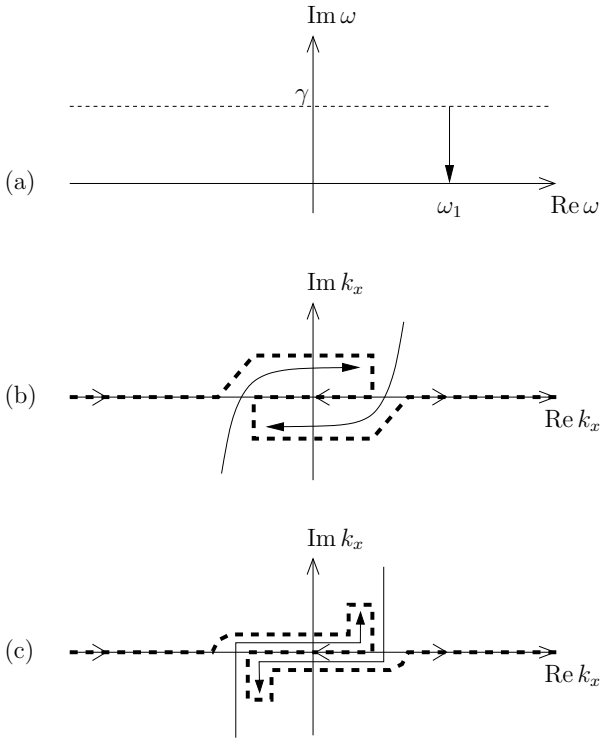

Figure 11: As $\mathrm{Im}\,\omega$ is reduced from γ to zero (a), k_z's branch points, $k_x = \pm\sqrt{\epsilon\mu}\omega/c$, move along the trajectories (b). By deforming branch cuts and integration paths, we get situation (c). In (b) the branch cuts are taken to be along the trajectories, while in (c) they are deformed into the solid lines.

where $K_z = \sqrt{\epsilon(\omega_1)\mu(\omega_1)\omega_1^2/c^2 - K_x^2}$. The expression for the Fresnel case is similar, but the fraction $-\mu\omega/2K_z$ is replaced with the Fresnel transmission coefficient, which is different for the two terms due to the sign change for K_{2z}.

If we instead took the limit $\sigma \to \infty$ before deforming the inverse Laplace transform, only the plane wave component K_x would be present. For the special case $K_x = 0$ we can still deform the inverse Laplace transform down to the real ω-axis, provided $\sqrt{\epsilon(\omega)\mu(\omega)}$ is analytic and zero-free for $\mathrm{Im}\,\omega > 0$. For large times, when only the frequency component ω_1 is present the field is given by

$$E(x,z,t) = -\frac{\mu(\omega_1)\omega_1}{2K_z} e^{iK_z z - i\omega_1 t}, \tag{40}$$

where $K_z = \sqrt{\epsilon(\omega_1)\mu(\omega_1)}\omega_1/c$. Only the positive sign for K_z is present, so if the plane wave limit $\sigma \to \infty$ (for $K_x = 0$) is taken before the monochromatic limit, simultaneous refraction does not occur. By comparing (40) to (39) in the special case $K_x = 0$ we observe that the resulting electric field depends on the order we took the monochromatic and plane wave limit. A discussion on the fact that these two limits do not commute in general is given in Section 7. From this it is understood that simultaneous refraction is a two-dimensional effect. In the case of a finite σ there will always be oblique waves with $k_x \neq 0$ excited, no matter how large σ is. After a sufficiently long time t these oblique waves will somehow establish waves along the z-direction with both signs for K_z. However, if $\sigma \to \infty$ is taken first, there will be no oblique waves excited. The simultaneous refracting waves can thus not be established. This latter situation is one-dimensional, as the excitation $u(x)$ is constant for all x, and $K_x = 0$.

A medium where $\epsilon(\omega) = \mu(\omega) = 1 + \chi(\omega)$, and $\chi(\omega)$ is a strong inverted Lorentz can be used to obtain simultaneous refraction. We will here use the parameters $F = -0.5$, $\omega_0 = 1$ and $\Gamma = 0.05$. The permittivity function $\epsilon(\omega)$ $(= \mu(\omega))$ for this medium is shown in Figure 12a. At the observation frequency $\omega_1 = 0.853$ the branch point trajectories as $\mathrm{Im}\,\omega$ is reduced from $\gamma = 5$ to 0 are shown in Figure 12b. Note that the gain at resonance is very large for this medium. As will be described in Sections 6 11 media with such a large gain are not suited for FDTD simulations or physical realization. Note that the

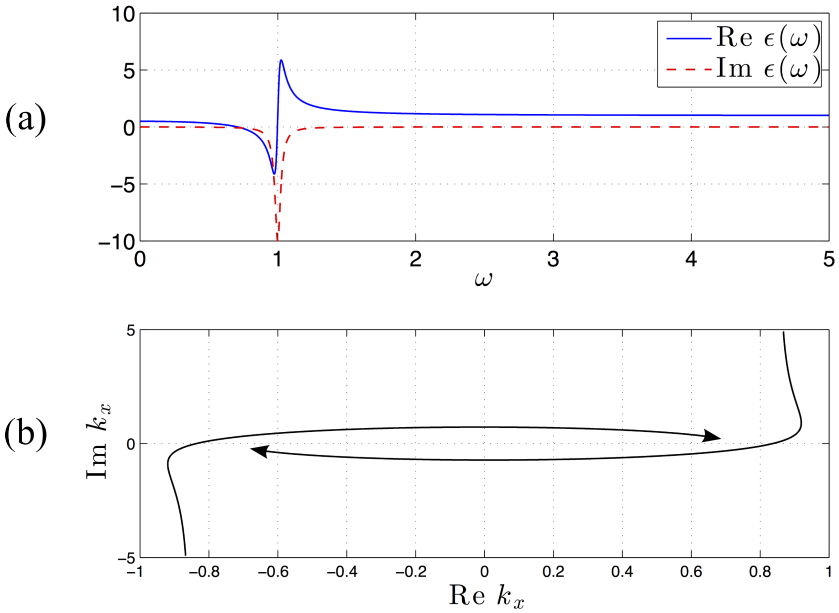

Figure 12: (a) $\epsilon(\omega) = \mu(\omega) = 1 + \chi(\omega)$, where $\chi(\omega)$ is given by the Lorentz model (11) with parameters $F = -0.5, \omega_0 = 1, \Gamma = 0.05$. (b) The branch point trajectories as $\mathrm{Im}\,\omega$ is reduced from $\gamma = 5$ to 0, at the observation frequency $\omega_1 = 0.853$. In all simulations and plots in this thesis the units are normalized, as will be explained in Section 10.

units in Figure 12 are normalized. This will be the case for all simulations and plots in this thesis, as will be explained in Section 10.

6 Transient behavior in gain media

The analysis of wave propagation in linear, passive media is usually done by considering a single real frequency (the monochromatic limit) and also often a single plane wave component (plane wave limit), separately. The monochromatic limit is approached by turning the source on at $t = 0$, and waiting a sufficiently long time, until all the transients die out ($t \to \infty$). The plane wave limit can be approximated by letting the width of the source being infinitely large ($\sigma \to \infty$). Physically these limits can thus never be reached, and for finite duration and source widths all frequencies and all plane wave components will be excited to some extent.

For passive media all transients decay as they propagate into the medium, and the necessary time for the transients to die out is usually relatively short. For gain media, however, the transients may grow as they propagate. We will here consider the situation where the maximum gain for a medium is found at another (real) frequency ω_g, than the observation frequency ω_1. If the gainy frequencies propagate in the $+z$-direction, this frequency will grow faster than the observation frequency as it propagates, and will thus dominate for large z. If we want to investigate a medium's optical response at the observation frequency ω_1 we should be certain the response we observe actually comes from this specific frequency. It will be shown in Section 6.1, that provided the inverse Laplace transform can be moved down to the real axis, all frequencies $\omega \neq \omega_1$ are expected to die out for large times.

It is simple to take the limit $t \to \infty$ in theory. However, as will become apparent, the required duration of an experiment before the transients have died out may be very large for media with large gain. When running time domain simulations it may be of interest to know when to expect the monochromatic limit to be reached at a given z. If the predicted duration is very long, one may want to adjust some parameters, to avoid having to simulate over such long durations. As the transients may grow with z, the larger z is, the longer duration is required for the transients to die out. At $z = 0$ the transients haven't traveled any distance, and have therefore not picked up any gain. The monochromatic limit is therefore reached after a short duration τ. As we increase z the required τ will increase, and how τ will increase with z is given by the difference in gain at ω_g and ω_1.

In section 6.2 we present a criterion for determining when the monochromatic limit is reached at a given z. The presented criterion is found to predict unnecessary long durations τ, and it is argued why this is the case. Another method, based on calculating the time domain solution through the inverse Laplace transform is presented in Section 6.3. If the time domain field at a given z is known, we can use time-frequency analysis to determine after which duration τ the observation frequency becomes dominant at this z.

For the excitation in time given by (32b) a lot of high frequencies are required to describe the abrupt onset at $t = 0$. If the source instead is smoothly turned on, the excitation of other frequencies than ω_1 will be reduced, and the monochromatic limit can thus be reached faster. A discussion on approaching the monochromatic limit in this way is presented in Section 6.5.

6.1 Understanding transient behavior using the residue theorem

The behavior in the monochromatic limit may be found by rewriting (36) into

$$E(x,z,t) = \frac{1}{2\pi}\int_{-\infty}^{\infty} \frac{E(x,z,\omega)}{V(\omega)} V(\omega)\exp\left(-i\omega t\right)\mathrm{d}\omega, \tag{41}$$

where $\frac{E(x,z,\omega)}{V(\omega)}$ is the transfer function from the excitation $V(\omega)$ to the resulting field $E(x,z,\omega)$. Note that $V(\omega)$ is a factor in $E(x,z,\omega)$, so the transfer function is independent of $V(\omega)$. With $V(\omega)$ given by (33b), the inverse transform (41) may be calculated using the residue theorem, by closing the contour by a large semi-circle in the lower half plane. This gives

$$E(x,z,t) = [\frac{E(x,z,\omega)}{V(\omega)}\exp\left(-i\omega t\right)]_{\omega=\omega_1} + \text{transients}(t). \tag{42}$$

The term transients(t) comes from the integration around all singularities and cuts in the lower half plane. Due to the negative imaginary part of the frequencies, the transients will decrease exponentially with time. For media where the inverse Laplace transform can be deformed down to the real ω-axis, the monochromatic limit thus exists for any finite (x,z):

$$E_{\omega_1}(x,z,t) = \frac{E(x,z,\omega_1)}{V(\omega_1)} \exp(-i\omega_1 t). \tag{43}$$

In theory it is very simple to take the monochromatic limit $t \to \infty$. However, in a time domain simulation (or an actual physical experiment) one would have to wait throughout the transient phase before the monochromatic response at the observation frequency may be observed. As mentioned above, the required duration τ before the monochromatic limit is reached may be very long for certain gain media. This is explained from (41) by noting that the transfer function may be very large for some of the transient frequencies, i.e. the frequencies around ω_{g}. In the current source situation the transfer function is found from (29) to be

$$\frac{E(x,z,\omega)}{V(\omega)} = \int_{\kappa(\omega)} -\frac{\mu\omega}{2k_z} U(k_x) e^{ik_x x + ik_z z} \mathrm{d}k_x. \tag{44}$$

Since $k_x \in \kappa(\omega)$ and $k_z(k_x,\omega)$ may be complex numbers, the exponential factor $e^{ik_x x + ik_z z}$ may be large for large (x,z). By rewriting $U(k_x)$ (Equation (33a)) in terms of the real and imaginary part of k_x we get

$$U(k_x) = \sigma\sqrt{2\pi} \exp[\frac{(k_{\mathrm{i}}^2 - (k_{\mathrm{r}} - K_x)^2)\sigma^2}{2}] \exp(-i(k_{\mathrm{r}} - K_x)k_{\mathrm{i}}\sigma^2), \tag{45}$$

where k_{r} and k_{i} are the real and imaginary parts of k_x, respectively. If $|k_{\mathrm{i}}| > |k_{\mathrm{r}} - K_x|$ for some $k_x \in \kappa(\omega)$, $U(k_x)$ will grow with σ, and may thus become very large. The k_x with large imaginary part will correspond to exponentially growing side waves. For media with strong gain, a large source width may thus strongly excite these exponentially growing side waves. The strongest excited k_x will be those close to the branch points $k_z = 0$, and the k_z in the denominator will increase the value of the integrand in (44) even more. Since the gain is strongest close to ω_{g}, these are the frequencies where the transfer function may be largest. This shows that the transfer function may be large for certain ω, even in the lower half plane. The transients (given by integrals around singularities and cuts) may thus be dominant for long durations τ, even though they decrease exponentially with time. It is also worth noting that if $|\mathrm{Im}\,\omega|$ for the singularities is very small, these transients will decay very slowly with time.

To determine for how long time the frequencies close to ω_{g} will dominate, one would have to know all the singularities and cuts for $\frac{E(x,z,\omega)}{V(\omega)}$ in the lower half plane of complex frequencies. Such singularities and cuts are present if e.g. $\kappa(\omega)$ is discontinuous with ω. It is hard to evaluate the integrals around those singularities in the general situation, and different methods for finding the necessary duration τ it takes to reach the monochromatic limit is therefore suggested in the following sections.

6.2 An excitation of finite duration

In the previous section the time dependency of the excitation was assumed to be given by (32b), i.e. a single frequency oscillation turned on at $t = 0$, which is never turned off. We will here instead consider the situation where the source is turned off after a duration τ, i.e.

$$v(t) = [H(t) - H(t-\tau)] \exp(-i\omega_1 t) \tag{46a}$$

$$V(\omega) = \frac{i}{\omega - \omega_1}[1 - e^{i(\omega-\omega_1)\tau}] = \tau \mathrm{sinc}[\frac{(\omega-\omega_1)\tau}{2}] e^{i\frac{(\omega-\omega_1)\tau}{2}}. \tag{46b}$$

For $t < \tau$ the physical response will be exactly the same in these two situations, as the system does not know that the source will be turned off some time in the future (causality). If we let $\tau > t_{\max}$, where $t_{\max}$ is the largest observation time, there is thus no difference between (32b) and (46a). But, it turns out that Equation (46b) gives us an advantage mathematically: Since $\mathrm{sinc}(x)$ is analytic at $x = 0$, there is no singularity at $\omega = \omega_1$, and the inverse Laplace transform may thus be calculated as an integral along the real ω-axis, without making use of the residue theorem. We have thus overcome one challenge from the previous section, regarding the integration around singularities and cuts in the lower half plane.

Equation (46b) also tells us how $V(\omega)$ changes with the duration of our experiment τ. We note that $V(\omega_1) = \tau$, so the observation frequency will be more and more excited as τ is increased (the source is kept turned on longer). This makes sense, as the source produces a signal with carrier frequency ω_1. For all other frequencies the magnitude $|V(\omega)|$ will be independent of τ. As τ is increased, $\mathrm{sinc}[\frac{(\omega-\omega_1)\tau}{2}]$ (and

$e^{i\frac{(\omega-\omega_1)\tau}{2}}$) will oscillate faster with ω. From this it becomes apparent that for $\tau \to \infty$ the source will be drowned down with a monochromatic signal at the observation frequency; all the other frequencies will cancel each other out in the inverse Laplace transform integral (29) due to the fast oscillations in $V(\omega)$. This means eventually only the observation frequency is present, i.e. the monochromatic limit is reached. For a finite point (x, z) the monochromatic limit is thus reached by letting the source stay on for a sufficiently long time $\tau \to \infty$, the same result as obtained in the previous section.

Parseval's theorem relates the energy of a signal $x(t)$ evaluated at all times t to the energy of the signal in terms of its Fourier transform $X(\omega)$,

$$\int_{-\infty}^{\infty} |x(t)|^2 \mathrm{d}t = \frac{1}{2\pi} \int_{-\infty}^{\infty} |X(\omega)|^2 \mathrm{d}\omega. \tag{47}$$

A criterion to determine when the monochromatic limit is reached is now suggested: The monochromatic limit is reached when a significant fraction f of the energy of the signal comes from a small bandwidth around the observation frequency ω_1. We can thus find how large τ must be to make

$$\frac{\int_\Delta |E(x, z, \omega)|^2 \mathrm{d}\omega}{\int_{-\infty}^{\infty} |E(x, z, \omega)|^2 \mathrm{d}\omega} > f, \tag{48}$$

where f is some fraction between 0 and 1. Δ is a bandwidth around ω_1, which should be chosen such that $\epsilon(\omega)\mu(\omega)$ is approximately the same as $\epsilon(\omega_1)\mu(\omega_1)$ for all $\omega \in \Delta$. We note that the monochromatic limit is not fully reached before $f \to 1$ for an infinitely small bandwidth Δ, which will only be the case for $\tau \to \infty$. We will in the following use a weak gain medium to see how Δ and f should be chosen, for (48) to be a suitable criterion for the monochromatic limit.

As an example, we now consider a medium where the permittivity and permeability are described by inverted Lorentzian functions,

$$\epsilon(\omega) = \mu(\omega) = 1 - \frac{F\omega_0^2}{\omega_0^2 - \omega^2 - i\Gamma\omega}, \tag{49}$$

where $F > 0$ is the strength of the active resonance, ω_0 is the resonance frequency and Γ is the bandwidth of the resonance. In this example the one-dimensional case ($K_x = 0, \sigma \to \infty$) is considered, and the parameters $F = 0.01$, $\omega_0 = 1$ and $\Gamma = 0.1$ are used. This gives a maximum gain at the resonance frequency $\operatorname{Im} n(\omega_0) = -0.1$. The real and imaginary part of $\epsilon(\omega)$ for these parameters are shown in Figure 13. The requirement $k_z \to +\omega/c$ as $\omega \to \infty$ gives that $k_z(\omega) = +\epsilon(\omega)\omega/c$. The imaginary part of k_z will thus be negative at all positive frequencies, $\operatorname{Im} k_z(\omega) < 0$ for all $\omega > 0$.

Figures 14 show the resulting field from simulations of the medium described by (49) after two different durations. The simulation results were achieved using the implemented FDTD program, which is described in Section 9. The observation frequency is taken to be $\omega_1 = 2$, where $k_z(\omega_1) \approx \omega_1/c$. In the monochromatic limit the medium should thus respond approximately as if it was vacuum, i.e. the field should not grow significantly with z. Since the source is abruptly turned on at $t = 0$ the signal will in the beginning contain all frequencies, not only ω_1. The frequencies around ω_0 will be amplified, so for large z these frequencies should dominate. As can be seen from Figures 14 this is also what happens in the simulations.

At resonance we have $\operatorname{Re} k_z(\omega_0) = \operatorname{Re} \epsilon(\omega_0)\omega_0/c = \omega_0/c = 1$ (normalized units, so $c = 1$). For the observation frequency we also have $\operatorname{Re} \epsilon(\omega_1) \approx 1$, so we get $\operatorname{Re} k_z(\omega_1) = \omega_1/c = 2$. The wavelength corresponding to a given frequency for a wave propagating inside a medium is given by $2\pi/|\operatorname{Re} k_z|$. The wavelength should therefore be $\lambda = 2\pi$ at resonance, and $\lambda \approx \pi$ at the observation frequency.

Figure 14a shows the fields after the duration $\tau = 314$. For $z < 50$, the wavelength is in fact 3.14, and the wave propagates with approximately no loss/gain. For $z > 50$ the field grows rapidly with z, and the wavelength is $\approx 2\pi$. It is reasonable to interpret this as that after the duration $\tau = 314$ the monochromatic limit $E_{\omega_1}(z, t)$ is reached for $z < 50$, while the transients corresponding to $\omega \approx \omega_0$ still dominate for $z > 50$. For $\tau = 314$ the ratio (48) is in fact approximately 1 for $z \ll 50$ and 0 for $z \gg 50$. The value for z where the ratio is 0.5 is $z = 51$. The method thus seems to produce reasonable results, and the value $f = 0.5$ marks the transition in z for where the monochromatic limit is reached and not.

In these calculations the bandwidth $\Delta = [1.95, 2.05]$ was chosen, i.e. the frequencies within a distance ± 0.05 from the observation frequency $\omega_1 = 2$. The size of this bandwidth does however not play an important role, as long as it does not include frequencies with a significant amount of gain, i.e. ω close to

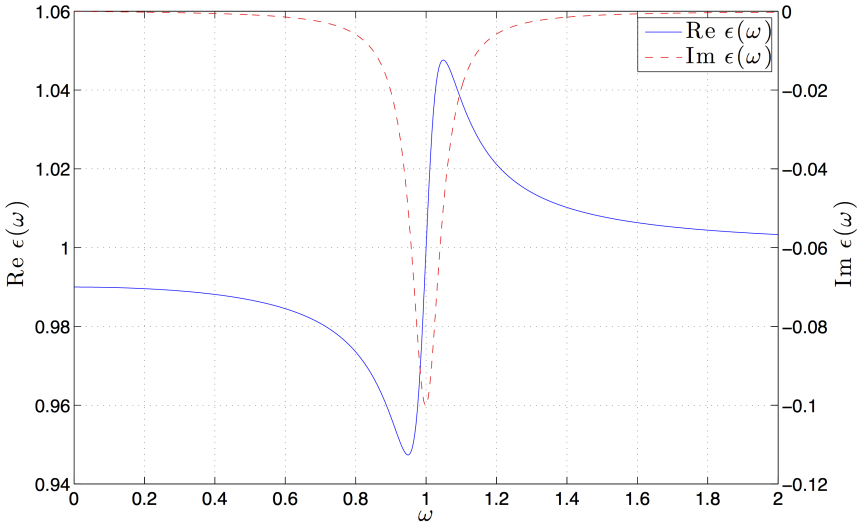

Figure 13: The real and imaginary part of $\epsilon(\omega)$ given by (49), with the parameters $F = 0.01$, $\omega_0 = 1$ and $\Gamma = 0.1$. Note that the scale on the y-axis for the real and imaginary part is different.

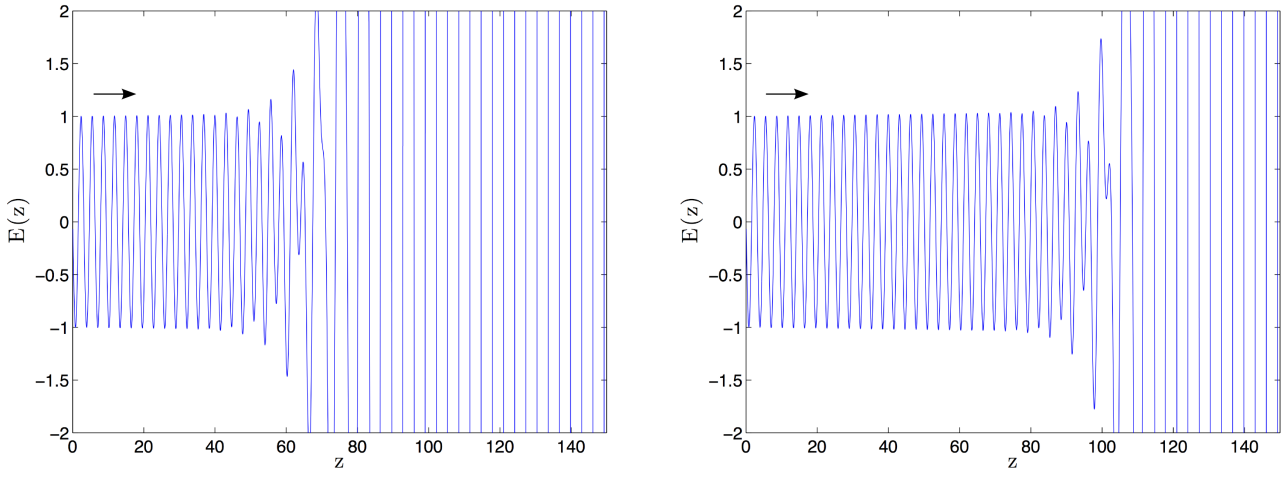

(a) (b)

Figure 14: The resulting electric field from time domain simulations of a medium where $\epsilon(\omega) = \mu(\omega)$ is given by Figure 13 after two different durations (a)$t = 314$ and (b)$t = 628$. The observation frequency $\omega_1 = 2$ was used. In (a) it is seen that the transients corresponding to frequencies close to the resonance frequency ω_0 grow rapidly with z, and dominate for $z > 50$. In (b) the transients have been convected a little further away, and now dominate for $z > 80$. The monochromatic limit was thus reached for z between 50 and 80 after a duration between $t = 314$ and 628.

$\omega_1 = 1$. This is because there are two possible frequency bands which may make significant contributions to the energy of the signal: A narrow band Δ_1 around the observation frequency ω_1 (due to the strong excitation of these frequencies), and a narrow band Δ_0 around the resonance frequency ω_0 (due to the large gain at these frequencies). The major energy contribution will for small and large z come from the bandwidths Δ_1 and Δ_0, respectively. As long as Δ_1 is included in Δ, while Δ_0 is not, the size of the bandwidth Δ is therefore not very important.

At $\tau = 628$ (Figure 14b) this "boundary" between where the monochromatic limit is reached and not has moved to $z \approx 80$. This shows that the transients in fact do die out with time, as predicted. The method based on (48) does however give that the value for z where the fraction (48) is 0.5 is $z = 55$, and thus suggests that the transients die out much more slowly than what they actually do in the time domain simulations. An explanation for why this is the case is now presented.

The suggested criterion for predicting whether the monochromatic limit is reached or not is based on Parseval's identity (47), which claims that the energy of the signal from all times is equal to the energy from all frequencies. In the example (Figures 14) z between 50 and 80 will for the times $t < 314$ be dominated by the resonance frequency, while for $t > 628$ the observation frequency will be dominant. The fields were however a lot larger in magnitude for the early times, due to the large gain at resonance. The integral of $|E(z,t)|^2$ will thus be weighted significantly more at earlier times (more energy due to large fields). We will therefore need the observation frequency to be dominant over a very long time before the total energy-contribution from this frequency can match the energy from the large fields at early times.

The criterion (48) does therefore not work exactly as intended. The criterion can be used to find durations τ where the monochromatic limit is reached, but the monochromatic limit will be reached locally in time way earlier than this predicted τ. The process which lead to this result did however make us realize this important fact: it is really whether the monochromatic limit is reached locally in time we are interested in. This suggest that the time domain solution should be found, which is the foundation for the method presented in the next section.

6.3 The time domain solution for a given z

As described in the previous section, comparing the energy-contribution from different frequencies at all times $0 < t < \tau$ is not a good way of predicting when the monochromatic limit is reached at a point z. What we are interested in is really whether at a given point z, after a duration τ, if the observation frequency dominant during a following short period T or not. The time domain solution at a given point (x, z) can be calculated directly, through the inverse Laplace transform (29). This will be done in the 1d case in this section. Complications with performing the same analysis in 2d are presented in 6.4. When the time domain solution is found, we can use time-frequency analysis to determine after which duration τ the monochromatic limit was reached in the medium considered.

If $k_z(\omega)$ is analytic in the upper half plane, the time domain field for $t < \tau$ is given by the inverse Fourier transform with respect to ω,

$$E(z,t) = \frac{1}{2\pi}\int_{-\infty}^{\infty} E(z,\omega)\exp(-i\omega t)\mathrm{d}\omega = \frac{1}{2\pi}\int_{-\infty}^{\infty}\frac{1}{2}\tau\mathrm{sinc}[\frac{(\omega-\omega_1)\tau}{2}]\exp(i\frac{(\omega-\omega_1)\tau}{2})\exp(ik_z(\omega)z - i\omega t)\mathrm{d}\omega. \tag{50}$$

The excitation (46a) is chosen so that the inverse transform then can be calculated along the real ω-axis.

We assume $\epsilon(\omega) = \mu(\omega) = 1 + \chi(\omega)$ where $\chi(\omega)$ is given by the Lorentz model (11). This gives

$$k_z(\omega) = \sqrt{\epsilon(\omega)\mu(\omega)}\frac{\omega}{c} = [1+\chi(\omega)]\frac{\omega}{c} = n(\omega)\frac{\omega}{c}, \tag{51}$$

where the positive sign of the square root is chosen to get $k_z(\omega) \to \omega/c$ as $\omega \to \infty$. For the medium to be active we must have a negative Lorentz strength, $F < 0$. Provided $|F| < 1$, k_z is then analytic for $\mathrm{Im}\,\omega > 0$.

The susceptibility $\chi(\omega)$ has two poles in the lower half plane, so the integrand in (50) has two essential singularities there. We can therefore not calculate the integral using the residue theorem. It is neither straightforward to evaluate the integral analytically along the real ω-axis. To calculate the time domain response of a Lorentzian medium was the topic for Brillouin and Sommerfeld's classical analysis [12]. They were only able to solve this problem within certain regimes, corresponding to first precursors etc. We should therefore rather calculate the inverse transform numerically.

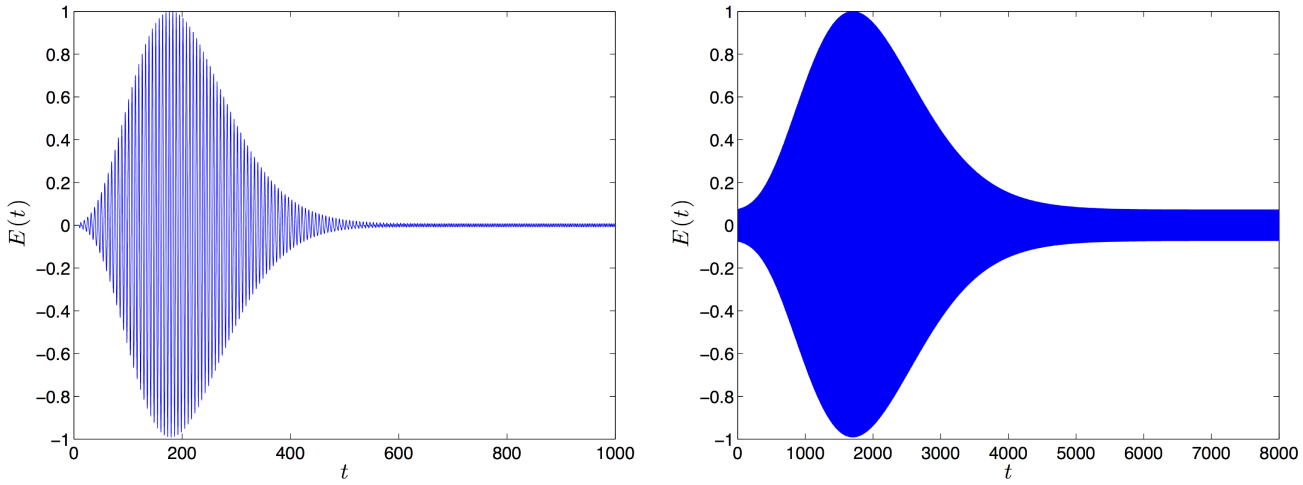

(a) (b)

Figure 15: The time domain solution of the electric field in two different media, at $z = 10$. The field was calculated through the inverse Fourier transform (50), using MATLAB's built in FFT-function. For both plots $\epsilon(\omega) = \mu(\omega)$ are given by inverted Lorentzian functions, with the parameters (a) $F = 0.1$, $\omega_0 = 1$, $\Gamma = 0.1$ and (b) $F = 0.01$, $\omega_0 = 1$, $\Gamma = 0.01$. The observation frequency $\omega_1 = 2$ was used in both calculations. In both media the field first grow large, due to large gain at some of the transient frequencies. Eventually these frequencies are convected away, and the monochromatic limit is reached. The electric field has in both figures been normalized to the maximum value of the field throughout the experiment duration. Note that the time axis has a different scale in the two figures.

The inverse Fourier transform (50) can be calculated using MATLAB's built in FFT-function. Figures 15 show the obtained time domain field at $z = 10$ for two symmetric Lorentz media with parameters $F = -0.1, \omega_0 = 1, \Gamma = 0.1$ and $F = -0.01$, $\omega_0 = 1$, $\Gamma = 0.01$. Both these media have a maximum gain $\operatorname{Im}\epsilon(\omega) = -1$ at resonance, but the bandwidth with gain is larger for the first medium. The observation frequency $\omega_1 = 2$ was used in both simulations.

It is not possible to see from the figures, but $E(t < 10) = 0$, as it takes time time $t = z/c$ for the field to travel from the source to our observation point $z = 10$. The amplitude of the field then grows for a while, until it reaches its maximum value, before it decays, and eventually stabilizes at a given value. The large field for early times is due to the large gain at some of the transient frequencies. Eventually these frequencies are convected away, and the monochromatic limit is reached. It is seen from the figures that this happens after the durations $t \approx 600$ and $t \approx 6000$ for the two media, respectively. For two media with the same maximum gain, a reduction of the bandwidth with gain with the factor 10 thus increase the time before the transients die out with the same factor 10.

That a reduction of Γ leads to an increased duration of the transient period can be understood by again interpreting the transients as integrals around the singularities and cuts in the lower half-plane of complex frequencies. The transients will then decay exponentially in time, with the exponential decay rate given by $\operatorname{Im}\omega$ for these singularities and cuts. The imaginary part of the zeros and poles of (49) is $-\Gamma/2$, so a reduction of Γ should indeed lead to a linear increased duration of the transient period.

The electric field has in both figures been normalized to the maximum value of the field throughout the experiment duration. For both media the gain at the observation frequency is negligible, so the amplitude at $z = 10$ will be approximately the same as at the source, which is 1. From this it is seen in the figures that the maximum field is larger in the medium with the largest bandwidth with gain. This also makes sense, as a larger fraction of the transient frequencies will be amplified in this medium.

We conclude this section by noting that for media with a large gain at other frequencies than the observation frequency, it may take a very long time before the transients for which the gain is large die out. Calculating the time domain response at a given point z through the inverse Fourier transform, can give us an indication of how long time it takes before the monochromatic limit is reached in such media.

6.4 Choosing τ and σ in the simulations

It was argued in Section 6.1 that if $|\mathrm{Im}\, k_x| > |\mathrm{Re}\, k_x - K_x|$ along the integration path, the transfer function (44) may become large for large σ. This is due to a strong excitation of growing side waves in the $\pm x$-directions. To be able to approximate the plane wave limit by letting the source width being very large we should thus have $|\mathrm{Im}\, k_x| < |\mathrm{Re}\, k_x - K_x|$ for all $k_x \in \kappa(\omega_1)$ at our observation frequency. It may however be that $|\mathrm{Im}\, k_x| > |\mathrm{Re}\, k_x - K_x|$ for $k_x \in \kappa(\omega)$ at other frequencies than ω_1. A large source width will thus make the transfer function at these frequencies very large. In time domain simulations, or actual physical experiments, should therefore not chose σ too large, as this will lead to a long necessary simulation time τ before the observation frequency becomes dominant. For K_x to be the dominant plane wave component at our observation frequency ω_1, σ should however not be chosen too small either.

For a given σ, the inverse Laplace-Fourier transform (41) may be calculated, to determine how long duration τ is required for the monochromatic limit to be reached. For each ω, the integration path $\kappa(\omega)$ must then be determined, as it is required for calculating the transfer function (44). Further, for each pair (k_x, ω) the longitudinal wave number k_z must be determined such that it is continuous with k_x and ω. Due to the complex $k_x \in \kappa(\omega)$ the inverse Fourier transform (44) will be a sum of possibly very large values, and a very small discretization Δk_x would thus be necessary. Performing the inverse Laplace-Fourier transform (41) numerically will thus require an extensive amount of computational power, and this will therefore not be done here.

To determine when the monochromatic limit will be reached in a 2d simulation we rather suggest to calculate the inverse Laplace transform in 1d (as was done in the Section 6.3), and keep in mind that in 2d the necessary duration may be even longer, due to possible strongly excited growing side waves. As mentioned above, the excitation of growing side waves can be limited by choosing a relatively small σ. We suggest that σ is chosen in the order of magnitude of $1/|\mathrm{Re}\, k_{x,\mathrm{bp}}|$, where $k_{x,\mathrm{bp}}$ is the branch point at the observation frequency, $k_{x,\mathrm{bp}} = \sqrt{\epsilon(\omega_1)\mu(\omega_1)}\omega_1/c$. Reducing the excitation of growing side waves through choosing a small σ does however come at a cost: At the observation frequency, a bundle of plane wave components k_x around K_x will then be excited to some extent, so the plane-wave characteristic of the wave is somehow destroyed.

6.5 Smoothening the onset of the source

The excitation of frequencies away from the observation frequency ω_1 can be reduced by turning on the source smoothly. The excitation (32b) is sharply turned on at $t = 0$, and a wide range of frequencies other than ω_1 are required to describe this abrupt change. The smoothest possible onset would be a gaussian wrapping of the monochromatic signal, i.e.

$$v_{\mathrm{g}}(t) = H(t) \exp\left(-(t - t_{\mathrm{d}})^2/(2w_{\mathrm{t}}^2)\right) e^{-i\omega_1 t}, \tag{52}$$

where t_{d} is the duration before the gaussian reaches its maximum value, and w_{t} is the width of the gaussian pulse. By letting $t_{\mathrm{d}} > w_{\mathrm{t}}$ and $w_{\mathrm{t}} \to \infty$ the excitation (52) would only contain the observation frequency ω_1. In a simulation finite values for t_{d} and w_{t} must be used, but even for quite small values the excitation of unwanted frequencies is drastically reduced.

For $t > t_{\mathrm{d}}$ the gaussian excitation is smoothly turned off again. This becomes a problem for finite durations and widths, as the source may be turned off before the monochromatic response of the medium becomes visible. If instead the integral of a gaussian is used, the source is smoothly turned on, but then kept at its maximum magnitude for $t \to \infty$. The integral of a gaussian is the error function, so the excitation

$$v_{\mathrm{e}}(t) = \frac{1}{2}(H(t) - H(t - \tau))(1 + \mathrm{erf}[\frac{(t - t_{\mathrm{d}})}{\sqrt{2}w_{\mathrm{t}}}])e^{-i\omega_1 t} \tag{53}$$

gives a smooth onset, and is kept on when it reach its maximum amplitude. The source is turned off after the time τ, to include the duration of the experiment in the Laplace transform (as was done in (46a)). The Laplace transform of (53) is given by

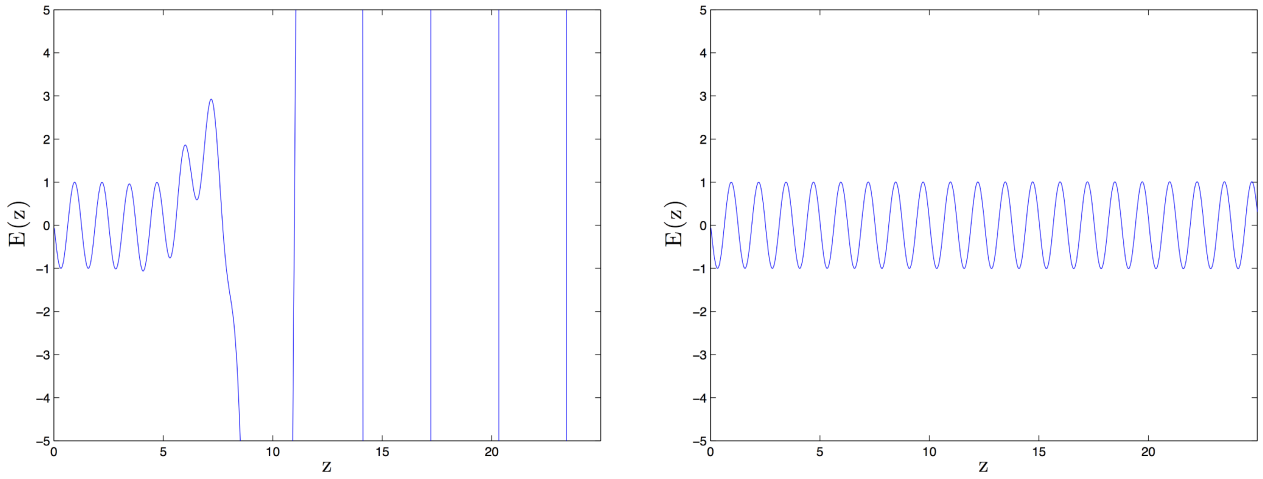

(a) (b)

Figure 16: Comparing simulation results for the two time excitations (32b) (Figure a) and (53) (Figure b). The investigated medium has $\epsilon(\omega) = \mu(\omega)$ both given as an inverted Lorentzian, with the parameters $F = \Gamma = 0.1$, $\omega_0 = 1$ and the observation frequency $\omega_1 = 5$. The Figures are captured after the same duration $\tau = 62.8$.

$$V_{\rm e}(\omega) = \frac{1}{2}\frac{i}{\omega-\omega_1}\times\{e^{i(\omega-\omega_1)t_{\rm d}-\frac{1}{2}(\omega-\omega_1)^2w_{\rm t}^2}{\rm erf}[\frac{t-t_{\rm d}}{\sqrt{2}w_{\rm t}}-i\frac{w_{\rm t}}{\sqrt{2}}(\omega-\omega_1)] - ({\rm erf}[\frac{t-t_{\rm d}}{\sqrt{2}w_{\rm t}}]+1)e^{i(\omega-\omega_1)t}\}_{t=0}^{t=\tau}. \tag{54}$$

Simulation results from an active resonance medium with $F = \Gamma = 0.1$, $\omega_0 = 1$ and $\omega_1 = 5$ are shown in Figure 16, where the excitations (32b) and (53) are compared. It is seen that the abrupt turned on oscillation contains a lot more of the resonance frequency, and is thus dominated by the large gain (Figure 16a). When the source is turned on smoothly (Figure 16b), only the observation frequency ω_1 is present after the same duration. When running the simulation a longer time, the resonance frequency becomes visible even for this excitation. This shows that turning the source on smoothly may decrease the excitation of other frequencies. To completely remove unwanted frequency content a very long onset-time is required, which will increase the necessary simulation time.

7 Physical instabilities

Wave propagation in semi-infinite gain media may involve instabilities. The waves are allowed to travel an infinitely large distance, picking up gain as they propagate, and may thus result in infinite fields. Diverging fields due to an infinite travelled distance $z \to \infty$ (and/or $x \to \pm\infty$), and which does not grow with time for a fixed point in space are called *convective instabilities* - the diverging fields are convected away. In certain cases the fields may also grow with time, even at a fixed point in space. Such instabilities are referred to as *absolute instabilities*.

In this section it is argued that due to instabilities associated with certain frequency-wavenumber components $E(k_x, z, \omega)$ it may not be possible to interpret the electromagnetic response of gain media in the single plane wave and monochromatic limit, as it usually is done for passive media. By examining the monochromatic and plane wave limits ($E_{\omega_1}(x, z, t)$ and $\lim_{\sigma\to\infty} E(x, z, t)$) we find that the order the limits are taken does not in general commute. Whether the fields goes to ∞ or not may also depend on which excitation $\lim_{\sigma\to\infty} u(x)$ is used to approach the plane wave limit (see attached paper, appendix A for details). The plane wave limit $\sigma \to \infty$ can in some cases cause instabilities to occur, as side waves corresponding to $k_z = 0$ will propagate the infinite distance from $\sigma = \pm\infty$ picking up gain, and thus leading to diverging fields. In other cases the limit $\sigma \to \infty$ can prevent instabilities from occurring, by limiting the excitation of the k_x's associated with the instabilities.

Section 7.3 and 7.4 describes media with $\epsilon(\omega)\mu(\omega)$ with single and double zeros for $\operatorname{Im}\omega > 0$, respectively. FDTD simulations of such media are presented in Section 12.5.

7.1 Analytic and zero-free $\sqrt{\epsilon\mu}$, plane wave limit ($\sigma \to \infty$)

We first consider the situation where $\sqrt{\epsilon(\omega)\mu(\omega)}$ is analytic in the upper half plane $\operatorname{Im}\omega > 0$. If the plane wave limit ($K_x \neq 0, \sigma \to \infty$) is taken first, in certain cases the monochromatic limit cannot be reached. In the plane wave limit only the plane wave component K_x is present. The electric field is in the current source situation then given by the inverse Laplace transform

$$E(x, z, t) = \frac{1}{2\pi} \int_{i\gamma-\infty}^{i\gamma+\infty} -\frac{\mu\omega}{2k_z} e^{iK_x x + ik_z z - i\omega t)} \mathrm{d}\omega. \tag{55}$$

If $k_z(\omega, K_x) = \sqrt{\epsilon(\omega)\mu(\omega) - K_x^2}$ has branch points for $\operatorname{Im}\omega > 0$ the inverse Laplace transform cannot be deformed all the way down to the real ω-axis, but must make detours around the branch cuts, as was shown in Figure 10a. The time domain signal will thus contain frequency components with $\operatorname{Im}\omega > 0$, meaning the fields will increase exponentially with time. This will be the case even for conventional weak gain media. Physically it is understood as follows. Since the source is turned on at $t = 0$, all ω will be excited to some extent. For some ω in the upper half plane we will have $k_z = 0$. As the plane wave limit is taken first, the side waves corresponding to $k_z = 0$ are allowed to travel an infinite distance (from $x = \pm\infty$), picking up gain as they propagate. Since the plane wave limit $\sigma \to \infty$ was taken first, no matter how large we chose t there will always arrive side waves which has propagated longer, and thus grown even larger than the side waves which arrived at any previous times. The fields will therefore grow with time, even for a fixed point (x, z), so we have an absolute instability. Due to this instability the monochromatic limit $E_{\omega_1}(x, z, t)$ can never be reached.

For the special case $K_x = 0$ we can move the ω-integration path all the way down to the real axis, since $k_z = \sqrt{\epsilon(\omega)\mu(\omega)}$ is analytic for $\operatorname{Im}\omega > 0$. The fields can thus be interpreted at real frequencies, and will not grow with time. This is because there will be no side waves excited when $\sigma \to \infty$. If we wait a sufficiently long time we will reach the monochromatic limit, and the fields are given by a single plane wave $K_x = 0$ and frequency ω_1. As described in Section 6 the time before the monochromatic limit is reached may however be very large if the gain of the medium is large at other frequencies than the observation frequency ω_1.

7.2 Analytic and zero-free $\sqrt{\epsilon\mu}$, monochromatic limit ($t \to \infty$)

Provided $\sqrt{\epsilon(\omega)\mu(\omega)}$ is analytic and zero-free for $\operatorname{Im}\omega > 0$ we can deform the integration path down to the real ω-axis. As was shown in Section 5 the inverse Fourier transform then might have to be taken

along a deformed integration path $\kappa(\omega)$. The monochromatic limit can then be reached by letting $t \to \infty$. The electric field in the current source situation can in this limit be written as

$$E(x,z,t) = \frac{e^{-i\omega_1 t}}{2\pi} \int_{\kappa(\omega_1)} -\frac{\omega_1 \mu(\omega_1)}{2k_z} U(k_x) e^{ik_x x + ik_z z} \mathrm{d}k_x. \tag{56}$$

For any finite σ, all $k_x \in \kappa(\omega_1)$ will be excited to some extent. If $\kappa(\omega_1)$ contains complex k_x, these components will grow in the $\pm x$-directions. For a conventional weak gain medium $\kappa(\omega)$ will be as shown in Figure 33. The part of the integration path where k_x must be complex is close to the branch points $k_z = 0$.

The k_x with largest $|\mathrm{Im}\, k_x|$ will be excited by far the most if σ gets really large. Note that these k_x's will correspond to $k_z \approx 0$. This means that the larger σ is, the more will the fields be dominated by exponentially growing side waves. If we try to take the plane wave limit for K_x close to the branch points we will thus get infinitely large fields. This is consistent with what was found in the previous section: If we wait an infinitely long time the growing side waves will have travelled an infinite distance, picking up gain, and make the fields grow infinitely large.

However, in this case, where the monochromatic limit was taken first, also the special case $K_x = 0$ will lead to infinitely large fields, provided $|\mathrm{Im}\, k_x| > |\mathrm{Re}\, k_x|$ at the branch points. For any finite σ all other k_x than $K_x = 0$ will be excited to some extent, also the side waves corresponding to $k_z = 0$. The excitation of other plane wave components will be related to the fact that the source has a finite width. It will take the time $t = \sigma/c$ for the side wave to propagate from $x = \pm\sigma$ to $x = 0$. At $x = 0$ the fields will therefore be the same for a finite σ as for $\sigma \to \infty$ for times less than σ/c. In the previous section we let $\sigma \to \infty$ first, so no matter how large we choose t the side wave will never reach $x = 0$. We now took the limit $t \to \infty$ first, so no matter how large we chose σ the side wave will always have propagated from the end of the source, even when we let $\sigma \to \infty$. Physically σ will always be finite, but we can choose σ very large, in attempt to approximate the plane wave limit. For any finite σ, the solution found when "taking the plane wave limit first" will thus describe the fields for $t \ll \sigma/c$, while "taking the monochromatic limit first" will describe the solution for $t \gg \sigma/c$.

For K_x where $|\mathrm{Re}\, k_x - K_x| > |\mathrm{Im}\, k_x|$ for all $k_x \in \kappa(\omega_1)$ the plane wave limit $\sigma \to \infty$ can be taken without getting infinitely large fields, even though the side waves still travel an infinite distance, picking up gain. Since the gaussian is such a smooth function, $U(k_x)$ decrease even more rapidly with σ than what the side waves grow, so all complex k_x are effectively removed from the integration path $\kappa(\omega)$. While taking the plane wave limit $\sigma \to \infty$ before the monochromatic limit $t \to \infty$ may lead to infinite fields for any excitation $u(x)$, taking the limits in the opposite order may in fact lead to finite fields provided the excitation is smooth enough (i.e. a gaussian). We have still waited for the side waves to propagate from the end of the source, but they were so weakly excited that they never appeared.

The gaussian excitation (32a) is somewhat unphysical, as it requires an infinite wide source even for finite σ. For any excitation $u(x)$ of finite support we will get $U(k_x) \to \infty$ as $\sigma \to \infty$ if there are any k_x with $|\mathrm{Im}\, k_x| > 0$ along $\kappa(\omega)$, independent of K_x. For example the excitation

$$u_t(x) = \mathrm{tri}[x/\sigma] e^{iK_x x}, \tag{57}$$

where $\mathrm{tri}[x/\sigma]$ is the triangular function, has Fourier transform

$$U_t(k_x) = \sigma \mathrm{sinc}^2[\sigma(k_x - K_x)/2], \tag{58}$$

which will increase with σ if $|\mathrm{Im}\, k_x| > 0$. Even though the gaussian excitation is unphysical, the fact that it makes it possible to take the plane wave limit is very interesting. It tells us that the growing side waves in a gain medium may be limited by making the source sufficiently smooth, and will disappear in the limit of a perfectly smooth source (gaussian).

If the maximum $|\mathrm{Im}\, k_x| \in \kappa(\omega_1)$ is very small, we can choose a large σ, and the side waves will still not be very dominant. The fields are then approximately given by the single plane wave and frequency components K_x and ω_1. As σ is increased the fields will be more and more disturbed by the growing side waves. Note that even though the side waves are not very dominant for the observation frequency ω_1 they could still be strongly excited for other frequencies ω, meaning the gain is larger at these frequencies. It may then take a very long time before the monochromatic limit is reached.

7.3 Non-analytic $\sqrt{\epsilon\mu}$

In Section 5.2 we considered a medium with non-analytic $\sqrt{\epsilon\mu}$, and looked at the possibility of moving the inverse Laplace transform integration path down to the real ω-axis by deforming the k_x-integration paths. It was shown that this is not possible because $\kappa(\omega)$ will not be continuous to the left and right of the branch point frequencies. Here we will instead take the plane wave limit $\sigma \to \infty$ first. It turns out that this apparently unstable medium will for large K_x become stable. It is crucial to remember that it is k_z, and not $\sqrt{\epsilon(\omega)\mu(\omega)}$, which is required to be analytic for $\mathrm{Im}\,\omega > 0$ (Equation (26)) for the field to be interpreted at real frequencies.

For concreteness, we will also here consider the case where the non-analytic points in the upper half plane are two single zeros. This is e.g. achieved by a nonmagnetic medium ($\mu = 1$) where $\epsilon(\omega)$ is given by

$$\epsilon(\omega) = 1 + \chi_{\mathrm{p}}(\omega) + \chi_{\mathrm{a}}(\omega). \tag{59}$$

Here $\chi_{\mathrm{p,a}}(\omega)$ are both given by the Lorentz model (11), where χ_{p} is a passive resonance ($F > 0$) and χ_{a} is an active resonance ($F < 0$). This $\epsilon(\omega)$ will have zeros in the upper half plane provided the active resonance is strong enough.

We will now instead consider the case where the plane wave limit ($K_x = 0$, $\sigma \to \infty$) is taken first. Since $k_z = \sqrt{\epsilon(\omega)\mu(\omega)}$ is non-analytic for $\mathrm{Im}\,\omega > 0$ we cannot deform the integration path down to the real ω-axis. The time domain solution will then contain frequencies growing with time. This is because the inverse Laplace transform contains frequencies in the upper half plane for which $k_z = 0$ even in the case $K_x = 0$. This corresponds to frequencies which do not propagate in any direction. Since these frequencies grow with time, but do not propagate, the field will grow with time even at a fixed point in space, so we have an absolute instability.

However, if we increase K_x the zeros of k_z may move down to the lower half plane $\mathrm{Im}\,\omega < 0$. If this is the case we can safely move the inverse Laplace transform down to the real ω-axis, and the monochromatic limit can be reached by waiting a sufficiently long time. We have thus "removed" the absolute instability by using a sufficiently large incident angle for the incoming wave. This may seem rather peculiar, but actually we should expect it: In the limit $K_x \to \infty$ we know that $k_z \to iK_x$, i.e. the fields should become evanescent there, independent of which medium is considered.

For any finite σ, all k_x will be present, also $k_x = 0$ for which the absolute instability is present. In a physical situation the fields will therefore always increase exponentially with time. This is also why we cannot take the monochromatic limit before the plane wave limit: As argued in the previous section, if we let $t \to \infty$ first, all plane wave components will be present, even though we let $\sigma \to \infty$ afterwards.

If the observation frequency is sufficiently far away from the zero in the upper half plane, the monochromatic limit may be reached over a certain time range, as the excitation of the unstable frequency is limited. Eventually the absolute instability will start to dominate, and the fields will diverge in time.

We conclude this section with noting that media with non-analytic $\sqrt{\epsilon\mu}$ (or with zeros for $\epsilon\mu$ in the upper half plane) will contain absolute instabilities, so possible application of such media may be limited.

7.4 Zeros of even order for $\mathrm{Im}\,\omega > 0$

If $\epsilon(\omega)\mu(\omega)$ has zeros of even order in the upper frequency plane, $\sqrt{\epsilon(\omega)\mu(\omega)}$ is analytic, and one may ask whether the inverse Laplace transform can be deformed down to the real axis. As explained in Section 5.2 this is not the case: Even though $\sqrt{\epsilon(\omega)\mu(\omega)}$ is analytic, the integration path $\kappa(\omega)$ will get "stuck" at $k_x = 0$ for the "even order zero"-frequencies. The time domain solution will thus contain frequency components increasing with time. For concreteness we will here consider the situation where $\epsilon(\omega)\mu(\omega)$ has two double zeros for $\mathrm{Im}\,\omega > 0$. Such a medium could for instance be obtained by letting $\epsilon(\omega) = \mu(\omega)$ be given as (59).

The argument above holds if we try to approach the monochromatic limit first (i.e. is valid for times $t \gg \sigma/c$). If we instead take the plane wave limit ($K_x = 0$, $\sigma \to \infty$) before the ω-integration path is deformed, we may actually deform the path down to the real axis, since $\sqrt{\epsilon(\omega)\mu(\omega)}$ is analytic for $\mathrm{Im}\,\omega > 0$, and only the plane wave component $K_x = 0$ is present. However, it turns out that media with even order zeros for $\mathrm{Im}\,\omega > 0$ must be treated with care. If ϵ and μ are given as suggested above, the electric and magnetic response must be **exactly** the same for the zeros of ϵ and μ to be located the same place. Even a tiny perturbation will split the double zero into two single zeros, and there will be

a branch cut between the two zeros. If this is the case the inverse Laplace transform can still be moved down to the real axis, but we must add integration paths around the branch cuts in the upper half plane. These frequency components will grow with time, so we have an absolute instability. Also this instability will disappear if the plane wave limit for large K_x is taken before the monochromatic limit, meaning for large K_x the response will be stable for $t \ll \sigma/c$.

8 Simultaneous refraction at low gain

As described in Section 5.3 simultaneous refraction will occur for media with $\epsilon(\omega) = \mu(\omega) = 1 + \chi(\omega)$, where $\chi(\omega)$ is an inverted Lorentz function with a strong resonance response. The observation frequency ω_1 must however be a little below the resonance frequency. As discussed in Section 6, due to the large gain at resonance it will then take a long time to reach the monochromatic limit $E_{\omega_1}(x, z, t)$. Large gain leads to large fields, which also make the media difficult to simulate (Section 11). Similar challenges are also expected in experimental realizations, with noise at resonance being strongly amplified. In practice we will eventually reach the gain saturation limit, and the linear field theory does not hold any longer. A large gain might also lead to instabilities, due to imperfections in the medium.

It is therefore of interest to search for simultaneous refracting media with low gain at all real ω, not only at the observation frequency ω_1. This section presents a method which can be used to find such media, based on the discussion on how to obtain a negative refractive index at low loss/gain done by [13].

To obtain simultaneous refraction the branch points of k_z, given by

$$k_x = \pm\sqrt{\epsilon(\omega)\mu(\omega)}\omega/c, \tag{60}$$

must move such that $\kappa(\omega)$ is forced into a zigzag path as $\operatorname{Im}\omega$ is reduced from γ to 0. Two key observations are made. First, the branch points must cross the real k_x-axis. It is argued in the attached paper (appendix A) that for passive media, where $\operatorname{Im} n(\omega) > 0$ for positive ω, the branch points cannot cross the real axis in the upper ω half plane. A requirement for simultaneous refraction to occur is thus that $\operatorname{Im} n(\omega) < 0$ for some positive ω. This again requires $\operatorname{Im}\epsilon(\omega) < 0$ and/or $\operatorname{Im}\mu(\omega) < 0$, i.e. the system must have gain.

Second, the branch point $+\sqrt{\epsilon(\omega)\mu(\omega)}\omega/c$ must move below origin. To achieve this we must have an accumulated negative complex phase for $\sqrt{\epsilon(\omega)\mu(\omega)}$ of at least $-\pi/2$, (or a positive phase more than $3\pi/2$) when $\operatorname{Im}\omega$ reaches 0. To evaluate the phase of $\epsilon(\omega)\mu(\omega)$ it is convenient to write it in complex form, $\epsilon(\omega)\mu(\omega) = |\epsilon(\omega)\mu(\omega)|e^{i\theta_{\epsilon\mu}(\omega)}$. The square root is then given by $+\sqrt{|\epsilon(\omega)\mu(\omega)|}e^{i\theta_{\epsilon\mu}(\omega)}$, where the positive sign is chosen to get $\sqrt{\epsilon(\omega)\mu(\omega)} \to +1$ as $|\omega| \to \infty$. For $\operatorname{Im}\omega = \gamma$ we thus have $\sqrt{\epsilon(\omega)\mu(\omega)} \approx 1$, i.e. $\theta_{\epsilon\mu} \approx 0$, provided γ is chosen large enough. As $\operatorname{Im}\omega$ is reduced, enough phase $\theta_{\epsilon\mu}$ should be accumulated for $+\sqrt{\epsilon(\omega)\mu(\omega)}\omega/c$ to move below origin before $\operatorname{Im}\omega$ reaches 0. By requiring $\epsilon(\omega)\mu(\omega)$ to be a rational function, the phase change can be found from its zero-pole-configuration. How this is done will be explained in Section 8.1.

To minimize the contribution from the integrals along the vertical detours in (37) the branch points should end up close to the real k_x-axis. This corresponds to a phase shift for $\sqrt{\epsilon(\omega)\mu(\omega)}$ of $\approx -\pi, \pm 2\pi, \pm 3\pi...$, or similarly for $\epsilon(\omega)\mu(\omega)$ of $\approx -2\pi, \pm 4\pi, \pm 6\pi...$ at $\operatorname{Im}\omega = 0$. Note that a phase change for $\epsilon(\omega)\mu(\omega)$ of $+2\pi$ does not lead to simultaneous refraction, as the branch point $+\sqrt{\epsilon(\omega)\mu(\omega)}\omega/c$ does not move below origin in that case. This will be the case for passive negative refracting media.

If the accumulated phase for $\epsilon(\omega)\mu(\omega)$ is larger than -2π the resulting zigzag-path will go back and forth multiple times, as shown in Figure 17 for the case $\theta_{\epsilon\mu} = -6\pi$. The second and third integral in (37) must then be scaled accordingly. If such a large phase is obtained, it is expected that the phase -2π could be obtained for a similar medium with less gain. As simultaneous refraction at low gain at all frequencies is what we seek, we therefore restrict the discussion to how to obtain a phase for $\epsilon(\omega)\mu(\omega)$ of -2π.

We note that for $k_x = 0$ we get $k_z = \sqrt{\epsilon(\omega)\mu(\omega)}\omega/c$, i.e. the same expression as the branch points with positive sign. By achieving branch points close to the real axis we thus also minimize the loss/gain for the forward propagating plane wave component $k_x = 0$. This may reduce the time it takes to reach the monochromatic limit drastically.

8.1 $\epsilon(\omega)\mu(\omega)$ as a rational function

For a medium to be simultaneous refracting a sufficient phase change for $\epsilon(\omega)\mu(\omega)$ is required as $\operatorname{Im}\omega$ is reduced from γ to 0. We will now require $\epsilon(\omega)\mu(\omega)$ to be rational, as this makes it fairly simple to understand how the phase of $\epsilon(\omega)\mu(\omega)$ change as ω is moved around in the complex plane: The phase of $\epsilon(\omega)\mu(\omega)$ is simply given by the location of ω relative to the poles and zeros of $\epsilon(\omega)\mu(\omega)$.

Rational functions are capable of describing $\epsilon(\omega)\mu(\omega)$ quite generally, as any function can be approximated by Taylor polynomials over a certain bandwidth. In fact, if $\epsilon(\omega)$ and $\mu(\omega)$ separately obey the

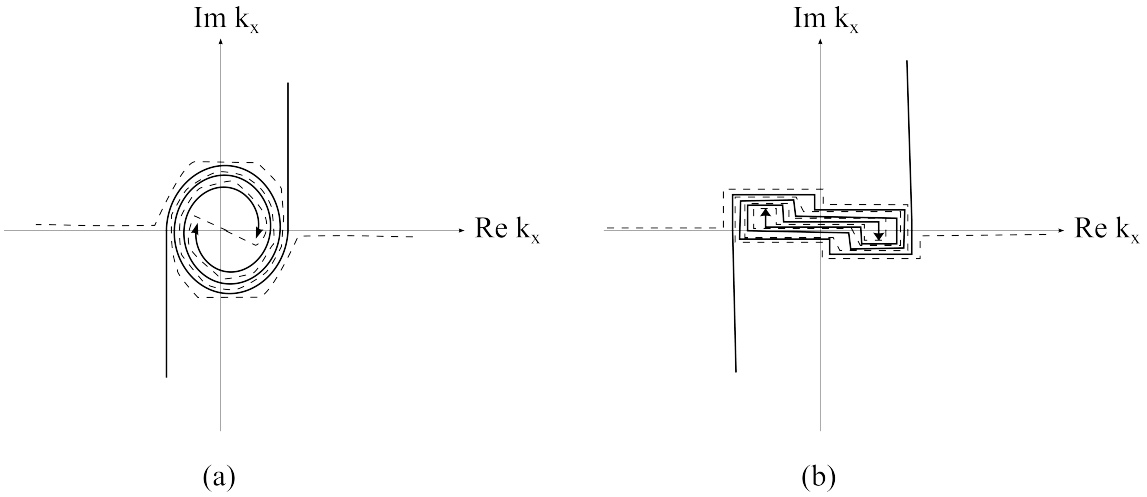

Figure 17: (a) A sketch of the branch point trajectories as $\mathrm{Im}\,\omega$ is reduced from γ to 0, if the phase shift of $\epsilon(\omega)\mu(\omega)$ was $\theta_{\epsilon\mu} = -6\pi$. The branch cuts, and the integration path $\kappa(\omega)$ can be deformed as shown in (b), where all vertical lines above and below $k_x = 0$ can be moved infinitely close to the real axis.

Kramer Kronig relations, $\epsilon(\omega)\mu(\omega)$ will be approximately rational: It has been shown that all functions obeying the KK-relations can be approximated by a sum of Lorentzians [14], which indeed will be rational. For $\epsilon(\omega)$ and $\mu(\omega)$ obeying the KK-relations they will separately be rational, and thus will also $\epsilon(\omega)\mu(\omega)$ be rational. Requiring $\epsilon(\omega)\mu(\omega)$ to be rational is therefore not a very strict constraint.

The requirement $\epsilon(\omega), \mu(\omega) \to 1$ as $|\omega| \to \infty$ gives that the number of zeros and poles must be equal [13]. It is convenient to group these in zero-pole pairs $(\omega_{0i}, \omega_{\mathrm{p}i})$. The symmetry properties of $\epsilon(\omega)$ and $\mu(\omega)$ gives that for every zero/pole $\omega_{0,\mathrm{p}}$ there will be a zero/pole at $-\omega^*_{0,\mathrm{p}}$, i.e. the zero/pole-configuration is symmetric with respect to the imaginary axis in the complex ω-plane. As these frequencies are far away from the observation frequency (which is some real, positive ω), they will contribute very little to the phase change of $\epsilon(\omega)\mu(\omega)$. By ignoring the contribution from these zeros and poles, we are left with the approximation

$$\epsilon(\omega)\mu(\omega) \approx \frac{(\omega - \omega_{\mathrm{z}1})(\omega - \omega_{\mathrm{z}2})...(\omega - \omega_{\mathrm{z}k})}{(\omega - \omega_{\mathrm{p}1})(\omega - \omega_{\mathrm{p}2})...(\omega - \omega_{\mathrm{p}k})}. \tag{61}$$

The complex argument of $\epsilon(\omega)\mu(\omega)$ is thus given by

$$\theta_{\epsilon\mu}(\omega) = \sum_i \arg(\omega - \omega_{\mathrm{z}i}) - \sum_i \arg(\omega - \omega_{\mathrm{p}i}), \tag{62}$$

i.e. a sum of angles in the complex plane given by the position of ω relative to the zeros and poles of $\epsilon(\omega)\mu(\omega)$.

Let us now consider the situation where $\epsilon(\omega) = \mu(\omega) = 1 + \chi(\omega)$, where $\chi(\omega)$ is given by the Lorentz model (11). The zero and pole of this function with $\mathrm{Re}\,\omega > 0$ are found to be $\omega_{\mathrm{z}} = +\sqrt{\omega_0^2 - \Gamma^2/4} - \frac{i\Gamma}{2}$ and $\omega_{\mathrm{p}} = +\sqrt{(1+F)\omega_0^2 - \Gamma^2/4} - \frac{i\Gamma}{2}$, respectively. The zeros and poles of $\epsilon(\omega)\mu(\omega)$ at these ω will be of double order. From (61) one may see that if the zeros and poles are placed far away from each other, the magnitude of $\epsilon(\omega)\mu(\omega)$ will be large for ω close to a pole (dividing a large number by a small number). Recall that F is the strength of the resonance, and increasing $|F|$ will increase the distance between the zero and pole. If $(F+1)\omega_0^2 > \Gamma^2/4$ and $\omega_0^2 > \Gamma^2/4$ the imaginary part of the zeros and poles will both be equal to $-i\Gamma/2$. The magnitude of $\epsilon(\omega)\mu(\omega)$ will thus also be large if Γ is small, as the frequencies around $\mathrm{Re}\,\omega_{\mathrm{p}i}$ will be closer to the pole.

The zeros and poles of $\epsilon(\omega)\mu(\omega)$ (marked as O^2 and X^2 respectively) for $\mathrm{Re}\,\omega > 0$ for a passive and active Lorentz are shown in Figures 18. For the passive Lorentz we have $F > 0$, so the double zero is to the right of the double pole. For the active Lorentz we have $F < 0$, so the double zero is located left of the double pole. The angles θ_{z} and θ_p are the angles the two vectors $(\omega_1 - \omega_{\mathrm{z}})$ and $(\omega_1 - \omega_{\mathrm{p}})$ make with the real axis, respectively. Trigonometry gives that $\theta = \theta_{\mathrm{p}} - \theta_{\mathrm{z}}$ for the active medium, and $\theta = \theta_{\mathrm{z}} - \theta_{\mathrm{p}}$ for the passive medium. The argument of a complex number is the angle it makes with the real axis.

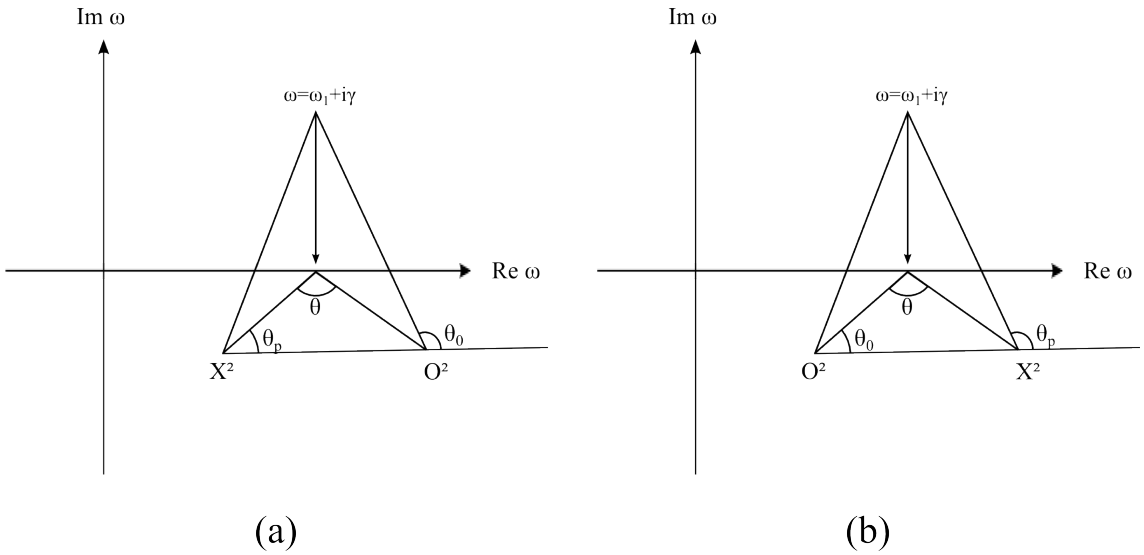

(a) (b)

Figure 18: The zero-pole configuration for $\epsilon(\omega)\mu(\omega)$ for a medium where $\epsilon(\omega) = \mu(\omega)$ is given by (a) a passive Lorentzian function and (b) an active Lorentzian function. Only the zeros and poles for $\mathrm{Re}\,\omega > 0$ are shown.

From (62) we then get $\theta_{\epsilon\mu} = 2\theta = 2(\theta_\mathrm{z} - \theta_\mathrm{p})$ for the passive medium, and $\theta_{\epsilon\mu} = -2\theta = 2(\theta_\mathrm{z} - \theta_\mathrm{p})$ for the active medium, where the factors 2 comes from that the poles and zeros are of double order. The phase of $\epsilon(\omega)\mu(\omega)$ is thus given by the angle which ω_1 makes with the double zero and pole.

What we really were interested in was the phase change for $\epsilon(\omega)\mu(\omega)$ as $\mathrm{Im}\,\omega$ is reduced from γ to 0, as indicated by the downwards arrow in the figures. We do however see that for $\mathrm{Im}\,\omega = \gamma$ the angle $\theta \approx 0$, at least if γ is chosen sufficiently large. We thus get that the angle $\theta_{\epsilon\mu}$ found for $\mathrm{Im}\,\omega = 0$ is the accumulated phase $\theta_{\epsilon\mu}$ we are interested in. The angle θ is positive. Since we want a negative phase $\theta_{\epsilon\mu} = -2\pi$ the active Lorentz can in fact be used to obtain simultaneous refraction, if $\theta \approx \pi$. This is achieved by placing the zero and poles far apart (i.e. a large F), and/or placing them close to the real axis (i.e. a small Γ). Both these approaches will as mentioned above increase the maximum $|\epsilon(\omega)\mu(\omega)|$, which is found for the frequencies close to the poles. If $\epsilon(\omega) = \mu(\omega) = 1 + \chi(\omega)$, i.e. a single Lorentz term should be used to obtain simultaneous refraction with low gain at one frequency the Lorentz term should be active, and have a large maximum gain (given by $|F/\gamma|$).

We should note that there are also zeros and poles symmetrically placed for $\mathrm{Re}\,\omega < 0$, but it was assumed here that the contribution to $\theta_{\epsilon\mu}$ from these zeros/poles are negligible. When this approximation holds can be seen from the geometric consideration we just did. If the distance between the zeros and poles in the half plane $\mathrm{Re}\,\omega < 0$ are a lot smaller than the distance from ω_1 to these zeros/poles, they will make the approximately the same angle with ω_1. Their contributions to $\theta_{\epsilon\mu}$ therefore approximately cancel out.

8.2 Negative $\sqrt{\epsilon(\omega)\mu(\omega)}$ at low gain for real ω

Dirdal and Skaar suggested a method for how to reduce the necessary maximum gain/loss for obtaining negative refraction in [15, 13]. We are searching for a medium with $\mathrm{Re}\,\sqrt{\epsilon(\omega)\mu(\omega)} < 0$, so we can use the medium they came up with, provided the phase change $\theta_{\epsilon\mu}$ is negative. The method works as follows. First place a double zero and pole relatively close to each other, and with a fairly large Γ such that the maximum $|\epsilon(\omega)\mu(\omega)|$ is small. The idea is now that if we place another double zero very close to the double pole, these two will almost cancel each other out in (61). Since the newly added double zero almost cancel out the effect of the double pole, we can either increase the distance between the original double zero and pole, or move all the zeros and poles towards the real axis, and still keep the maximum gain relatively small. The number of zeros and poles must however be the same, so we must place out two more poles. But where to place them? If they are placed far away from the other zeros and poles we will end up with the same problem with a large $|\epsilon(\omega)\mu(\omega)|$ as earlier. We thus place another double

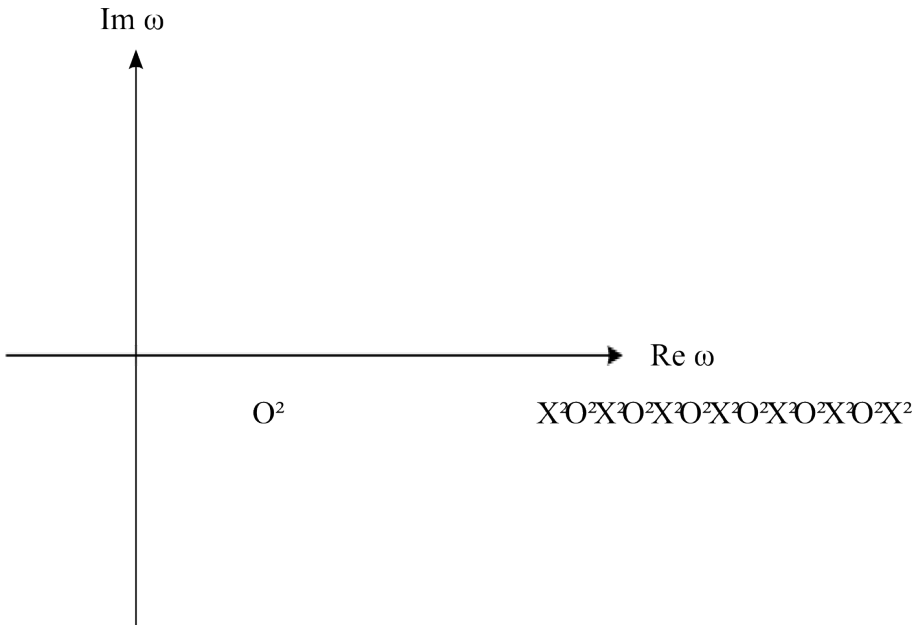

Figure 19: The zero-pole configuration of $\epsilon(\omega)\mu(\omega)$, where a band of zeros and poles have been introduced to reduce the maximum gain of a possible simultaneous refracting medium. The double zeros are marked as O^2 and the double poles as X^2.

zero next to the already existing cluster of zeros and poles. If this procedure is repeated over and over again we end up with a band of zeros and poles, as shown in Figure 19.

We can assign one zero/pole from each double zero/pole to each of the functions $\epsilon(\omega)$ and $\mu(\omega)$, and thus get $\epsilon(\omega) = \mu(\omega)$. The medium just engineered can be written as a sum of Lorentz functions, where the number of zero-pole pairs will equal the number of Lorentz functions. This gives $\epsilon(\omega) = \mu(\omega) = 1 + \sum_{i=1}^{N} \chi_i(\omega)$. Here each $\chi_i(\omega)$ is given by a single zero-pole pair (and their symmetric zero-pole pair at $\mathrm{Re}\,(\omega) < 0$). The resulting $\epsilon(\omega)$ $(= \mu(\omega))$ from such a zero-pole-band medium is shown in Figure 20a. To create this medium 150 Lorentz functions were used. It is seen in Figure 20b that the branch point $k_x = +\sqrt{\epsilon(\omega)\mu(\omega)}\omega/c$ moves below origin at the observation frequency $\omega_1 = 0.97$, so this medium is expected to be simultaneous refracting. The branch points end up close to the real axis, so the integrals around vertical detours in (37) are small. The maximum gain is reduced with a factor 5 compared to the medium described by Figure 12.

The effect of the zeros and poles in the band to some extent cancelled each other out. This lead to a smaller maximum gain, while $\mathrm{Re}\,\sqrt{\epsilon(\omega)\mu(\omega)} < 0$ still is obtained over some frequency range. In [13] this was done using passive resonances (zeros placed to the right of poles), where the band goes towards smaller $\mathrm{Re}\,\omega$. To obtain simultaneous refraction the phase change must be negative, so active resonances were therefore used here, and the band goes towards larger frequencies. The larger the frequency band is (i.e. the more Lorentz functions are used), the more can the maximum gain be reduced. This reduction in gain does however come at a cost: the bandwidth where $\mathrm{Re}\,\sqrt{\epsilon(\omega)\mu(\omega)} < 0$ is reduced.

By examining the resulting function in Figure 20 we see that the zero-pole-band created an asymmetric $\mathrm{Im}\,\epsilon(\omega)$, with a steep variation just above the frequencies with $\mathrm{Re}\,\sqrt{\epsilon(\omega)\mu(\omega)} < 0$, and a softer change for even larger frequencies. The reduction in maximum gain is thus related to this steep variation in $\mathrm{Im}\,\epsilon(\omega)(= \mathrm{Im}\,\mu(\omega))$. This can be understood from the Kramers-Kronig relations, as will be described in Section 12. The more Lorentz functions are used to describe this asymmetric $\mathrm{Im}\,\epsilon$, the more can the maximum gain be reduced. Obtaining $\mathrm{Re}\,\sqrt{\epsilon(\omega)\mu(\omega)} < 0$ at low loss/gain through a such a steep variation in $\mathrm{Im}\,\epsilon$ has also been suggested earlier [15], where it was shown that to get a linear reduction in gain, an exponential increase in steepness is required. This corresponds to an exponential reduction in the bandwidth with $\mathrm{Re}\,\sqrt{\epsilon(\omega)\mu(\omega)} < 0$. It is therefore not convenient to reduce the gain much more than what was done in the medium described Figure 20, as for small bandwidths, long durations for the the monochromatic limit to be reached is required.

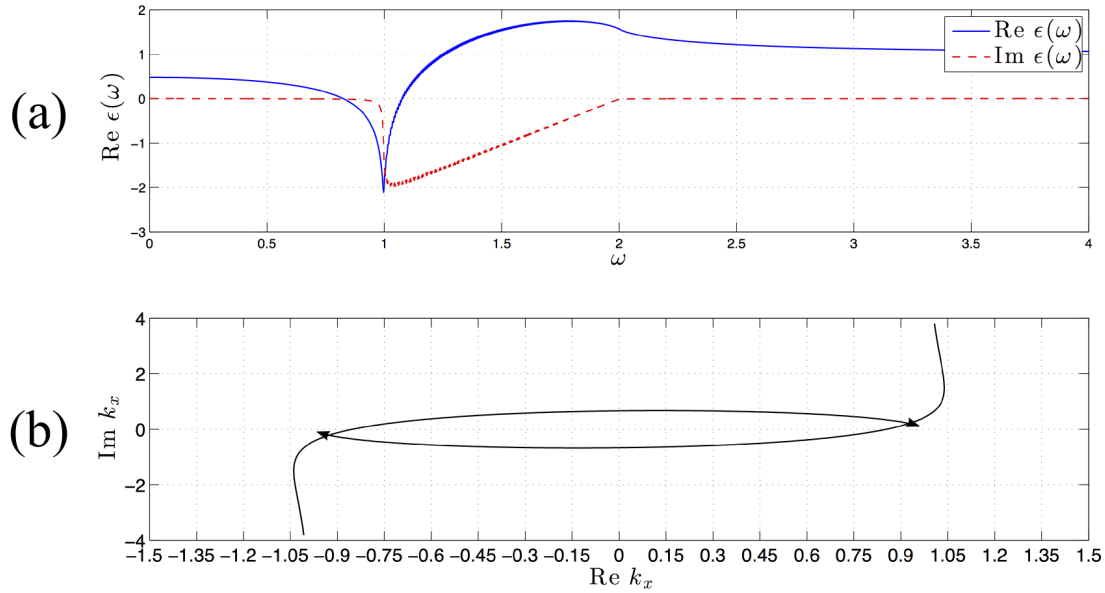

Figure 20: (a) A medium where $\epsilon(\omega) = \mu(\omega)$ are both given as a sum of 150 Lorentzian functions with different resonance frequencies and strengths. The medium is designed to achieve simultaneous refraction with a minimal gain at all frequencies. (b) The branch point trajectories as $\mathrm{Im}\,\omega$ is reduced from $\Gamma = 4$ to 0, at the observation frequency $\omega_1 = 0.97$.

8.3 Monochromatic limit for simultaneous refracting medium with low gain

The medium with $\epsilon(\omega) = \mu(\omega)$ described by Figure 20a is expected to be simultaneous refracting for the observation frequency $\omega_1 = 0.97$. The maximum gain for this medium is $\max|\mathrm{Im}\,\epsilon(\omega)| \approx -2$ at $\omega \approx 1.05$. For all Lorentzian functions used to create the medium, the bandwidth $\Gamma = 0.01$ was used, and we should thus expect the transients to die out approximately as in Figure 15. The time domain solution at $z = 2\pi$, i.e. approximately one wavelength at the observation frequency for this medium, is shown in Figure 21a.

In Figure 21 it looks like the transients die much faster than for the medium in Figure 15. The time domain response is however somewhat bumpy. This effect is believed to be due to interference between the transients from the band of frequencies with gain. As seen in Figure 21b these bumps do not completely die out until $t \approx 5000$, so it actually takes this long time before the monochromatic limit is reached, i.e. approximately the same as for the medium in Figure 15 after all. This analysis was performed in 1d, and as argued in Section 6.4 it is expected to take even longer to reach the monochromatic limit in 2d, due to possible amplified side waves making the transfer function large.

We did not include the smooth source into this analysis. It was shown in Section 6.5 that a smooth onset may in fact reduce the dominance of the gainy frequencies, even for a medium with relatively large maximum gain, $\max|\mathrm{Im}\,\epsilon(\omega)| = -1$. This was however for the case where the observation frequency ($\omega_1 = 5$) was far away from the gainy frequencies ($\omega \approx 1$). For media with large gain, with a observation frequency very close to the gainy frequencies, the onset period must be extremely large to reduce the excitation of the gainy frequencies significantly. It is not possible to simulate for such long times with FDTD due to lack of computational power.

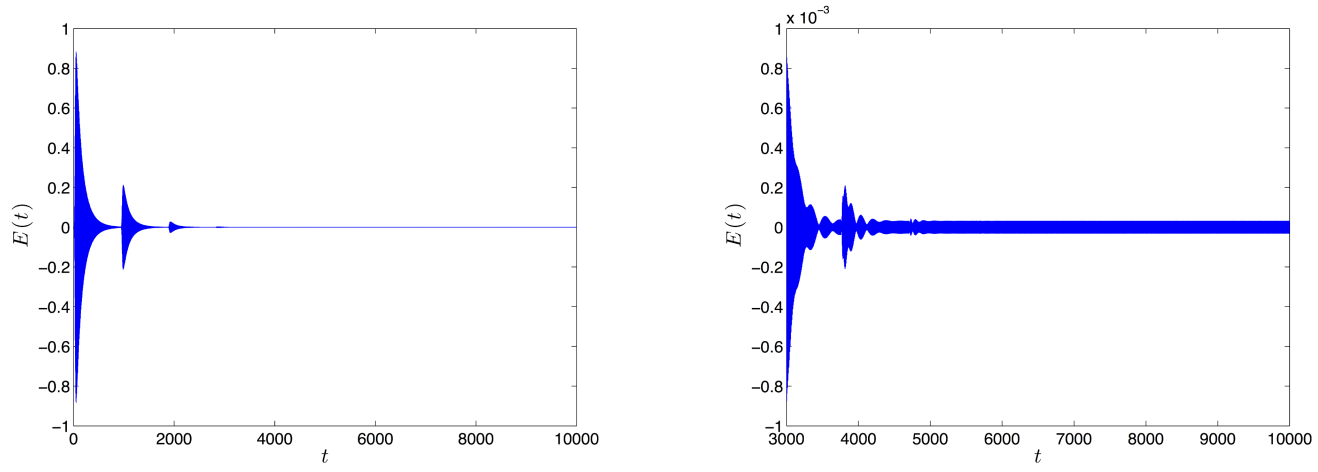

(a) (b)

Figure 21: (a) The time domain solution at $z = 2\pi$ in the medium with $\epsilon(\omega) = \mu(\omega)$ given as in Figure 20. (b) Zoomed in on large t in Figure (a).

9 FDTD

Finding analytic solutions to the time dependent Maxwell's equations is not possible except for in a few special cases. If the derivatives in Maxwell's equations are written out as finite differences it is possible to iteratively find a numerical estimate for the time domain solution. The basic method of solving the standard wave equation through making use of finite differences reaches back to Courant et al in 1928 [16]. Applying this method to solve Maxwell's equations was first suggested by Yee in 1966 [17]. The method is known as the finite difference time domain (FDTD) method, since it is based on expressing derivatives as finite differences, and it aims to estimate the solution in the time domain.

In his "proof of concept" paper Yee only solved Maxwell's equations for a medium with constant ϵ and μ. Dispersive media were treated by Luebbers et al. [18], where the convolution is computed as a discrete sum, and the electric field assumed to be constant in each term of the sum. They also show that if the susceptibility frequency response is described by the Debye model the convolution can be calculated recursively, which leads to a huge improvement on the necessary computational power. In 1992 [19] they showed that the convolution can be calculated recursively also for susceptibilities expressed by a Lorentz function. They further showed that if the susceptibility is a sum of Lorentz functions the same recursive method can be applied to each susceptibility term separately. This idea is very interesting, as Dirdal and Skaar [14] recently showed that every function that obeys the Kramer-Kronig relations can be approximated by a superposition of Lorentzians. Since the convolution can be computed recursively for a Lorentzian, it will in some situations be convenient to approximate the susceptibility function as a superposition of Lorentzians, and then apply the recursive convolution method.

Together with his student Kelley, Luebbers further improved the recursive convolution method by approximating the electric field as a linear function (instead of a constant) for each term in the discrete convolution sum. This improvement leads to higher accuracy compared to other methods (using the same resolution in space and time).

In this section the most important equations used in these methods are derived in detail. Some of the notation will deviate slightly from what is used in the original papers, to make it correspond better to the theory in the previous sections.

9.1 The Standard FDTD Method (Yee)

In the standard Yee FDTD method the derivatives in Maxwell's equations are replaced by finite differences, and the field values approximated at discrete points in time and space: $\mathbf{E}(x,y,z,t) \approx \mathbf{E}(i\Delta x, j\Delta y, k\Delta z, n\Delta t)$ for which Yee uses the notation $\mathbf{E}^n(i,j,k)$. This gives for the curl equations

$$\nabla \times \mathbf{E}^n = -\frac{\mathbf{B}^{n+\frac{1}{2}} - \mathbf{B}^{n-\frac{1}{2}}}{\Delta t} \tag{63a}$$

$$\nabla \times \mathbf{H}^{n-\frac{1}{2}} = \frac{\mathbf{D}^{n+1} - \mathbf{D}^n}{\Delta t} - J \tag{63b}$$

where the position coordinates has been left out for simplicity. Since the magnetic field is needed to calculate the next value of the electric field, and visa versa, the calculation is done in a leap-frog manner. A calculation is done every half time step, where it alternates which of the fields are updated. This is why the notation $\pm 1/2$ is used in the time dependence for $\mathbf{H}$. The magnetic fields are also calculated at a grid shifted $1/2$ in the x and z-directions (for H_z and H_x respectively), as the points used to approximate spatial derivatives are shifted an equal distance in opposite directions away from the point where the derivative is calculated.

In a three dimensional situation Equation (63a) and (63b) give a system of 6 scalar equations. For the 2D system with electric field polarized in the y-direction, as described in Section 3, only three of these equations will be present. Note that the coordinate system here used is shifted from what is used in Yees paper. This is to make it correspond to correspond to the theory in Section 3. Coordinates in the form (i,j) will therefore correspond to $(i\Delta x, j\Delta z)$.

$$\frac{D_y^{n+1} - D_y^n}{\Delta t} = \frac{\Delta H_x}{\Delta z} - \frac{\Delta H_z}{\Delta x} \tag{64a}$$

$$\frac{B_x^{n+\frac{1}{2}} - B_x^{n-\frac{1}{2}}}{\Delta t} = \frac{\Delta E_y}{\Delta z} \tag{64b}$$

$$\frac{B_z^{n+\frac{1}{2}} - B_z^{n-\frac{1}{2}}}{\Delta t} = -\frac{\Delta E_y}{\Delta x} \tag{64c}$$

The current density has been assumed to be zero everywhere, $J^n(i,j) = 0$. Since the current density is related to the electric field through the conductivity ($J(\omega) = \sigma(\omega)E(\omega)$) setting $J = 0$ is equivalent to including the conductivity in the electric susceptibility function.

By assuming that ϵ and μ have constant values, along with $\mathbf{B} = \mu\mathbf{H}$ and $\mathbf{D} = \epsilon\mathbf{E}$, Yee rearranges the Equations (64), and get

$$E_y^{n+1}(i,j) = E_y^n(i,j) + \frac{1}{\epsilon}\frac{\Delta t}{\Delta z}[H_x^{n+\frac{1}{2}}(i+\frac{1}{2},j) - H_x^{n+\frac{1}{2}}(i-\frac{1}{2},j)] \\ - \frac{1}{\epsilon}\frac{\Delta t}{\Delta x}[H_z^{n+\frac{1}{2}}(i,j+\frac{1}{2}) - H_z^{n+\frac{1}{2}}(i,j-\frac{1}{2})] \tag{65a}$$

$$H_x^{n+\frac{1}{2}}(i,j+\frac{1}{2}) = H_x^{n-\frac{1}{2}}(i,j+\frac{1}{2}) + \frac{1}{\mu}\frac{\Delta t}{\Delta z}[E_y^n(i,j+1) - E_y^n(i,j)] \tag{65b}$$

$$H_z^{n+\frac{1}{2}}(i+\frac{1}{2},j) = H_z^{n-\frac{1}{2}}(i+\frac{1}{2},j) - \frac{1}{\mu}\frac{\Delta t}{\Delta x}[E_y^n(i+1,j) - E_y^n(i,j)] \tag{65c}$$

A (perfectly conducting) metallic obstacle is introduced by forcing the electric field to be zero in an area of the simulation domain. Also at the boundaries of the domain the fields are kept at 0 for all times. A propagating wave is produced by setting initial values for both the electric and magnetic field, where some of the initial values are non-zero for $t = 0$. The solution at all later times t can be found through iteration, by using equation (65a)-(65c).

9.2 Convolution as a discrete sum

In [18] Luebbers presents a way for adopting Yees method to dispersive media. The convolution integral (equation (9a)) is expressed as a sum, where the electric field is assumed to be constant at each term of the sum. Using the Yee notation D and E are then related through

$$D^n = \epsilon_0 E^n + \epsilon_0 \sum_{m=0}^{n-1} E^{n-m} \int_{m\Delta t}^{(m+1)\Delta t} \chi(\tau)\mathrm{d}\tau \tag{66}$$

For the next time step the equation becomes

$$D^{n+1} = \epsilon_0 E^{n+1} + \epsilon_0 \sum_{m=0}^{n} E^{n+1-m} \int_{m\Delta t}^{(m+1)\Delta t} \chi(\tau)\mathrm{d}\tau \tag{67}$$

Equation (66) and (67) can be inserted in equation (64a). Some manipulation of the resulting equation yields

$$E_y^{n+1} = \frac{1}{1+\chi^0}\{E_y^n + \psi^n + \frac{\Delta t}{\epsilon_0 \Delta z}[H_x^{n+\frac{1}{2}}(i+\frac{1}{2},j) - H_x^{n+\frac{1}{2}}(i-\frac{1}{2},j)] \\ - \frac{\Delta t}{\epsilon_0 \Delta x}[H_z^{n+\frac{1}{2}}(i,j+\frac{1}{2}) - H_z^{n+\frac{1}{2}}(i,j-\frac{1}{2})]\} \tag{68}$$

where the definitions

$$\chi^m = \int_{m\Delta t}^{(m+1)\Delta t} \chi(\tau)\mathrm{d}\tau, \tag{69}$$

$$\Delta\chi^m = \chi^m - \chi^{m+1} \tag{70}$$

and

$$\psi^n = \sum_{m=0}^{n-1} E_y^{n-m} \Delta\chi^m \tag{71}$$

have been made.

If the susceptibility is independent of frequency one gets $\chi^m = \Delta\chi^m = 0$ for all m, and Equation (68) reduces to Equation (65a) as it should. As pointed out in [18] the Equations for the magnetic response would be identical to (65b) and (65c) for a non-magnetic medium. If the medium has a magnetic response the same procedure as for the electric fields can be followed: approximate the magnetic convolution (Equation (9b)) as a discrete sum, insert this into Equation (64b) and (64c), and manipulate these equations to get

$$H_x^{n+\frac{1}{2}} = \frac{1}{1+\chi_m^0}\{H_x^{n-\frac{1}{2}} + \psi_{\mathrm{m}x}^n + \frac{\Delta t}{\mu_0 \Delta z}[\Delta E_y^n(i,j+1) - E_y^n(i,j)]\} \tag{72a}$$

$$H_z^{n+\frac{1}{2}} = \frac{1}{1+\chi_m^0}\{H_z^{n-\frac{1}{2}} + \psi_{\mathrm{m}z}^n - \frac{\Delta t}{\mu_0 \Delta x}[\Delta E_y^n(i+1,j) - E_y^n(i,j)]\} \tag{72b}$$

where the notation $\chi_{\mathrm{m}x}^m$ and $\chi_{\mathrm{m}z}^m$ etc is used for the magnetic susceptibility terms.

9.3 Recursive convolution for Lorentzian susceptibility functions

The summation term in Equation (68) will have to be calculated for every time step (as the electric field values are "shifted" compared to the χ^m values for every new step). It would therefore save a lot of computation time if one could get rid of this term. Luebbers shows that for media where the susceptibility is described by the Debye [18] or Lorentz [19] model, the calculation of the sum can be done recursively, where the new value is given as an exponential function times the previous value. The derivation for a Lorentzian model will be presented here.

For a Lorentzian medium the susceptibility in the frequency domain is given by

$$\chi(\omega) = \frac{F\omega_0^2}{\omega_0^2 - \omega^2 - i\Gamma\omega} = \frac{F\omega_0^2}{(\omega-\omega_1)(\omega+\omega_1^*)} \tag{73}$$

where $\omega_1 = \sqrt{\omega_0^2 - \frac{\Gamma^2}{4}} - \frac{i\Gamma}{2}$ and ω_1^* its complex conjugate.

The inverse Fourier transform can be calculated using the Residue theorem, where the closed path C is chosen to be the real axis and a semicircle with infinite radius in the lower half plane. The integration can be done along the real axis as the susceptibility has no singularities (as zeros or poles) in the upper half plane. The integral path C in Equation (6) should be a counter clockwise path, while the chosen path goes clockwise. This adds an additional minus sign to the expression, which gives

$$\chi(t) = -\frac{1}{2\pi}\oint_C \frac{F\omega_0^2}{(\omega_1-\omega)(\omega_1^*+\omega)} e^{-i\omega t}\mathrm{d}\omega \tag{74}$$

By applying the residue theorem we get

$$\chi(t) = \frac{iF\omega_0^2}{\omega_1+\omega_1^*}(e^{-i\omega_1 t} - e^{i\omega_1^* t}) = \frac{F\omega_0^2}{2i\Omega_1}(e^{i\Omega_1 t} - e^{-i\Omega_1 t})e^{-\frac{\Gamma}{2}t} = \frac{F\omega_0^2}{\Omega_1} sin(\Omega_1) e^{-\frac{\Gamma}{2}t} \tag{75}$$

where $\Omega_1 = \mathrm{Re}\,\omega_1 = \sqrt{\omega_0^2 - \frac{\Gamma^2}{4}}$ has been introduced. It turns out that it is useful to introduce the complex quantity $\hat{\chi}(t) = \frac{iF\omega_0^2}{\Omega_1} e^{-i\omega_1 t}$. This is because $\hat{\chi}(t+\Delta t) = \hat{\chi}(t)e^{-i\omega_1\Delta t}$ which makes it possible to derive a recursive formula for the convolution. Note that $\mathrm{Re}\,\{\hat{\chi}(t)\} = \chi(t)$.

The convolution integral then becomes

$$\hat{\chi}^m = \int_{m\Delta t}^{(m+1)\Delta t} \hat{\chi}(\tau)\mathrm{d}\tau = \frac{F\omega_0^2}{\omega_1\Omega_1}(1 - e^{-i\omega_1\Delta t})e^{-i\omega_1 m\Delta t} \tag{76}$$

which gives

$$\hat{\chi}^0 = \frac{F\omega_0^2}{\omega_1\Omega_0}(1 - e^{-i\omega_1\Delta t}) \tag{77a}$$

$$\Delta\hat{\chi}^0 = \frac{F\omega_0^2}{\omega_1\Omega_0}(1 - e^{-i\omega_1\Delta t})^2 \tag{77b}$$

A complex version of the summation variable ψ^n is used to represent the sum using the complex susceptibility, $\hat{\psi}^n = \sum_{m=0}^{n-1} E_y^{n-m}\Delta\hat{\chi}^m$. The exponential character of the susceptibility allows for the complex summation variable to be calculated recursively

$$\hat{\psi}^n = \Delta\hat{\chi}^0 E^n + e^{-i\omega_1\Delta t}\hat{\psi}^{n-1} \tag{78}$$

where $\psi^n = \mathrm{Re}\{\hat{\psi}^n\}$. In the first time step $\hat{\psi}^{-1} = 0$ is used (since $E(t < 0) = 0$).

9.4 Piecewise Linear Recursive Convolution (Luebbers & Kelley)

In the previous sections the electric field was assumed to have a constant value between the time steps when calculating the convolution integral. By replacing this constant value with a linear approximation between the two points Kelley and Luebbers claim to increase the accuracy drastically without any increased demand for computational power.

Using this new approximation the convolution integral (Equation (9a)) becomes

$$\begin{aligned} D^n &= \epsilon_0 E^n + \epsilon_0 \int_0^{n\Delta t} E(n\Delta t - \tau)\chi(\tau)d\tau \\ &= \epsilon_0 E^n + \epsilon_0 \sum_{m=0}^{n-1} \int_{m\Delta t}^{(m+1)\Delta t} (E^{n-m} + \frac{E^{n-m-1} - E^{n-m}}{\Delta t}(\tau - m\Delta t))\mathrm{d}\tau \end{aligned} \tag{79}$$

In a more compact form this becomes

$$D^n = E^n + \sum_{m=0}^{n-1}\{E^{n-m}\chi^m + (E^{n-m-1} - E^{n-m})\xi^m\} \tag{80}$$

where χ^m is given as in the previous section, and

$$\xi^m = \frac{1}{\Delta t}\int_{m\Delta t}^{(m+1)\Delta t} (\tau - m\Delta t)\chi(\tau)\mathrm{d}\tau \tag{81}$$

For a Lorentzian medium also ξ^m can be computed recursively, through introducing the complex quantity

$$\hat{\xi}^m = \frac{1}{\Delta t}\int_{m\Delta t}^{(m+1)\Delta t} (\tau - m\Delta t)\hat{\chi}(\tau)\mathrm{d}\tau = -\frac{F\omega_0^2}{\Omega_1\omega_1\Delta t}[\frac{i}{\omega_1}(1 - e^{-i\omega_1\Delta t}) + \Delta t e^{-i\omega_1\Delta t}]e^{-i\omega_1 m\Delta t} \tag{82}$$

where $\xi^m = \mathrm{Re}\{\hat{\xi}^m\}$.

If $D^{n+1} - D^n$ in Equation (64a) is calculated using Equation (80), and manipulating the equation one gets

$$\begin{aligned} E^{n+1} = \frac{1}{1 + \chi^0 - \xi^0}\{(1 - \xi^0)E^n + \frac{\Delta t}{\epsilon_0\Delta z} + \psi^n + \frac{\Delta t}{\epsilon_0\Delta z}[H_x^{n+\frac{1}{2}}(i + \frac{1}{2}, j) - H_x^{n+\frac{1}{2}}(i - \frac{1}{2}, j)] \\ - \frac{\Delta t}{\epsilon_0\Delta x}[H_z^{n+\frac{1}{2}}(i, j + \frac{1}{2}) - H_z^{n+\frac{1}{2}}(i, j - \frac{1}{2})]\} \end{aligned} \tag{83}$$

where $\psi^n = Re\{\hat{\psi}^n\}$ now is given by the modified complex function

$$\hat{\psi}^n = (\Delta\hat{\chi}^0 - \Delta\hat{\xi}^0)E^n + \Delta\hat{\xi}^0 E^{n-1} + e^{-i\omega_1\Delta t}\hat{\psi}^{n-1} \tag{84}$$

and the first step ψ^0 is again calculated using the fact that $\hat{\psi}^{-1} = 0$.

10 Implementation

Kelley and Luebbers PLRC-method for susceptibilities given as a Lorentzian function was implemented in MATLAB, in 1 and 2 dimensions. The 2D version of the script is attached in appendix B. How the boundary conditions were implemented, and the most critical parameters were chosen are explained in this section.

The size of the simulation domain is given by $N_x \mathrm{d}x \times N_z \mathrm{d}z$, where N_x and N_z are the number of grid points in the x and z-direction and $\mathrm{d}x, \mathrm{d}z$ the grid spacings. The simulation runs over a time $N_t \mathrm{d}t$ where N_t is the number of time steps and $\mathrm{d}t$ is the time step.

The electric field is saved at all time steps, to make it possible to evaluate which direction the field propagates. The size of the electric field matrix will therefore be $N_x \times N_z \times N_t$. The magnetic field matrixes are reused every time step. The two previous time steps are needed when calculating the convolution summation variable (84), so a $N_x \times N_z \times 2$ matrix is needed for each of H_x and H_z. If we are only interested in the electric field at the last time step, the matrix size of E can be reduced to only keep the previous time step, as for the magnetic field.

Since the medium is assumed to be semi-infinite the propagating waves must never reach the boundary of the simulation domain. N_x and N_z must therefore scale with N_t, so for the simulation to run over a long time the matrix sizes will be large, and the simulation will take a long time to run due to lack of memory.

In the simulations normalized frequencies are used. For example, for Lorentzian media the resonance frequency ω_0 is taken to be 1. To find the actual physical quantities all frequencies should thus be scaled with ω_0, and other quantities accordingly. For $\omega_0 = 1$ the unit time step $\Delta t = 1/N_{\mathrm{per}}$ is such that $T = 2\pi$, where $T = N_{\mathrm{per}}\Delta t$ is the time duration of one time period at ω_0, and N_{per} is the number of samples used to describe one such period. The speed of light in vacuum is set to $c = 1$, so one time unit corresponds to one spatial unit. To get a desired response at optical frequencies the matamaterials should be designed to have a resonance frequency corresponding to $\lambda = 400 - 700$nm, i.e. in the order of 10^{15}Hz. One time unit would then correspond to a duration in the order of femto seconds, and one spatial unit corresponds to lengths in the order of some hundreds of nano meters.

10.1 The source

For both the situation with a current source in $z = 0$ and the Fresnel boundary situation the source was implemented as a forced oscillation in H_x along the left boundary. This corresponds physically to an oscillating current source in this plane, as described by (28). This current source is assumed to be ideal, so the fields outside the source will not affect the fields at the source plane. In the situation with a current source in $z = 0$ only the right half plane $z > 0$ is simulated; the fields for $z < 0$ will be exactly the same due to the symmetry of the situation.

In the 2D simulation the amplitude of the excitation is modulated by (32a). A perfect gaussian excitation would require $N_x = \infty$, so (32a) was truncated after 3σ as shown in Figure 22. N_x must the be chosen such that the distance from the truncation to the end of the domain is larger than the wave can propagate during the time $N_t \mathrm{d}t$.

The plane-like character of the waves produced by the source will increase with σ. However, there will be a tradeoff between the plane-like character and computational speed, as a larger σ will require a larger N_x. $\sigma = 10$ was used in most of the 2D simulations.

10.2 1d and 2d

As explained in the paper (appendix A) the plane wave and monochromatic limits does not commute in general, i.e. the solution may depend on which limit is taken first. In the simulations the width of σ must be chosen before the simulation is started. For any finite σ in a 2D simulation the plane wave limit is never reached, and the monochromatic limit is approached first, by letting the simulation run over a sufficiently long time.

A simulation in 1D corresponds to a plane wave propagating in the z-direction, and will thus simulate the situation where the plane wave limit $\sigma \to \infty$ with $K_x = 0$ is taken first, and the monochromatic limit is taken afterwards by letting the simulation run over a long time.

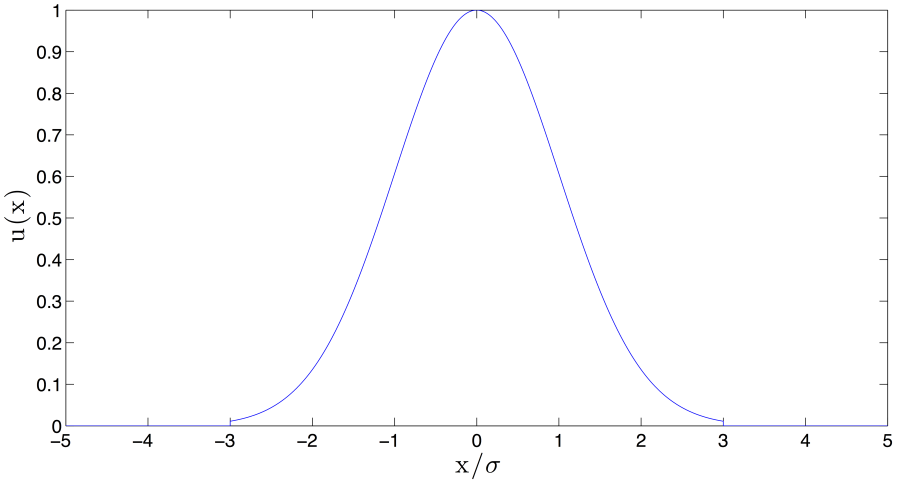

Figure 22: A gaussian excitation profile, truncated after 3σ. The unit along the x-axis is σ.

10.3 Step size

The grid spacings $\mathrm{d}x, \mathrm{d}z$ and the time spacing $\mathrm{d}t$ must be chosen such that enough data points are present to represent the wavelengths in space and oscillation periods in time. The position steps are taken to be equal in both directions, $\mathrm{d}x = \mathrm{d}z$. They must also fulfill the stability criterion given by [20]:

$$v_{\max}\mathrm{d}t \leq (\frac{1}{\mathrm{d}x^2} + \frac{1}{\mathrm{d}z^2})^{-1/2} \tag{85}$$

Here $v_{\max}$ is the maximum phase velocity expected within the model, and is taken to be c. With $\mathrm{d}x = \mathrm{d}z$, the time step can be chosen as $\mathrm{d}t = a \cdot \mathrm{d}x$ with $a = 0.9$ in the 1D program, and $a = 0.7$ in the 2D program. If the simulation gives an unstable solution it may help to reduce a. To minimize the simulation time the largest value which still makes the solution stable should be chosen for a.

11 Artificial reflections

When simulating gain media (using the implemented FDTD program) over a long duration, an unexpected effect appears: a wave propagating backwards can be seen close to the source. The spatial simulation domain is larger than $ct_{\max}$ (where $t_{\max}$ is the maximum simulation time) in all directions, so the backward propagating wave is not a reflection from the boundaries of the grid. The backward wave grows in time, so shortly after the backward wave is seen, it becomes the dominant propagation, and the validity of the FDTD solution is destroyed. It looks like the signal produced by the source is reflected somewhere inside the medium, and that these reflections grow as they propagate towards the source. The reflected wave may pick up gain as it propagates. As the backward wave grows with time, it is reasonable to assume that the reflections occur further and further away from the source. These artificial reflections occur both in 1d and 2d simulations. For simplicity we will consider the one-dimensional situation.

The backward wave was investigated using a single active resonance, where the refractive index is described by (49), using different values for the parameters F, Γ and the observation frequency ω_1. The resonance frequency $\omega_0 = 1$ was used in all simulations. In Figure 23 the electric field is plotted at normalized time $t = 167$ and $t = 219$. The parameters $F = 0.1$, $\Gamma = 0.1$ and $\omega_1 = 5$ were here used.

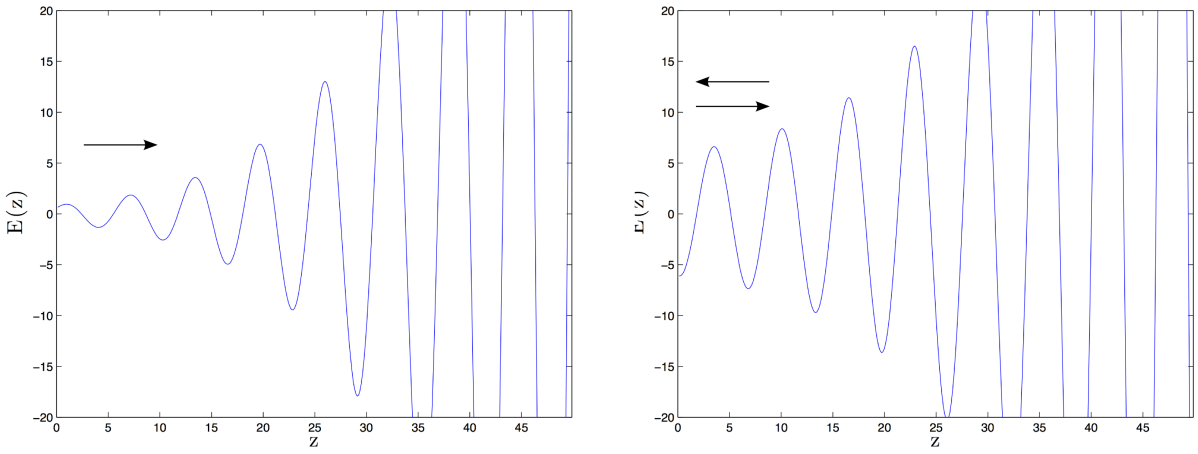

(a) (b)

Figure 23: Simulation results after two different durations, for a medium with $\epsilon(\omega) = \mu(\omega)$ given by an inverted Lorentzian, with the parameters $F = 0.01, \Gamma = 0.1$ and $\omega_0 = 1$, with the resonance frequency as the observation frequency, $\omega_1 = \omega_0$. (a) $t = 750$. The generated signal propagates away from the source, and grows in the z-direction due to the gain. (b) $t = 841$. The validity of the simulation solution is destroyed by an unexpected reflected wave, which propagates towards the source.

Section 11.1 tries to explain the artificial reflections in terms of errors caused by discretization of the electric field in space. The reflections were investigated using different values for F, Γ and ω_1, and it is argued in Section 11.2 that this explanation must be wrong. Section 11.3 suggest a different explanation; that the origin for the reflections are errors in the calculated FDTD solution caused by the numerical resolution of MATLAB.

Due to the occurrence of such artificial reflections, the implemented FDTD program are only able to simulate strong gain media for very short durations τ, before the validity of the solution is destroyed.

11.1 Reflections due to discretization errors

It was first believed that the reflections are caused by errors related to the discretization in space and time. The FDTD solution from the electric field at a given point z will differ from the real the real field $E_{\text{real}}(z)$ with an error $\Delta E(z)$. The initial assumption was that this error will lead to a reflected field $rE_{\text{real}}(z)$ traveling towards the source, where r is the reflection coefficient, which is assumed to be

independent of z. If the entire error signal is reflected we get $E_{\text{FDTD}} = E_{\text{real}}(z) + \Delta E(z) = (1+r)E_{\text{real}}(z)$ [6]. The reflection coefficient is thus given by

$$r = \Delta E(z)/E_{\text{real}}(z). \tag{86}$$

A reflected wave $\Delta E(z) = rE_{\text{real}}(z)$ would then be generated at every point z, and may grow as it propagates towards the source. For the artificial reflections to become visible at z close to 0, they must reach an amplitude in the same order of magnitude as the source signal, which is 1. This will happen for reflections originating from some distance z_0 into the medium. Reflections from $z < z_0$ will be ignored.

Since a linear approximation for $E_{\text{real}}(z)$ is used to calculate the derivatives in Maxwell's equations, the error $\Delta E(z)$ is expected to be of second order, i.e. $\Delta E(z) \approx \frac{\mathrm{d}^2 E_{\text{real}}(z)}{\mathrm{d}z^2}(\Delta z)^2$. It is argued in Section 6 that frequencies around resonance will dominate for large z, due to the large gain. As a rough estimate for the field at large z we will thus use a monochromatic plane wave at resonance,

$$E(z) \approx E_0 \exp\left(ik_z(\omega_0)z - i\omega_0 t\right). \tag{87}$$

E_0 here represents how much the frequencies around resonance are excited by the source, and will be some fraction between 0 and 1 (depending on the observation frequency and the duration of the simulation). The second derivative of (87) with respect to z will be $-k_z^2 E(z)$. If the gain is low ($F \ll 1$) we have $|k_z| = 2\pi/\lambda$, which then gives

$$|\Delta E(z)| \approx (2\pi\Delta z/\lambda)^2 |E(z)|. \tag{88}$$

The reflection coefficient is thus approximated by

$$r \approx (2\pi\Delta z/\lambda)^2. \tag{89}$$

The criterion for when the artificial reflections becomes visible is set to

$$|rE(z)\exp\left(ik_z(\omega_0)z - i\omega_0 t\right)| = rE_0 \exp\left(2|\mathrm{Im}\, k_z(\omega_0)|z\right) > 1, \tag{90}$$

i.e. when the reflections reach an amplitude larger than the source excitation at $z = 0$. This gives the expression for z_0, where the first visible artificial reflections come from:

$$z_0 = \frac{-\ln r - \ln E_0}{|2\mathrm{Im}\, k_z(\omega_0)|}. \tag{91}$$

The time t_{err} before the artificial reflections destroy the validity of the simulation will be the time the frequency components close to ω_0 takes to propagate to z_0, get reflected, and propagate back to $z = 0$, i.e. a total distance $2z_0$. This gives

$$t_{\text{err}} = 2z_0/c = \frac{-2\ln 2\pi/\lambda - 2\ln\Delta z - \ln E_0}{|\mathrm{Im}\, k_z(\omega_0)|}. \tag{92}$$

11.2 Investigation of artificial reflections, using an active resonance

Simulations were run using different values for F, Γ, Δz, Δt and ω_1, and the following observations were made:

- Reflections are dominated by the resonance frequency, no matter which observation frequency is used.
- The time before the artificial reflections appear seems to be independent of Δz and Δt.
- The time before the artificial reflections appear decreases if the maximum gain or the bandwidth with gain is increased.
- The artificial reflections only occur for large fields.

[6] It is reasonable to assume that half of the error signal propagates in each direction, but this factor of 1/2 is left out for simplicity

In the simulation which produced Figure 23 the artificial reflections became visible after $t \approx 800$. At these parameters $\operatorname{Im} k_z(\omega_0) = -0.1$, and $\operatorname{Re} k_z(\omega_0) = 1$, so $\lambda = 2\pi$. The spatial step $\Delta z = 0.1323$ was used. Since the resonance frequency was used as the observation frequency, we will have $E_0 \approx 1$. Estimating the error time using (92) then gives $t_{\text{err}} = -2 \ln 0.1323/0.1 = 40.5$, which is a lot smaller than the observed error time of 800. If the reflections were due to discretization errors we would thus expect them to appear a lot sooner than what they actually do. Discretization errors can therefore not be what causes the occurrence of the unexpected backward wave.

Based on the derivation in the previous section we may then ask why artificial reflections do not occur sooner. If the discretization errors lead to reflections from the FDTD-grid, this could somehow be explained by that the impedance of the medium is slightly different at two adjacent points in the grid. It is shown in [21] that despite the inherent approximations in the FDTD method, the impedance in the grid is exactly the same in the continuous world, i.e. independent on the discretization Δz.

The assumptions that were done in Section 11.1 were all very rough. The expression (92) is however quite consistent with the observations listed above:

- That the reflections are dominated by the resonance frequency ω_0 makes sense, as they are errors being amplified, and the gain is largest at ω_0.
- The dependence on E_0 is logarithmic, so a observation frequency very far from resonance, or a very long duration τ is needed to change E_0 significantly.
- If the bandwidth Γ is increased, E_0 will increase, and thus reduce t_{err}.
- If the maximum gain is increased, $\operatorname{Im} k_z(\omega_0)$ will increase, and thus reduce t_{err}.

An explanation similar to the one given in Section 11.1, but where the "reflection coefficient" is of several orders of magnitude smaller, could thus be reasonable. This is what is presented in the next section.

11.3 Reflections due to numerical precision of MATLAB

As the reflections only occur if the fields grow large, we now suggest that they are caused by the numerical precision of MATLAB.

MATLAB represents floating-point numbers in either double precision or single precision format. The default is double precision, but you can make any number single precision with a simple conversion function. A value stored as a double requires 64 bits, where 52 bits represents all the digits, and the rest are used to store the exponent and sign of the value. In practice this means the number $1 + \delta$ in MATLAB is identically equal to 1 for $\delta \leq 1/2^{53}$. Because of this the calculated electric field values will differ from the "real" FDTD solution with a magnitude $|E(x, z, t)|/2^{53}$. For media with large gain, the electric field values will range over many orders of magnitude. At a given point this small error will be negligible, but the error may spread towards lower z where the field is smaller. An error signal is thus induced. This signal is assumed to be white noise, and will thus contain all frequencies, including frequencies around resonance, which will grow fast as they propagate towards the source. When this error signal reach a magnitude of around 1 at $z = 0$ it becomes visible, and the FDTD solution is thus not reliable any more.

If we assume the entire error induced from the numerical precision errors is reflected at every point z, we can get a similar expression as (92), by inserting the "reflection coefficient" $r = 1/2^{-53}$ in (91):

$$t_{\text{err}} = 2z_0/c = \frac{106 \ln 2 - \ln E_0}{|\operatorname{Im} k_z(\omega_0)|}. \tag{93}$$

If we again assume $E_0 \approx 1$ (since $\omega_1 = \omega_0$) we get $t_{\text{err}} = 735$ for the simulation in Figures 23, which is not very far from the observed error time.

Due to the logarithmic dependence of t_{err} with respect to r, reducing the numbers of bits by a factor should thus lead to t_{err} being reduced with the same factor. When the simulation which lead to Figure 23 was run using "single" precision, the artificial reflections became visible after $t \approx 400$, i.e. about half the time from when "double" precision was used. It is therefore reasonable to believe that numerical precision is what causes the artificial reflections.

We will not go more in depth on the origin of these artificial errors. We rather note that for media with strong gain the implemented FDTD program cannot be trusted over long simulation times, as numerical errors are being amplified and destroys the validity of the solution. These errors are believed to be related to the numerical precision of the calculations done in MATLAB.

12 Simulation results

Negative refractive index is a novel optical property, which can be achieved using metamaterials. The Sections 12.1 to 12.3 will present different types of media which can be used to obtain a negative refractive index, and simulations of them. Section 12.4 briefly introduces the concept of evanescent gain, and simulation results showing the occurrence of evanescent gain in a weak gain medium. In Section 12.5 media with zeros in the upper half plane are simulated, with results showing that the fields do in fact grow with time in such media. This is consistent with what was found in Section 7.3 and 7.4.

To find possible negative refracting media it may be useful to consider the Kramers-Kronig relations. The Kramers-Kronig relations relates the real and imaginary parts of any function that is analytic in the upper half plane. In this Section we will assume that $\epsilon(\omega)$ and $\mu(\omega)$, and thereby also the refractive index $n(\omega)$ obey the Kramers-Kronig relations:

$$\mathrm{Re}\, n(\omega_1) = 1 + \frac{2}{\pi}\mathcal{P}\int_0^\infty \frac{\omega \mathrm{Im}\, n(\omega)}{\omega^2 - \omega_1^2}\mathrm{d}\omega \tag{94a}$$

$$\mathrm{Im}\, n(\omega_1) = -\frac{2\omega_1}{\pi}\mathcal{P}\int_0^\infty \frac{\mathrm{Re}\, n(\omega)}{\omega^2 - \omega_1^2}\mathrm{d}\omega, \tag{94b}$$

where $\mathcal{P}$ means the principle value. We note that the factor $\frac{\omega}{\omega^2-\omega_1^2}$ in (94a) is positive for $\omega > \omega_1$, and negative for $\omega < \omega_1$. To obtain $\mathrm{Re}\, n(\omega_1) < 0$ we must thus have either $\mathrm{Im}\, n(\omega) < 0$ for $\omega > \omega_1$ and/or $\mathrm{Im}\, n(\omega) > 0$ for $\omega < \omega_1$. It is also worth noting that $\mathrm{Im}\, n(\omega)$ at the frequencies close to ω_1 is weighted the most, as the denominator gets small. It is therefore possible to obtain $\mathrm{Re}\, n(\omega_1) < 0$ with $\mathrm{Im}\, n(\omega_1) \approx 0$ at an observation frequency ω_1, if there is a steep drop in $\mathrm{Im}\, n(\omega)$ just above or below this frequency.

The active medium described in Section 12.3 is expected to be simultaneous refracting. Even though the maximum gain has been reduced through the steep variation in $\mathrm{Im}\, n(\omega)$, the gain is still too large for the medium to be suited for being simulated using the implemented FDTD program. The fields grow rapidly with z, and the validity of the solution is after a short duration destroyed by artificial reflections. FDTD simulations were therefore not able to reveal the effect of simultaneous refraction.

12.1 Passive negative refracting medium

If $\epsilon(\omega)$=$\mu(\omega)$, also the refractive index $n(\omega) = \sqrt{\epsilon(\omega)\mu(\omega)}$ must be given by the same function. The positive sign of the square root must be chosen to get $n(\omega) \to \omega/c$ as $\omega \to \infty$. According to the argument given above we may obtain a refractive index using a medium with a large positive $\mathrm{Im}\, n(\omega)$ below the observation frequency. We may for instance use a passive Lorentzian medium

$$\epsilon(\omega) = \mu(\omega) = n(\omega) = 1 + \frac{F\omega_0^2}{\omega_0^2 - \omega^2 - i\Gamma\omega}, \tag{95}$$

provided that the strength of the resonance F is large enough. The imaginary part of a Lorentzian decays faster in magnitude than the real part, as ω is increased. By choosing F very large it is thus possible to obtain $\mathrm{Re}\, n(\omega) \approx -1$ and $\mathrm{Im}\, n(\omega) \approx 0$ at a given frequency ω_1. In the following simulations the parameters $F = 100$, $\omega_0 = 1$ and $\Gamma = 0.1$ were used. The real and imaginary parts of this refractive index ($n(\omega) = \epsilon(\omega) = \mu(\omega)$) are shown in Figure 24. The observation frequency $\omega_1 = 7.14$ gives $n(\omega_1) = -1 + 0.03i$. In the 1d simulation the situation with a current source at $z = 0$ was used, as shown in Figure 25. It is clearly seen that the wave propagates towards the source, which is due to the negative $\mathrm{Re}\, n(\omega)$. For large z the Brillouin and Sommerfeld precursors can be seen. Figure 26 shows a 2d simulation of the Fresnel case, where the negative index medium is located to the right, and vacuum is to the left. The source is located all the way to the left, marked with a bold line. The wave is traveling towards the boundary, and is refracted at a negative angle. This is consistent with what was stated in Section 3.3 for a medium with $\epsilon = \mu = -1$. The energy is absorbed by the medium, as $\mathrm{Im}\, k_z > 0$, and the Poynting vector $\mathbf{S}$ for the transmitted wave is directed away from the boundary. This is as we would expect from a passive medium.

The 1d simulation was performed for the situation where the negative refracting medium fills the entire space, and a current source is located in the plane $z = 0$. This was done to demonstrate that backward waves are generated even when there are no other medium present, so backward waves are not produced by interaction with a boundary. The field was only simulated for $z > 0$, due to the symmetry

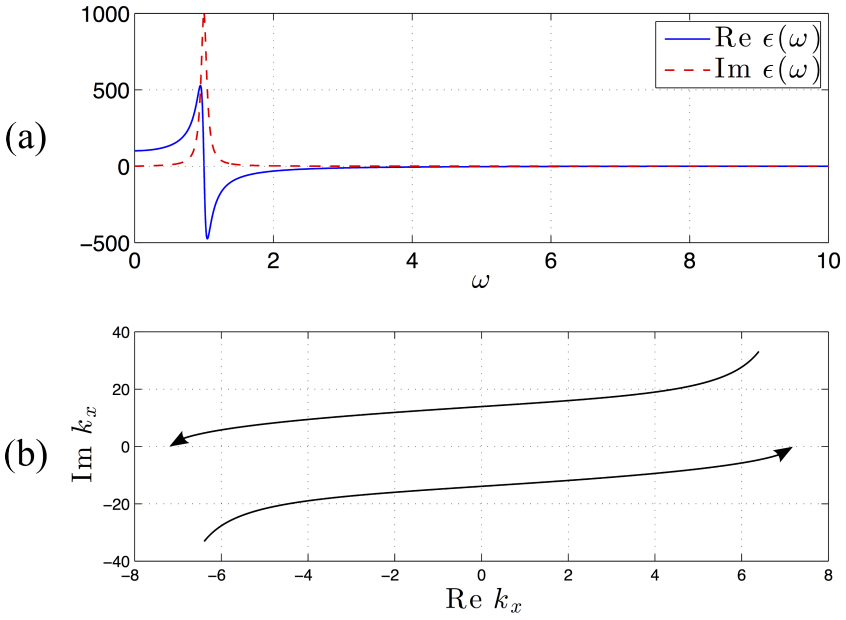

Figure 24: (a) The real and imaginary parts of $\epsilon(\omega) = \mu(\omega) = 1 + \chi(\omega)$ where $\chi(\omega)$ is given by the Lorentz model (11), with the parameters $F = 100$, $\omega_0 = 1$ and $\Gamma = 0.1$. (b) The resulting branch point trajectories as $\mathrm{Im}\,\omega$ is reduced from $\gamma = 30$ to 0, at the observation frequency $\omega_1 = 7.14$. We note that the branch points do not cross the real k_x-axis, so $\kappa(\omega)$ can be taken along the real axis. This is the case for all passive media.

of the situation. The 2d simulation was performed in the Fresnel case, to demonstrate that the wave is in fact refracted at a negative angle. The boundary is at $z = 0$, as indicated in the figures.

A negative refractive index could similarly be obtained by a large negative peak of $\mathrm{Im}\, n(\omega)$ above the observation frequency, e.g. as was shown in Figure 12 ($n(\omega) = \epsilon(\omega) = \mu(\omega)$). As discussed in Section 6, a large gain at other frequencies than the observation frequency, $\omega \neq \omega_1$ will make it hard to reach the monochromatic limit. Such media cannot be simulated by the implemented FDTD program, as the fields grow very large, and artificial reflections eventually destroy the validity of the solution.

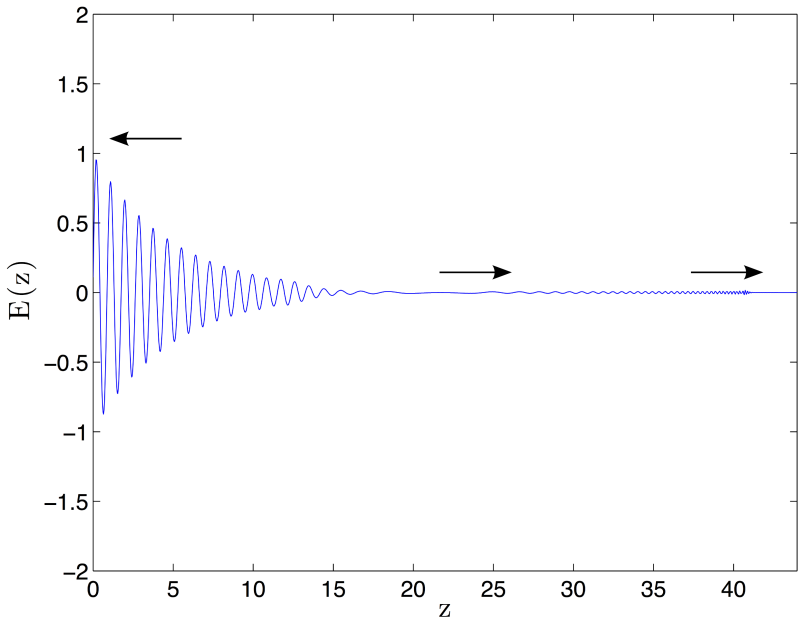

Figure 25: The resulting electric field from a 1d simulation of a medium where $\epsilon(\omega) = \mu(\omega)$ is described by Figure 24a. The image was captured after the duration $t = 44$. Close to $z = 0$ a backward wave is established. The small field which is seen at large z is the low frequency Brillouin precursor at $z \approx 20$, and the high frequency Sommerfeld precursor at $z \approx 40$. The precursors propagate at approximately the speed $c/n(0)$ and c, respectively.

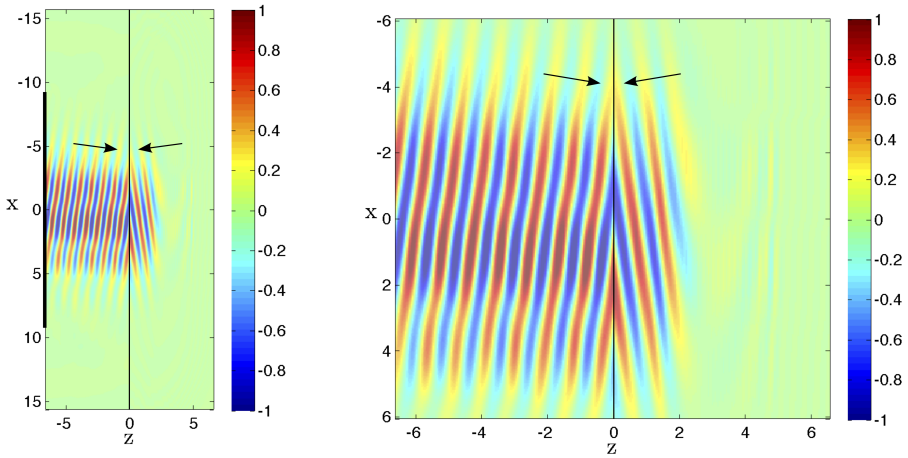

(a) (b)

Figure 26: The resulting electric field from a 2d simulation for a medium where $\epsilon(\omega) = \mu(\omega)$ is described by Figure 24a. The image was captured after the duration $t = 13.2$. It is seen that the wave is refracted at a negative angle, and propagates towards the boundary.

12.2 Non-magnetic negative refraction

It was argued in Section 3.4 that negative refraction can also be obtained in non-magnetic media, e.g. by the CFW-medium. In the CFW-medium $\mu = 1$ (non-magnetic), and ϵ is given by a sum of a passive and an active Lorentzian

$$\epsilon(\omega) = 1 + \frac{F_1\omega_{01}^2}{\omega_{01}^2 - \omega^2 - i\Gamma_1\omega} + \frac{F_2\omega_{02}^2}{\omega_{02}^2 - \omega^2 - i\Gamma_2\omega}, \tag{96}$$

where $F_1 > 0$ (passive) and $F_2 < 0$ (active). The refractive index is given as $n(\omega) = \sqrt{\epsilon(\omega)}$, where the sign should be chosen such that $n(\omega) \to +\omega/c$ as $\omega \to \infty$. The permittivity function $\epsilon(\omega)$ and the corresponding refractive index $n(\omega)$ is plotted in Figures 27, where the parameters of (96) are chosen such that we get $\mathrm{Re}\, n(\omega) < 0$ in a short frequency range.

It is worth noting that $\mathrm{Im}\, n(\omega) > 0$ for all ω, even though $\mathrm{Im}\, \epsilon(\omega) < 0$ for the frequency range where $\mathrm{Re}\, n(\omega) < 0$. A negative $\mathrm{Im}\, \epsilon$ means the medium has gain, which was a requirement for obtaining non-magnetic refraction. Since the medium has gain, it may seem strange that the imaginary part of $n(\omega)$ is positive, meaning the fields decay in the z-direction. This is explained as follows. Since the medium has $\mathrm{Re}\, \epsilon(\omega_1) > 0$ and $\mathrm{Re}\, \mu(\omega_1) > 0$ at the observation frequency, the vectors $\mathbf{E}, \mathbf{H}$ and $\mathbf{k}$ will form a right handed system. This means $\mathbf{k}$ and $\mathbf{S}$ will indeed be parallel, even though the refractive index is negative. Since $\mathrm{Re}\, n(\omega)$ is negative (which gives $\mathrm{Re}\, k_z < 0$ for small k_x), $\mathbf{k}$ points towards the boundary, so also the Poynting vector $\mathbf{S}$ points towards the boundary. The backward wave thus grows as it propagates towards the boundary. When it reaches the boundary it has an amplitude larger than the incident wave. The amplified backward wave thus leaves the medium, and may be interpreted as an "amplified reflection". The positive $\mathrm{Im}\, n(\omega)$ thus means that the fields grow in the $-z$-direction, rather than decay in the $+z$-direction.

Simulation results from the medium described by Figures 27 are shown in Figures 28 and 29. The parameters $F_1 = 2.44$, $\omega_{01} = 2.64$, $\Gamma_1 = 0.151$ and $F_2 = -0.14$, $\omega_{02} = 3.77$, $\Gamma_2 = 0.151$ were used, with the observation frequency $\omega_1 = 3.883$. In the 1d simulation (Figure 28) it is seen that the fields decay very fast with z inside the medium, which is due to the relatively large positive $\mathrm{Im}\, n(\omega_1)$. Since the backward wave reach a larger magnitude than the incident wave (due to the gain), the excess energy leaves the medium, and appears as an amplified reflection. As seen from the figure, the reflection grows in magnitude for a while, before it stabilizes at a maximum amplitude of almost 5. The incident wave has an amplitude of 1, which gives a reflection coefficient of almost 4. The 2d simulation shows that the wave is refracted at a negative angle, even though this may be hard to see due to the strong decay of the field in the z-direction.

Both 1d and 2d simulations were here performed in the Fresnel case, with vacuum to the left, and the non-magnetic negative refracting medium to the right. This was done to demonstrate that there is an amplified reflected wave present. In Figure 28 the low frequency Brillouin precursor can be seen for z between 20 and 40, and the high frequency Sommerfeld precursor is seen at $z \approx 60$.

It is worth noting that the gain of this medium is relatively high. For other media, this high gain may have lead to rapidly growing fields, which again leads to artificial reflections destroying the validity of the simulation. The reason this does not happen for this medium is that the frequencies for which the medium has gain are refracted negatively. The gain is therefore working towards the boundary, so the fields don't propagate a long distance, and thus never grow very large.

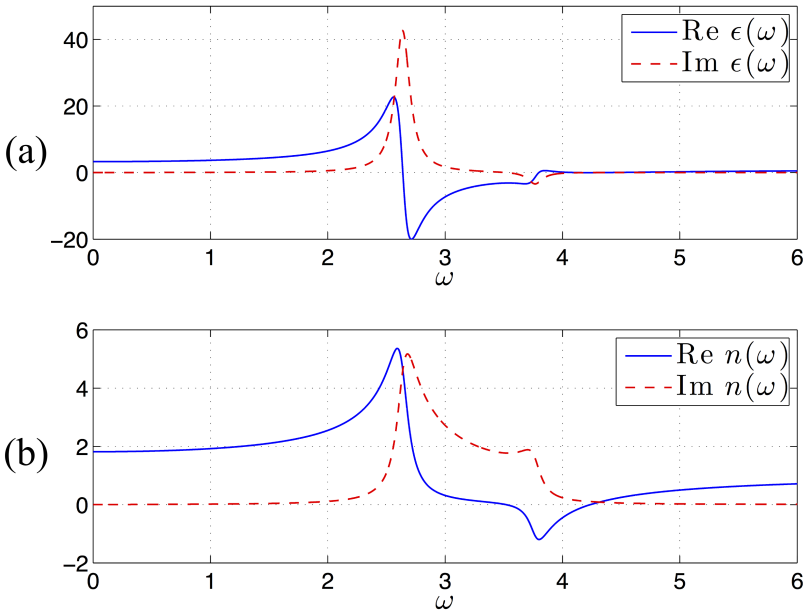

Figure 27: (a) The permittivity and (b) the refractive index for the medium described by $\mu = 1$ and $\epsilon(\omega)$ given by (96). The parameters $F_1 = 2.44, \omega_{01} = 2.64, \Gamma_1 = 0.151$ and $F_2 = -0.14, \omega_{02} = 3.77, \Gamma_2 = 0.151$ were used. The refractive index is clearly negative for the frequencies around 3.8.

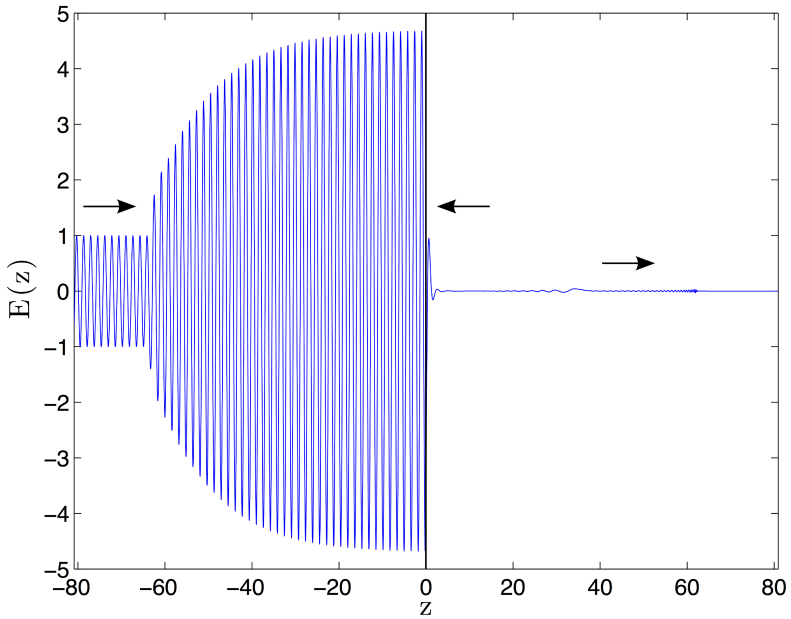

Figure 28: Non-magnetic negative refraction in the Fresnel situation. The non-magnetic medium, which is described by Figures 27, is located at $z > 0$. The medium has gain, which gives a reflection coefficient larger than 1. The reflected wave has almost reached back to $z \approx -60$. It is seen that the amplitude of the negative refracted wave has gradually been growing, and has now reached its stable value of almost 5 at $z = 0$. The Brillouin and Sommerfeld precursors are seen at $z \approx 30$ and $z \approx 60$, respectively. The figure was captured after the duration $t = 145$.

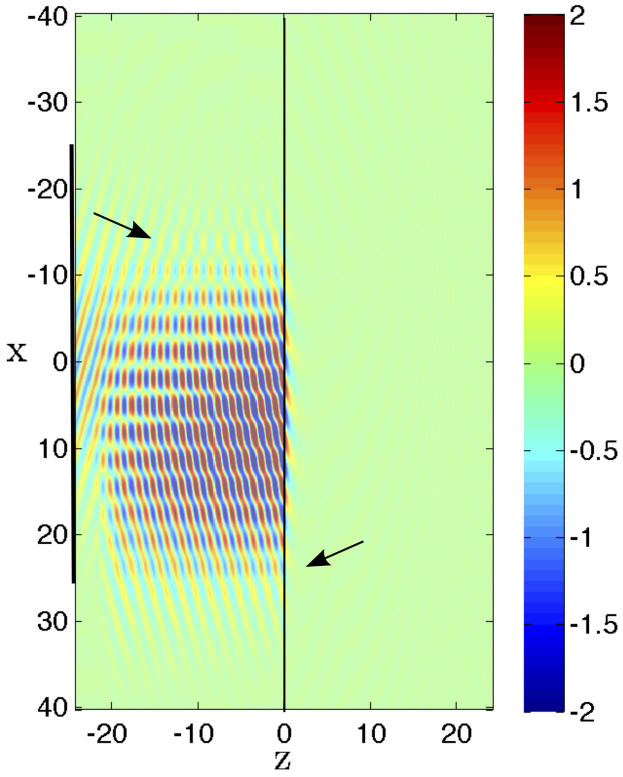

Figure 29: Non-magnetic negative refraction in 2d. The non-magnetic medium, which is described by Figures 27, is located at $z > 0$. The reflected wave has an amplitude of almost 4. The backward propagating wave is coming from the top right corner, so the incident wave is in fact refracted at a negative angle. The image was captured after the duration $t = 48$.

12.3 Negative refraction with low loss/gain

The strength of the passive resonance in Figure 24a may seem unnecessary large. One could obtain negative refraction using a much smaller resonance strength, but this would give a larger $\mathrm{Im}\, n(\omega_1)$, meaning the fields decay more rapidly with z. It was shown by Nistad and Skaar that negative refraction at very low loss/gain can be obtained through a steep change in $\mathrm{Im}\, n(\omega)$ close to the observation frequency [15]. Dirdal and Skaar later showed that all functions obeying the Kramers-Kronig relations can be approximated by a sum of Lorentzians [14]. This will thus also be the case for the steep-variation refractive index found in [15], so this medium can be simulated using the implemented FDTD program. The refractive index for two media where such a steep drop in $\mathrm{Im}\, n(\omega)$ is used to obtain negative refraction are shown in Figures 30. As can be seen from the Figures the reduction of maximum gain/loss has come at the expense of a smaller bandwidth with $\mathrm{Re}\, n(\omega) < 0$. Both media are left handed, and $\epsilon(\omega) = \mu(\omega) = n(\omega)$.

Results from 1d simulations of both media are shown in Figures 31. Both simulations were done in the current source situation. Figure 31a shows that a backward wave is present for z close to 0. For z between 60 and 180 the Brillouin and Sommerfeld precursors can be seen. As seen in Figure 31b, the transients in the gain medium grow rapidly with z. It is however possible to detect a backward wave close to $z = 0$. Due to the large gain, this medium can only be simulated over a short time period before artificial reflections destroy the solution.

From Figure 30b it is seen that for the passive medium the branch point trajectories do not cross the real k_x-axis, so the inverse Fourier transform can be taken along the real k_x-axis. Figure 30d shows that for the active medium the branch point trajectories are similar to those in Figure 11b. The inverse Fourier transform must then be taken along a zig-zag path, similar to in Figure 11c, and the medium described by Figure 30c is therefore expected to be simultaneous refracting.

Figures 32a and (b) show the resulting electric field from 2d simulations of the same media. Both simulations were done in the situation with a current source at $z = 0$, and the medium under investigation fills the entire space. The small source width $\sigma = 2$ was used, to limit the presence of exponentially growing side waves, in accordance with the discussion in Section 6.4.

It is seen that for the passive medium (Figure 32a) a backward wave is established. For the active medium the fields grow rapidly with z, as in the 1d-case. The deformation theory suggests that the active medium should be simultaneous refracting in the monochromatic limit $E_{\omega_1}(x, z, t)$; both signs of k_z should be present. Along the line $x = 0$ the expected response is thus a "standing wave". Due to the rapidly growing fields artificial reflections destroy the validity of the FDTD solution, and the monochromatic limit is therefore never reached in the simulations.

As was shown in Section 8.3, the monochromatic limit for this active medium (Figure 30c) is reached at $z = 2\pi$ after $\tau \approx 5000$. This is in the 1d-case, and it is expected to take even longer to reach the monochromatic limit in 2d, due to the presence of growing side waves. The transients grow so rapidly that it was by no means possible to simulate for such a long time.

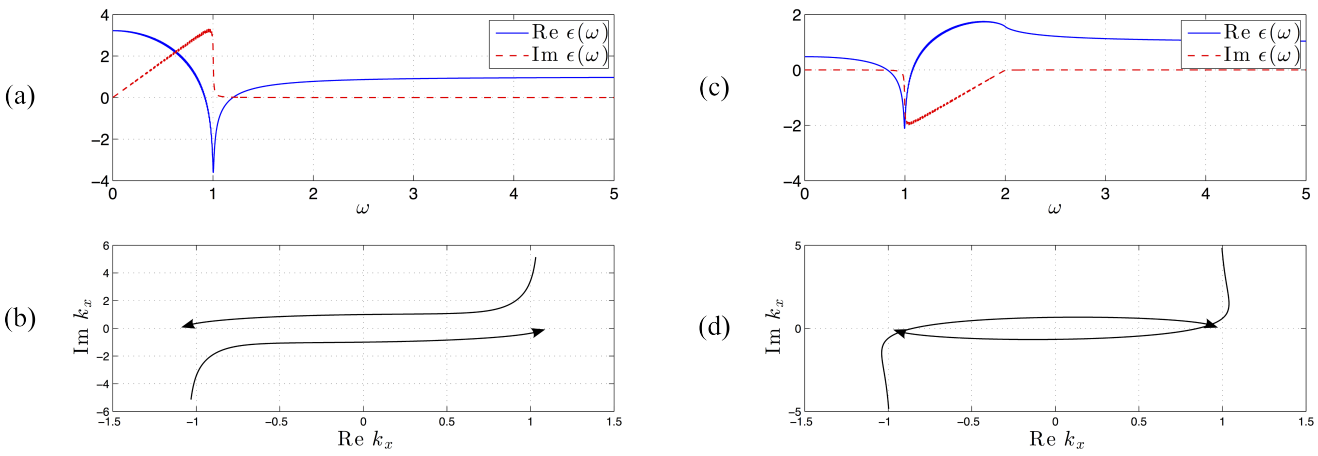

Figure 30: (a) The real and imaginary parts of $\epsilon(\omega)$ given as a sum of 150 passive Lorentzians, with parameters tuned to get a steep variation in $\mathrm{Im}\,\epsilon(\omega)$ at $\omega \approx 1$. (b) The branch point trajectories for a medium described by $\epsilon(\omega) = \mu(\omega)$ given as in (a), as $\mathrm{Im}\,\omega$ is reduced from $\gamma = 5$ to 0 at the observation frequency $\omega_1 = 1.06$. (c) and (d) Similar as for (a) and (b), but where the Lorentzians are active. The observation frequency $\omega_1 = 0.97$ was used.

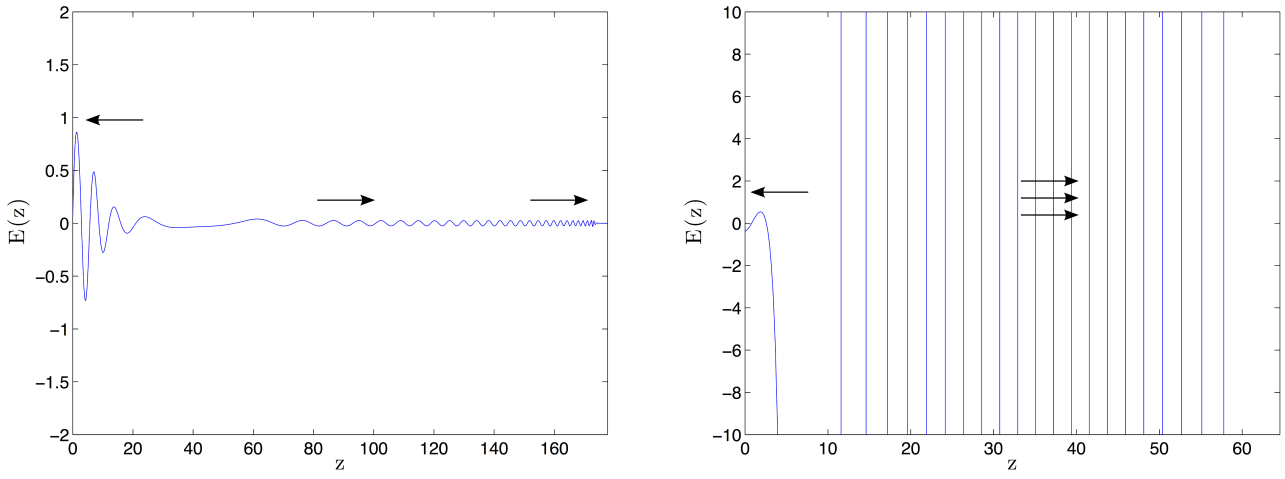

Figure 31: The Figures (a) and (b) show the resulting fields from 1d simulations of media where $\epsilon(\omega) = \mu(\omega)$ are given by Figure 30a and (c), respectively. Both figures were captured after the same duration $t = 180$. Note that the axes in the figures are different. The observation frequency $\omega_1 = 1.06$ was used for the passive medium (Figure (a)), and $\omega_1 = 0.97$ was used for the active medium (Figure (b)).

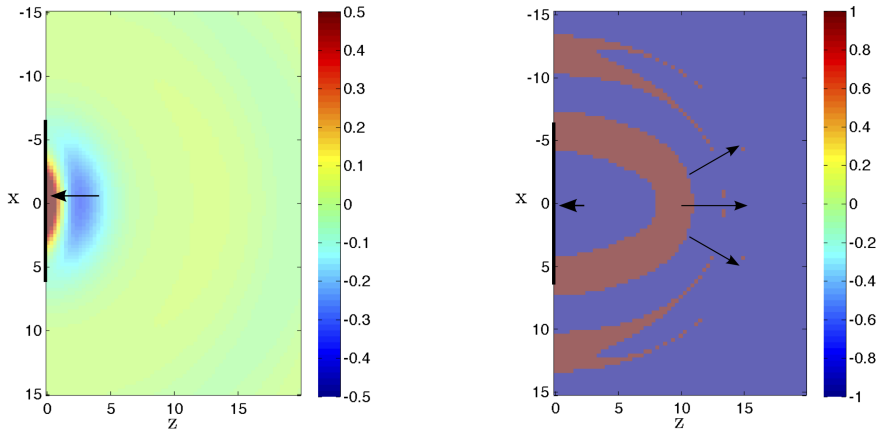

(a) (b)

Figure 32: 2d simulations of the media with $\epsilon(\omega) = \mu(\omega) = n(\omega)$ given by Figures 30: (a) the passive medium (Figure 30a) and (b) the active medium (Figure 30b). The simulations were done in the situation where a current source is located at $z = 0$, and the medium fills the entire space. The source, indicated by the bold line all the way to the left, produce an incident wave with $K_x = 0$ (normal incidence). In (a) it is seen that a backward wave is established inside the passive medium. The observation frequency $\omega_1 = 1.06$ was used. In (b) it is seen that the fields grow rapidly, due to large gain at other frequencies than the observation frequency $\omega_1 = 0.97$. Both figures are captured after the duration $t = 43.5$.

12.4 Evanescent gain

When light hits a boundary surface between a high index medium and a low index medium, total internal reflection occurs for incident angles larger than a critical angle $\theta > \theta_c$. Boundary conditions for the electric and magnetic fields give that there must however still be an electric field inside the low index medium. It can be shown that this field decays with z, i.e. the wave number k_z has an positive imaginary part. This will be the case for real ϵ and μ.

If the low index medium has loss/gain, the evanescent field should also somehow be altered. Due to the boundary conditions the reflected wave should sense any such perturbation. How to determine the electromagnetic response if the low index medium has loss/gain has been discussed extensively over the last decades [22, 23, 24, 25, 26]. One of the issues discussed is whether the reflectivity may exceed unity if the medium has gain, which is referred to as *evanescent gain*. It is argued in [26] that evanescent gain may or may not occur, this will depend on the global properties of the permittivity function $\epsilon(\omega)$ (for a non-magnetic medium, $\mu = 1$). For a weak gain medium with small dispersion, they show evanescent gain should be present.

Which direction the wave propagates, and whether the gain works towards or away from the boundary is determined by the signs of $\operatorname{Re} k_z$ and $\operatorname{Im} k_z$, so the problem is essentially to determine the correct sign of k_z. The deformation path-framework can therefore be used to understand this phenomenon. If k_z is chosen according to (26), the deformation theory ensures that k_z is zero-free, and continuous with k_x and ω along the inverse Fourier-Laplace integration surface. As argued in the attached paper we must also have $k_z \to ik_x$ for $k_x \to \infty$ for a fixed ω, and $k_z \to +\omega/c$ for $\omega \to \infty$ for a fixed k_x, independent of the properties of the medium we're investigating.

We now consider a weak gain medium, for concreteness we assume the medium is non-magnetic ($\mu = 1$), and $\epsilon(\omega)$ is given by a weak inverted Lorentzian,

$$\epsilon(\omega) = 1 - \frac{F\omega_0^2}{\omega_0^2 - \omega^2 - i\Gamma\omega}, \tag{97}$$

and set the resonance frequency as our observation frequency, $\omega_1 = \omega_0$. The parameters $F = 0.05$, $\omega_0 = 1$ and $\Gamma = 0.1$ were used in the simulations which produced Figure 34.

Provided $F < 1$, $\epsilon(\omega)$ will be analytic and zero-free for $\operatorname{Im}\omega > 0$, so the inverse Laplace transform

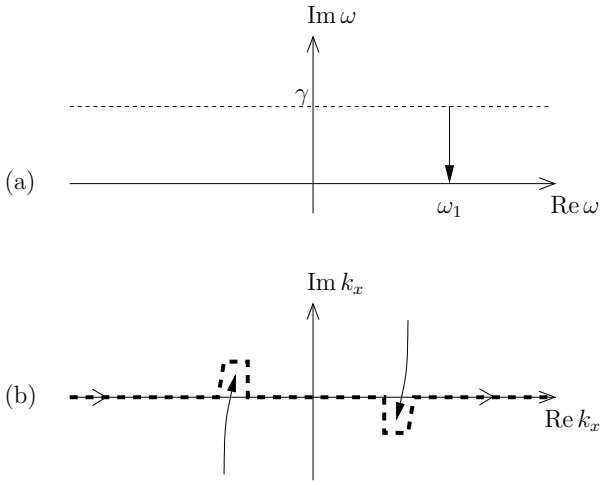

Figure 33: As $\mathrm{Im}\,\omega$ is reduced from γ to zero (a), k_z's branch points, $k_x = \pm\sqrt{\epsilon\mu}\omega/c$, moves along the trajectories in (b) for a weak gain medium. The integration path in the k_x-domain must detour around these branch points.

can be moved down to the real axis. At a given frequency the branch points will move as shown in Figure 33b. Note that the resulting integration path $\kappa(\omega)$ contains vertical detours with complex k_x. These detours are largest at the resonance frequency. It may be tempting to simply overlook these detours, so that the inverse Fourier transform is taken along the real k_x-axis, as it would be for a passive medium. This is however not possible, due the branch cuts from the zeros of k_z, which cross the real k_x-axis. For $k_x = 0$ we have $k_z = \pm\sqrt{\epsilon(\omega)}\omega/c$, where the sign of the square root must be chosen such that $k_z \to +\omega/c$ as $\omega \to \infty$. For $\epsilon(\omega)$ given by (97) we get $\mathrm{Im}\,k_z < 0$ for small k_x. If we increase k_x along the real axis, requiring k_z to be continuous with k_x we would get $k_z \to -ik_x$ as $k_x \to \infty$, in contradiction to the requirement from the paper. But, as we cross the branch cut the sign of k_z must be switched (see Section 2.5). This will give $k_z \to +ik_x$ as $k_x \to \infty$, in accordance with the requirement from the paper. (The branch cuts thus ensure that the sign of k_z can be chosen such that k_z approach both limits $k_z \to +\omega/c$ as $\omega \to \infty$ and $k_z \to ik_x$ as $k_x \to \infty$, and still is continuous with k_x and ω along the inverse Fourier-Laplace transform integration surface).

FDTD simulations show that the field is in fact evanescent for $|K_x| > |\mathrm{Re}\,k_{x,\mathrm{bp}}|$, where $k_{x,\mathrm{bp}}$ is the branch points for k_z. For $|K_x| < |\mathrm{Re}\,k_{x,\mathrm{bp}}|$ the fields grow with z, also as the theory predicted ($\mathrm{Im}\,k_z < 0$). The resulting fields are shown in Figures 34 for the two cases. In the simulations the medium for $z > 0$ is the weak gain medium described by (97), while the medium for $z < 0$ is a high index (non-dispersive) dielectric medium, with $\epsilon = 4$ and $\mu = 1$. Figure 34(d) shows that the reflected field has an amplitude larger than 1, implying that evanescent gain is present. In the simulations Maxwell's equations are solved in the time domain. One may therefore take the simulations as an independent verification for that the deformation theory can be used to understand when evanescent gain is possible or not. In the simulations the incident angle θ is determined by the carrier wavenumber K_x of the approximately plane waves produced by the source; where the critical angle θ_c will correspond to $K_x = 1$.

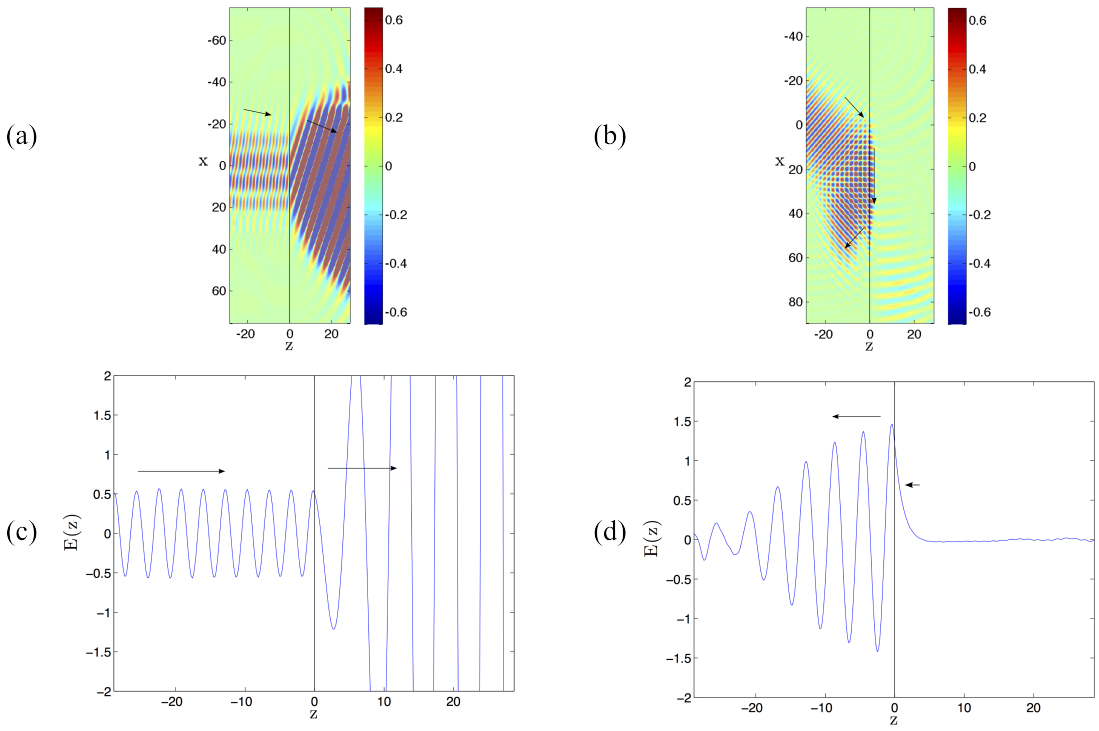

Figure 34: The incident wave propagates from a high index medium ($\epsilon = 4$), to a low index gain medium located at $z > 0$, for two different incident angles: (a) $\theta < \theta_c$ ($K_x = 0.3$). Only a small fraction of the field is reflected at the boundary. (b) $\theta > \theta_c$ ($K_x = 1.3$). A large fraction is reflected at the boundary. (c) The field from Figure (a) along the line $x = 0$. The field increases with z inside the medium, so $\mathrm{Im}\, k_z < 0$. (d) The field from Figure (b) along the line $x = 40$. The field decrease with z inside the medium, so $\mathrm{Im}\, k_z > 0$. The maximum amplitude of the incident wave is 0.65, while the maximum amplitude at the boundary $z = 0$ is 1.5. The reflection coefficient is thus larger than 1, so evanescent gain is present.

12.5 Absolute instabilities for media with $\sqrt{\epsilon\mu}$ with zeros for $\mathrm{Im}\,\omega > 0$

It was argued in Section 7.3 and 7.4 that for media with $\epsilon(\omega)\mu(\omega)$ with zeros in the upper half plane $\mathrm{Im}\,\omega > 0$, the fields should diverge in time, even at a fixed point in space. FDTD simulations of such media verify that this is the case. This happens even when the zeros in the upper half plane are of even order, which in theory should result in a stable medium, in the 1d case.

The non-magnetic medium ($\mu = 1$) with ϵ given by

$$\epsilon(\omega) = 1 + \frac{F_1\omega_{01}^2}{\omega_{01}^2 - \omega^2 - i\Gamma_1\omega} + \frac{F_2\omega_{02}^2}{\omega_{02}^2 - \omega^2 - i\Gamma_2\omega}, \tag{98}$$

with the parameters $F_1 = 1.5$, $\omega_{01} = 0.8$, $\Gamma_1 = 0.15$, $F_2 = -0.15$, $\omega_{02} = 1.1$ and $\Gamma_2 = 0.3$, has a zero of even order for $\epsilon(\omega)\mu(\omega)$ in the upper half plane, at $\omega_z = -1.18 + i0.026$. Figure 35a shows the resulting field from a 1d simulation of this medium, while Figure 35b shows the resulting field from a 1d simulation of a medium where $\epsilon(\omega) = \mu(\omega)$ both are equal to (98). For the latter medium the zero for $\epsilon(\omega)\mu(\omega)$ in the upper half plane is of even order. The 1d simulation corresponds to the situation where the plane wave limit $K_x = 0$, $\sigma \to \infty$ is taken initially, so only the plane wave component $K_x = 0$ is present. The non-magnetic medium should thus have an absolute instability, where the fields grow exponentially with time, with the exponential growth rate equal to $\mathrm{Im}\,\omega_z = 0.026$. The symmetric medium ($\epsilon = \mu$) should in theory be stable, at least if the electric and magnetic response are in fact exactly identical.

The simulations show that the electric field grow with time in both media. Through evaluating the electric field at a given z over time, it is found that the field amplitude do in fact grow with an exponential growth rate ≈ 0.025, i.e. in good agreement with the theoretical predicted value. For the non-magnetic medium (Figure 35a) the field has grown largest close to $z = 0$, as this is where the field has been present over the longest time. The observation frequency $\omega_1 = 1.2$ was used in the simulations. If an observation frequency further apart from the zero in the upper half plane was used, it would take a longer time before the instability becomes visible, as the instability becomes less excited. However, for large times the field will eventually be dominated by the instability.

It is believed that the reason the field grow with time even for the symmetric medium is that the electric and magnetic field are calculated separately at shifted points in space and time in the simulations. Numerical errors then cause the resulting electric and magnetic response to differ slightly, even though the same parameters were used for $\epsilon(\omega)$ and $\mu(\omega)$. As explained in Section 7.4 such small perturbations will split the double zero into to single zeros, which leads to an absolute instability.

Even in the simulation world, where no physical impurities or random generated noise are present, even order zeros in the upper half plane thus lead to an absolute instability. In an actual physical experiment there will always be some sort of perturbations present, and media with even order zeros in the upper frequency plane therefore have limited use.

As explained in Section 7.3, taking the plane wave limit $\sigma \to \infty$ for a large K_x may in fact prevent the instability from occurring. Results from a 2d simulation of the non-magnetic medium given by (98), using a large K_x, is shown in Figure 36. The field is evanescent, and does not grow with time throughout the duration of the simulation. In the simulation a finite σ is used, so all k_x are excited to some extent, also $k_x = 0$. For very long experiment durations we should thus expect the instability to eventually become visible, even for this large K_x. The 2d simulation was done in the situation with a current source at $z = 0$, and only the field for $z > 0$ was simulated due to symmetry.

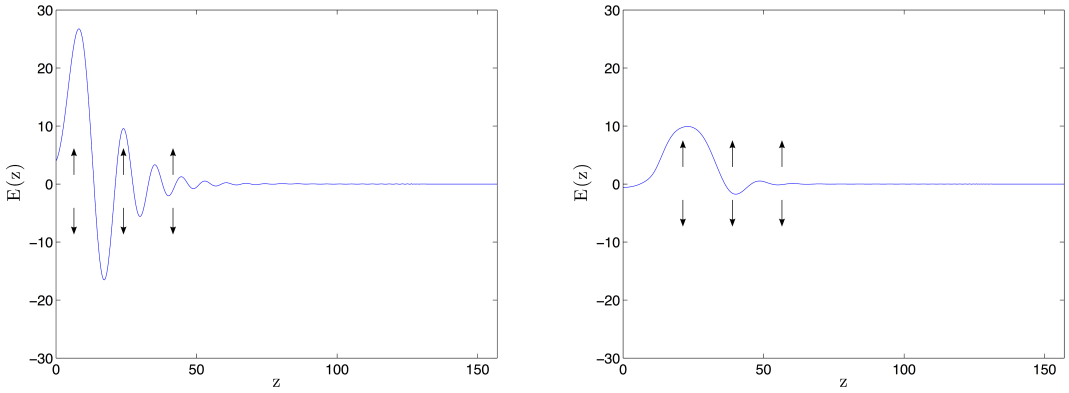

(a) (b)

Figure 35: 1d simulation of the two media (a) $\mu = 1$ and ϵ given by (98) and (b) $\epsilon(\omega) = \mu(\omega)$ both given by (98). The fields grow with time in both media. The simulations were done in the current source situation, where only the fields for $z > 0$ are simulated due to symmetry. Both figures were captured after the same duration, $t = 129$. The arrows in the figures indicate that the fields grow with time.

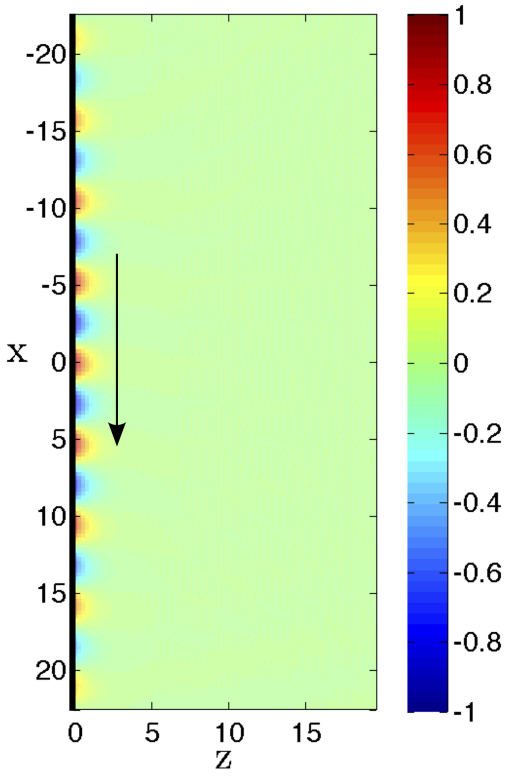

Figure 36: Simulation results showing that an absolute instability disappears for large K_x. The field propagate along the x-axis, and decay fast with z due to the large "incident angle". The bold line at $z = 0$ indicates the source.

13 Discussions and conclusion

Fourier-Laplace analysis was used to predict the existence of media exhibiting simultaneous refraction, i.e. refracting both positively and negatively at the same time. This novel property will occur in media where when deforming the inverse Laplace transform integration path down to the real ω-axis, the branch points in the k_x-plane move such that the k_x-integration path is forced into a zigzag-pattern at our observation frequency ω_1. For this to be possible the medium must have gain. It was argued that this effect is two-dimensional, meaning that the side waves somehow establish waves along the z-axis with both signs of k_z.

It was found that to obtain simultaneous refraction in a medium where $\epsilon(\omega) = \mu(\omega) = 1 - \chi(\omega)$, where $\chi(\omega)$ is given by the Lorentz function, the strength of the Lorentz function must be very large, meaning the maximum gain of the medium must be large. It was further showed that the required gain can be minimized through introducing a steep drop in the imaginary parts of ϵ and μ just above the observation frequency.

The deformation theory was also used to analyze possible instabilities in infinite or semi-infinite gain media. It was found that for media where $\sqrt{\epsilon\mu}$ is non-analytic or has zeros in the upper half plane, the inverse Laplace transform cannot be moved down to the real ω-axis, and such media will therefore have an absolute instability, meaning the fields will grow with time even at a fixed point in space. It is further shown that due to the possible presence of instabilities, it is not necessarily possible to interpret the fields in the monochromatic and plane wave limits in media with gain, as it usually is done for passive media. Even for media where the monochromatic limit exists, it is shown that for certain media it may take a very long time for the transients to die out.

A FDTD program was implemented in MATLAB, to be used for simulating some of the novel media which were analyzed using the Fourier-Laplace theory. A range of negative refracting media were simulated, with results consistent with what the theory predicts. Simulation results showing evanescent gain were presented. For media with a non-analytic $\sqrt{\epsilon\mu}$ in the upper half plane, the simulations do in fact show that the fields grow with time, i.e. an absolute instability is present. For media with a large gain the program fails after just a short duration, due to artificial reflections destroying the validity of the solution. These reflections were shown to originate from the numerical precision of MATLAB.

Due to these artificial reflections, simulations were not able to reveal the effect of simultaneous refraction. The reflections only occur for very large fields. At our observation frequency ω_1 the gain for the optimized medium is very low, and in the monochromatic limit the fields should thus not be very large. A large gain at other frequencies very close to ω_1 does however make the field grow rapidly in the transient period, which is why the artificial reflections occur. The maximum gain of the optimized medium may be further reduced through an even steeper change in $\operatorname{Im} n(\omega)$. This will however come at the cost of an even smaller bandwidth with $\operatorname{Re} n(\omega) < 0$, which is not desirable, as this will increase the necessary duration for the monochromatic limit to be reached.

Through turning on the source sufficiently smoothly, one may prevent the excitation of the frequencies with large gain. Since the gain is so large, the necessary onset period will however be extremely long, so it is not possible to follow this approach in our simulations, due to lack of computational power.

It is important to remember that it is in the real, physical world, not the FDTD world we live in. Even though artificial reflections due to numerical errors would not occur in an actual physical experiment, we would however run into similar problems. In the real world there will always be some noise or impurities, which eventually will excite the gainy frequencies leading to huge fields. The media in this analysis were assumed to be infinite, or semi-infinite. In practice the theory here presented is thus only valid for very short time periods, as the light very soon will reach the outer boundaries of the medium it propagates within. The theory does however tell us about the actual optical properties of the investigated medium, and helps us understand the origin of instabilities. In media with absolute instabilities the fields will diverge with time, so possible application of such media may be limited.

14 Further work

14.1 Perfectly Matched Layers

In the implemented FDTD program the spatial domain was chosen so large that the fields never reached the outer boundaries throughout the simulations. This is because the investigated media where assumed to be infinite or semi-infinite. If we want to run simulations over very long times this may however lead to a memory leakage. This problem could be overcome by making use of Perfectly Matched Layers (PML) techniques [27]. A perfectly matched layer is an artificial absorbing layer. Waves which hit this layer will simply be absorbed, rather than reflected. By applying a PML technique it may thus be possible to limit the extent in the x- and z-directions, and by this allow for simulating for long times. Perfectly matched layers are however not absolute reflection free. It is of high importance that the reflections are kept at an absolute minimum, as we want to investigate the properties of a semi-infinite medium. The absorption at the boundaries must therefore be larger than the round-trip gain of the medium, otherwise the fields will grow with time.

Implementation of a PML technique may also in fact help overcome the problem with artificial reflections. The artificial reflections occur because the fields grow very large. If the spatial domain is chosen small enough that the transients never grow any large we have thus prevented the artificial reflections from occurring. Implementation of PML boundary conditions should thus make it possible to simulate for large enough times to reveal the effect of simultaneous refraction.

14.2 Metamaterials beyond the Kramers-Kronig relations

Dirdal and Skaar recently showed that the Kramers-Kronig relations may be a too strict limitation on $\epsilon(\omega)$ and $\mu(\omega)$. For instance, the split ring resonator medium, which only consists of passive components, must have gain for large frequencies for the Kramers-Kronig relations to be obeyed. The Kramers-Kronig relations are really just relating mathematical functions, which do not necessarily have any physical meaning. The effective medium theory metamaterial models are based on requires the structures to be much smaller than the wavelength of the light. For very high frequencies the models thus collapse. That a passive medium seems to have gain may therefore be understood as that the frequencies where the medium is gainy is outside the metamaterial frequency range. At these frequencies $\mu(\omega)$ will just be a mathematical function, and has nothing to do with the physical properties of the medium.

The Kramers-Kronig relations showed us that gain above the observation frequency was necessary for obtaining simultaneous refraction. It may therefore be worth looking into whether this gain may be "hidden" outside the metamaterial frequency range, as is the case for the inverted transmission line medium.

A Fourier theory of linear gain media

My contribution: Section III and Section IV: Choice of excitations, and associated analysis. Section V.D and V.E: Choice of medium, analysis, numerical experiments, and discussions. Section VI: Conclusion.

Fourier theory of linear gain media

Hans Olaf Hågenvik,[1] Markus E. Malema,[1] and Johannes Skaar[1]

[1] *Department of Electronics and Telecommunications, Norwegian University of Science and Technology, NO-7491 Trondheim, Norway*[*]

(Dated: June 16, 2014)

The analysis of wave propagation in linear, passive media is usually done by considering a single real frequency (the monochromatic limit) and also often a single plane wave component (plane wave limit), separately. For gain media, we demonstrate that these two limits generally do not commute; for example, one order may lead to a diverging field, while the other order leads to a finite field. Moreover, the plane wave limit may be dependent on whether it is realized with a rect function excitation or gaussian excitation of infinite widths. We consider wave propagation in gain media by a Fourier–Laplace integral in time and space, and demonstrate how the correct monochromatic limit or plane wave limit can be taken, by deforming the integration surface in complex frequency–complex wavenumber space. We also give the most general criterion for absolute instabilities. The general theory is applied in several cases, and is used to predict media with novel properties. In particular, we show the existence of isotropic media which in principle exhibit simultaneous refraction, meaning that they refract positively and negatively at the same time.

I. INTRODUCTION

Fourier theory makes it possible to consider single frequencies and plane wave components separately, in describing electromagnetic wave propagation in linear, passive media. This leads to huge simplification in analysis and interpretation, especially for dispersive (and/or spatially dispersive) media. Nevertheless, we must have in mind that real physics happens in the time–spatial domain, not in frequency–wavenumber space; the monochromatic and plane wave limits can never be realized in practice. The monochromatic limit is approached by turning on the excitation at some time $t = 0$ [1], and waiting a sufficiently long time until the transients have died out. The plane wave limit is approached by letting the width of the excitation be sufficiently large.

For active media (gain media), it is clearly of large interest to use the same Fourier theory, by decomposing the field into frequency components and/or plane waves. There is, however, a number of obstacles. The most obvious one is that active media are inherently nonlinear due to gain saturation [2]. In practice, this can be dealt with by verifying that the magnitude of the solution is less than the threshold for gain saturation. If it is not, then the excitation must be reduced accordingly, or the solution must be rejected. If there are divergences associated with the linear solution, the solution must be rejected in any case.

Another problem is that the Fourier transform not necessarily exists. A remedy is to use the Laplace transform, decomposing the time-domain fields into exponentially increasing functions $\exp(-i\omega t)$ for $\mathrm{Im}\,\omega > 0$ (see Sec. II). Once the solution has been found, it can often be continuated towards real frequencies, enabling simpler interpretation (Sec. III). One may argue that the Fourier transform should be sufficient for the relevant situations, since diverging solution must be rejected anyway. However, this strategy is dangerous, as imposing Fourier transform analysis may give the impression of false, stable solutions.

An extensively discussed problem in the context of active media, is the determination of the sign of the longitudinal wavenumber k_z. This problem is far from trivial, even e.g. in the context of total internal reflection from a weakly amplifying medium [3–5]. More recently, the problem has been discussed in the context of the wave vector or refractive index of more advanced active media including active metamaterials [6–9].

We are not going to treat this problem here, as it now seems to be agreement that the sign of the longitudinal wavenumber must be determined by ensuring it is analytic in the upper half-plane of complex frequency, and such that $k_z \to +\omega/c$ for $\omega \to \infty$ [7–11]. Here ω is the (possibly complex) frequency and c the vacuum light velocity. However, we will take the analysis one important step further; by considering a double Fourier–Laplace transform with respect to space and time. Clearly, for realistic situations, the fields can neither have infinite durations nor infinite widths. In addition to turning the field excitations on at $t = 0$, it turns out to be crucial to let them have finite widths, to see how the medium behaves in practice. Indeed, even though a particular medium does not show absolute instabilities for plane wave excitations, it can support absolute instabilities in the presence of other excitations.

Once the general theory governing causal finite beam propagation has been discussed, it is of interest to consider the monochromatic limit and plane wave limit. A number of peculiar but interesting results arise. First of all, the monochromatic and plane wave limits do not commute in general; for very common situations with conventional gain media, one order leads to finite fields, while the other order leads to infinite fields. Second of all, the plane wave limit may depend on the way it is

[*] johannes.skaar@ntnu.no

taken; if it is realized using a finite-support excitation or a gaussian excitation, eventually of infinite widths. Our analysis leads to a better understanding of the nontrivialities associated with earlier, monochromatic and plane-wave analyses of active media. It also can be used to predict new classes of active media, with novel responses. For example, we predict the presence of isotropic media which exhibit simultaneous refraction, i.e., both positive and negative refraction simultaneously. While this is a novel and surprising response, it may be argued that the required gain is unrealistically high, and makes both realization and time-domain simulations challenging or even impossible, at least for the proposed media.

Previously, Kolokolov [4] and Grepstad and Skaar [5] have treated the problem of Fourier–Laplace transform analysis of active media. However, Kolokolov only considered the special case with weak or no dispersion. Dispersion has important consequences for the theory, as it turns out to fundamentally change the method of deformation in the complex frequency–wavenumber space. The dispersion, possibly engineered by metamaterials, may lead to new classes of active media, as shown by the different possible behaviors in frequency–wavenumber space. Grepstad and Skaar did not perform a complete analysis, since they did not consider the deformation in frequency–wavenumber space, including the monochromatic limit for finite beams.

The article is structured as follows. In Sec. II, we state the problem and discuss the assumptions in detail, before analyzing the fields using the Laplace transform (in time) and Fourier transform (in space). In Sec. III we discuss how we may approach real frequencies for media without absolute instabilities. This happens at the expense of deforming the integration path in the complex wavenumber (k_x) space. In Sec. IV we discuss the plane wave limit, and the interpretation of divergences and non-commutativity. The theory is applied to the understanding of existing media and novel media in Sec. V. In particular, we show the presence of simultaneous refraction, before concluding in Sec. VI.

II. LAPLACE AND FOURIER TRANSFORM ANALYSIS

We restrict the analysis to linear, time-shift invariant, isotropic, homogeneous media without spatial dispersion. Moreover, we assume the following asymptotic behavior for the product of permittivity and permeability, as $\omega \to \infty$ [12]: $\epsilon(\omega)\mu(\omega) = 1 + \mathcal{O}(\omega^{-2})$. Finally, we assume that the medium does not support superexponential instabilities, meaning that any field solution should not grow faster with time than an exponential.

In the analysis we consider an infinite or semi-infinite medium. Of course, there are no infinite gain media in practice; what is meant by "infinite" here is that the smallest distance from an observation point to the boundary of the medium is larger than $ct_{\max}$, where c is the vacuum light velocity and $t_{\max}$ is the maximum duration of the experiment. To approach steady state (or the monochromatic limit) we will later require $t_{\max}$ to be large. Then we must have in mind that the dimensions of the gain medium must be accordingly large. Considering an infinite or semi-infinite medium helps us understand the optical response given solely by the medium's properties – all effects related to interactions with surrounding media have been ruled out.

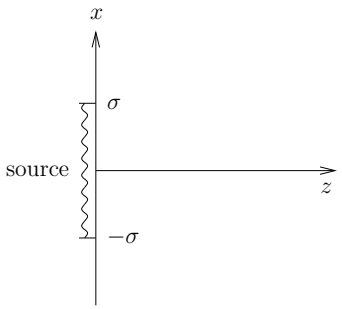

FIG. 1. An excitation is located at $z = 0$ in a homogeneous medium. In the figure the special case with finite width 2σ is shown.

We will assume that the medium is dark for $t \leq 0$. This assumption needs some clarification. To establish the active medium, an energy pump must be turned on before $t = 0$. When the system does not support instabilities, we can imagine that the pump was turned on a long time before $t = 0$, such that any transients have died out. If there are instabilities, however, any disturbance will blow up with time. We could assume that the pump is turned on slowly before $t = 0$, sufficiently smooth such that no significant transients are generated as a result of the pump, but sufficiently fast such that the (small) transients do not grow too much before $t = 0$. We do not consider the existence of such a trade-off further; we rather demand that any transients from the pump or from other perturbations or fluctuations in the system, must be included into the analysis. This is done by including them into the excitation of the system, to be defined below.

It is also in order to comment the linearity assumptions in some detail. The amplitude in any practical medium will be limited by nonlinear effects such as gain saturation. When we refer to "diverging fields", or "instabilities", it strictly means that the fields grow until they are limited by gain saturation. Clearly, in such cases the linear analysis is only accurate for a limited duration. In the absence of instabilities, the analysis is clearly accurate for all times, provided the excitations are sufficiently weak.

For simplicity we limit the discussion to propagation in two dimensions, x and z, and transversal electric (TE) fields. Let $\mathcal{E}(x, z, t)\hat{\mathbf{y}}$ be the physical electric field, pointing in the y-direction $\hat{\mathbf{y}}$. Since the medium is active, the field may diverge with time t. We have limited our atten-

tion to active media that leads to fields growing at most exponentially (see [13]):

$$|\mathcal{E}(x,z,t)| \leq E_0 \exp(\gamma t). \tag{1}$$

Here E_0 and γ are constants independent of x, z, and t. Consider a source located at the plane $z=0$, producing fields in the half-spaces $z>0$ and $z<0$ (see Fig. 1). By (1) the electric field is Laplace transformable:

$$E(x,z,\omega) = \int_0^\infty \mathcal{E}(x,z,t)\exp(i\omega t)\mathrm{d}t, \tag{2}$$

for $\operatorname{Im}\omega > \gamma$. Furthermore, $E(x,z,\omega)$ can be Fourier transformed wrt. x, to obtain the plane wave spectrum

$$E(k_x,z,\omega) = \int_{-\infty}^\infty E(x,z,\omega)\exp(-ik_x x)\mathrm{d}x. \tag{3}$$

The inverse transform can be written

$$\begin{aligned}(2\pi)^2\mathcal{E}(x,z,t) &= \\ &= \int_{i\gamma-\infty}^{i\gamma+\infty}\int_{-\infty}^{\infty} E(k_x,z,\omega)\exp(ik_x x - i\omega t)\mathrm{d}k_x\mathrm{d}\omega \\ &= \int_{-\infty}^{\infty}\int_{i\gamma-\infty}^{i\gamma+\infty} E(k_x,z,\omega)\exp(ik_x x - i\omega t)\mathrm{d}\omega\mathrm{d}k_x,\end{aligned} \tag{4}$$

where, in the last equality, we have used Fubini's theorem to interchange the order of integration. This is permitted provided $E(k_x,z,\omega)$ is absolute integrable wrt. ω and k_x, and k_x and ω. Once we have found a solution to Maxwell's equations, we must verify that the solution is consistent with the assumption. For the solutions in the present article, it is argued in Appendix A that the fields are absolute integrable provided the excitation is. A sufficient condition for absolute integrability is therefore e.g. that the excitation (to be defined shortly) can be written $U(k_x)V(\omega)$ for absolute integrable functions $U(k_x)$ and $V(\omega)$. This translates to an excitation in the (x,t)-domain of the form $u(x)v(t)$, for continuous functions $u(x)$ and $v(t)$.

We consider a source in the plane $z=0$ (Fig. 1), infinitely thin, but possibly of infinite width. In general, we may have sources everywhere; in that case, we would have to superpose the fields resulting from the different sources. For $z\neq 0$, Maxwell's equations mean that $\left(\mathrm{d}^2/\mathrm{d}z^2 - k_x^2 + \epsilon\mu\omega^2/c^2\right)E(k_x,z,\omega) = 0$. Furthermore, the transversal (x-component) of the magnetic field is given by $-i\omega\mu H(k_x,z,\omega) = \mathrm{d}E(k_x,z,\omega)/\mathrm{d}z$. Hence, we can express

$$E(k_x,z,\omega) = A(k_x,\omega)\mathrm{e}^{ik_z z} + B(k_x,\omega)\mathrm{e}^{-ik_z z} \tag{5a}$$

$$H(k_x,z,\omega) = -\frac{k_z}{\omega\mu}\left[A(k_x,\omega)\mathrm{e}^{ik_z z} - B(k_x,\omega)\mathrm{e}^{-ik_z z}\right] \tag{5b}$$

for $z<0$, and

$$E(k_x,z,\omega) = C(k_x,\omega)\mathrm{e}^{ik_z z} + D(k_x,\omega)\mathrm{e}^{-ik_z z} \tag{6a}$$

$$H(k_x,z,\omega) = -\frac{k_z}{\omega\mu}\left[C(k_x,\omega)\mathrm{e}^{ik_z z} - D(k_x,\omega)\mathrm{e}^{-ik_z z}\right] \tag{6b}$$

for $z>0$. Here

$$k_z^2 = \epsilon\mu\frac{\omega^2}{c^2} - k_x^2. \tag{7}$$

The four functions $A(k_x,\omega)$, $B(k_x,\omega)$, $C(k_x,\omega)$, and $D(k_x,\omega)$ are connected by the electromagnetic boundary conditions, which in turn, are dependent on the source. For a current source, $E(k_x,z,\omega)$ is continuous across the source plane, while $H(k_x,0^+,\omega) - H(k_x,0^-,\omega) = J(k_x,\omega)$, where $J(k_x,\omega)$ is the (Fourier–Laplace transformed) surface current source. With reflection symmetry about the plane $z=0$, this means that

$$A = D, \tag{8a}$$

$$B = C, \tag{8b}$$

$$\frac{2k_z}{\omega\mu}(A-B) = J(k_x,\omega). \tag{8c}$$

Clearly, both unknown functions A and B cannot be found from (8). Moreover, since the medium potentially is active, we cannot use principles like requiring the source to do positive work, or field decay as $z\to\infty$. We must invoke the principle of causality in its most fundamental form.

First we note that the sign of k_z can be chosen arbitrarily in (5) and (6); a change of sign means only that the functions C and D (and A and B) are interchanged. Since $\epsilon(\omega)$ and $\mu(\omega)$ are analytic for $\operatorname{Im}\omega>\gamma$, and tend to unity as $\omega\to\infty$ there, we choose the sign such that for a fixed k_x,

$$\begin{aligned}&k_z(k_x,\omega) \text{ is analytic for } \operatorname{Im}\omega>\gamma, \text{ and} \\ &k_z(k_x,\omega)\to +\omega/c \text{ as } \omega\to\infty \text{ in the region } \operatorname{Im}\omega>\gamma.\end{aligned} \tag{9}$$

Assuming that the medium and the source are at rest for $t<0$, the fields as described by (6) are causal. Thus they satisfy the conditions of Titchmarsh' theorem for diverging functions, (B6) and (B7) (see Appendix B). This means that $C(k_x,\omega)\mathrm{e}^{ik_z z}$ and $D(k_x,\omega)\mathrm{e}^{-ik_z z}$, separately, satisfy these conditions. From the initial value theorem and the fact that $k_z c = \omega + \mathcal{O}(\omega^{-1})$, it is intuitively clear that the factor $\mathrm{e}^{-ik_z z}$ shifts the beginning of the associated time-domain response to earlier times by an amount z/c. Thus $D(k_x,\omega)\mathrm{e}^{-ik_z z}$ can only be compatible with causality for all $z>0$ if $D(k_x,\omega)\equiv 0$[1].

---

[1] A rigorous argument goes as follows (here we suppress the k_x-dependence for clarity): Since $D(\omega)\exp(-ik_z z)$ is required to satisfy (B7) for all z, and since $k_z c = \omega + \mathcal{O}(\omega^{-1})$, we have for sufficiently large γ:

$$\int_{-\infty}^{\infty}|D(\omega'+i\gamma)|^2\mathrm{d}\omega' \leq 2K(z)\exp(-2\gamma z/c). \tag{10}$$

Here $K(z)$ is independent of γ. If $d(t)$ is the inverse Laplace transform of $D(\omega)$, then $d(t)\exp(-\gamma t)$ is the inverse Laplace transform of $D(\omega+i\gamma)$. Thus, from Parseval's relation, $\int_0^\infty |d(t)|^2\exp(-2\gamma t)\mathrm{d}t = \frac{1}{2\pi}\int_{-\infty}^{\infty}|D(\omega'+i\gamma)|^2\mathrm{d}\omega'$. Combina-

We have thus arrived at the causality result: In (5) and (6), we have

$$A = D = 0, \tag{12a}$$

$$B = C = -\frac{\omega\mu}{2k_z} J(k_x, \omega), \tag{12b}$$

and the sign of k_z is to be determined according to (9). In Appendix A we prove that the function $k_z(k_x, \omega)$ is zero-free in a region $\mathrm{Im}\,\omega > \gamma$; thus B is analytic there[2].

We now consider the usual situation described by the Fresnel equations, where we have different media on each side of the plane $z = 0$, and there is no source at $z = 0$ but rather somewhere in the medium on the left-hand side ($z < 0$). Clearly, we can use the identical causality argument on the right-hand side ($z > 0$), to obtain (9) and $D = 0$. The electromagnetic boundary conditions $E(k_x, 0^+, \omega) = E(k_x, 0^-, \omega)$ and $H(k_x, 0^+, \omega) = H(k_x, 0^-, \omega)$ then give the reflection and transmission coefficients

$$\frac{B}{A} = \frac{\mu_2 k_{1z} - \mu_1 k_{2z}}{\mu_2 k_{1z} + \mu_1 k_{2z}}, \tag{13a}$$

$$\frac{C}{A} = \frac{2\mu_2 k_{1z}}{\mu_2 k_{1z} + \mu_1 k_{2z}}, \tag{13b}$$

where $k_{iz}^2 = \epsilon_i \mu_i \omega^2/c^2 - k_x^2$. Here subscript 1 and 2 stand for the medium to the left and right, respectively.

It is important to note that the results so far have been derived for $\mathrm{Im}\,\omega > \gamma$. In Sec. III we will consider the possibility of continuating the solutions towards real frequencies.

III. TOWARDS REAL FREQUENCIES

To facilitate interpretation and computation, it is useful to examine if we can move the inverse Laplace transform contour (Bromwich path) in (4) down to the real ω-axis, such that it describes an inverse Fourier transform. For the active media and systems where this is possible, we have only convective instabilities [14, 15]: Then, nondiverging excitations lead to nondiverging fields for every fixed point (x, z). This means that any growing wave must be convected away. On the other hand, if the Bromwich path cannot be moved down to the real axis due to singularities or cuts, the transform can be described as an inverse Fourier transform plus integrals around the nonanalytic points. Since the latter integrals diverge with time, we have absolute instabilities, meaning that the fields diverge even at fixed points in space.

For a wide range of active media of interest, it turns out to be possible to move the Bromwich path in (4) down to the real axis, at the expense of deforming the integration path in the k_x-domain [15]. This is what we will consider in the following. The clue here is to realize that the integrand is analytic in both k_x and ω, so integration paths can be deformed until they reach singularities. To this end we assume that $\epsilon\mu$ does not have singularities or zeros for $\mathrm{Im}\,\omega \geq 0$; situations with zeros in the upper half-plane will be discussed later. Under these conditions $\sqrt{\epsilon\mu}$ is analytic and zero-free for $\mathrm{Im}\,\omega \geq 0$. We consider the evaluation of the physical field in the spatial and time domain, according to (4), but along a possibly deformed surface Γ in the (k_x, ω)-domain:

$$(2\pi)^2 \mathcal{E}(x, z, t) = \int_\Gamma E(k_x, z, \omega) \exp(ik_x x - i\omega t) \mathrm{d}k_x \mathrm{d}\omega \tag{14}$$

Consider Fig. 2a-b, showing the original integration paths in the ω- and k_x-domains. For all ω in the indicated domain D_ω, the branch points of k_z, i.e., $k_x = \pm\sqrt{\epsilon\mu}\omega/c$, are located in the domain D_{k_x}. Now, consider the short piece of the integration path that lies in D_ω. For these ω values, the idea is to deform the corresponding k_x integration path, as shown in Fig. 2c. This can safely be done, since $k_z(k_x, \omega)$ is analytic wrt. k_x away from the branch cuts.

The next step is to interchange the order of integration (using Fubini's theorem). For each k_x in the path in Fig. 3b, we can deform the short piece of the ω-path, obtaining the path in Fig. 3a. Repeating the procedure for two neighboring pieces of the ω-integration curve, we obtain the situation in Fig. 4, generally with two different integration curves in the k_x-domain. In simple situations like the one in the figure, we could use a single, common integration curve in the k_x-domain, for both pieces in the ω-domain. In general, to get rid of the vertical integration curves between the two domains in Fig. 4a, we must require the existence of a common integration curve in the k_x-domain detouring the interface between the neighboring domains (Fig. 4c). If this is always the case, we can continue the deformation in the ω-domain until the integration curve coincides with the real axis:

$$\mathcal{E}(x, z, t) = \frac{1}{2\pi} \int_{-\infty}^{\infty} E(x, z, \omega) \exp(-i\omega t) \mathrm{d}\omega, \tag{15}$$

where

$$E(x, z, \omega) = \frac{1}{2\pi} \int_{\kappa(\omega)} E(k_x, z, \omega) \exp(ik_x x) \mathrm{d}k_x. \tag{16}$$

---

tion with (10) yields

$$\int_0^T |d(t)|^2 \mathrm{d}t \leq \exp(2\gamma T) \int_0^T |d(t)|^2 \exp(-2\gamma t) \mathrm{d}t \tag{11}$$

$$\leq \exp(2\gamma T) \int_0^\infty |d(t)|^2 \exp(-2\gamma t) \mathrm{d}t \leq \frac{K(z)}{\pi} \exp(-2\gamma(z/c - T)).$$

valid for any z and T, and for sufficiently large γ. Letting $z/c > T$, it is apparent that we can make the right-hand side as small as we wish, by letting γ be sufficiently large. Thus $d(t)$ vanishes for $t < T$. Since T was arbitrary, $d(t)$ vanishes everywhere.

[2] If we had chosen the opposite sign for k_z in (9), we would have obtained $B = C = 0$. If we had chosen the sign in another, arbitrary way, we would have obtained $A = D = 0$ for some frequencies, and $B = C = 0$ else. Such choices are inconvenient (but perfectly valid) as k_z and the four functions A, B, C, and D get nonanalytic.

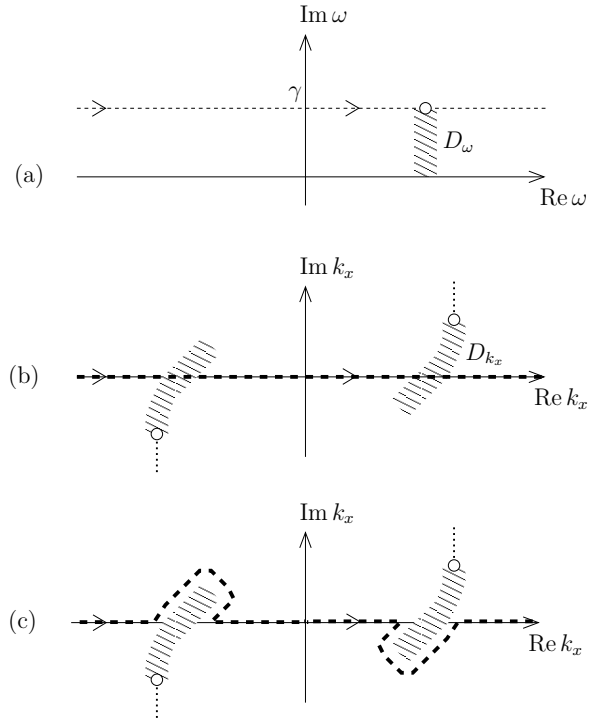

FIG. 2. The dashed lines correspond to the integration paths in (4): (a) ω-domain; (b) k_x-domain; and (c) deformed path in the k_x-domain for the ω indicated by a circle in (a). The domain D_{k_x} corresponds to the set of values $k_x = \pm\sqrt{\epsilon\mu}\omega/c$ for $\omega \in D_\omega$. The open circles in the k_x-plane correspond to the open circle in the ω-plane. The dotted vertical lines indicate branch cuts for $k_z(k_x, \omega)$ for the particular ω as indicated by the open circle. We proved in Appendix A that $k_z(k_x, \omega)$ is analytic wrt. k_x, for $\operatorname{Im}\omega = \gamma$ and real k_x; thus the branch cuts must avoid the real k_x-axis. In the figure we take them to be vertical, starting at the circles.

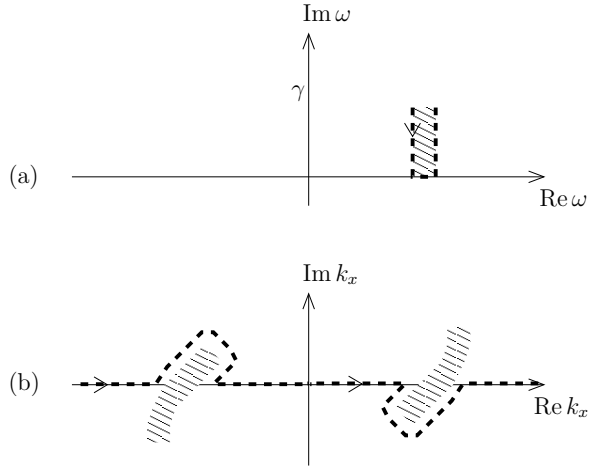

FIG. 3. Deformation in the ω-domain. For each k_x in the path in (b), the integration path in D_ω can be deformed (a).

Here $\kappa(\omega)$ is the deformed path in the k_x-domain, for each ω. Since $\operatorname{Im}\omega = 0$ in (15), the resulting field will not diverge with time. Thus in these situations, there are no absolute instabilities, and (16) can be interpreted as the usual frequency-domain field for real ω.

We have required the existence of a common k_x-integration curve for any two neighboring ω's. A sufficient condition is that $\sqrt{\epsilon\mu}$ is analytic for $\operatorname{Im}\omega \geq 0$: Consider the trajectories of k_z's branch points, $k_x = \pm\sqrt{\epsilon\mu}\omega/c$, as we reduce $\operatorname{Im}\omega$ from γ to zero. For two neighboring values of $\operatorname{Re}\omega$, these two trajectories will become arbitrarily close as the two $\operatorname{Re}\omega$'s approach each other.

We have also required that $\epsilon\mu$ be zero-free for $\operatorname{Im}\omega \geq 0$. While even order zeros give analytic square root, they induce another problem: At the zero the two branch points in the k_x-domain coincide so the integration curve get "stuck".

The frequency-domain field $E(x, z, \omega)$ is related to the physical, time-domain field in the so-called monochromatic limit. From (15),

$$\mathcal{E}(x, z, t) = \frac{1}{2\pi}\int_{-\infty}^{\infty} \frac{E(x, z, \omega)}{V(\omega)} V(\omega)\exp(-i\omega t)\mathrm{d}\omega, \quad (17)$$

where $\frac{E(x,z,\omega)}{V(\omega)}$ is the transfer function from the excitation $V(\omega)$ to the resulting field $E(x, z, \omega)$. Note that $V(\omega)$ is a factor in $E(x, z, \omega)$, so the transfer function is independent of $V(\omega)$. We can for example take a unit-step modulated complex exponential as the excitation[3]:

$$v(t) = H(t)\exp(-i\omega_1 t), \quad H(t) = \begin{cases} 0, & t < 0 \\ 1, & t > 0 \end{cases}, \quad (18)$$

with Laplace transform

$$V(\omega) = \frac{i}{\omega - \omega_1}. \quad (19)$$

The inverse transform (17) can be found with the residue theorem, by closing the contour by a large semicircle in the lower half-plane:

$$\mathcal{E}(x, z, t) = \left[\frac{E(x, z, \omega)}{V(\omega)}\exp(-i\omega t)\right]_{\omega=\omega_1} + \text{transients}(t). \quad (20)$$

Here the term transients(t) is a result of the integration around all singularities and cuts in the lower half-plane,

[3] This excitation is not continuous at $t = 0$. Thus its Laplace transform (19) is not absolutely integrable with respect to ω; a condition that must be satisfied to apply Fubini's theorem to (4). However, we can come as close as we wish to the excitation (18) while satisfying the condition, by letting $H(t)$ be slightly smoothened at $t = 0$. This makes (19) valid for arbitrarily large ω, before it starts to decay faster.

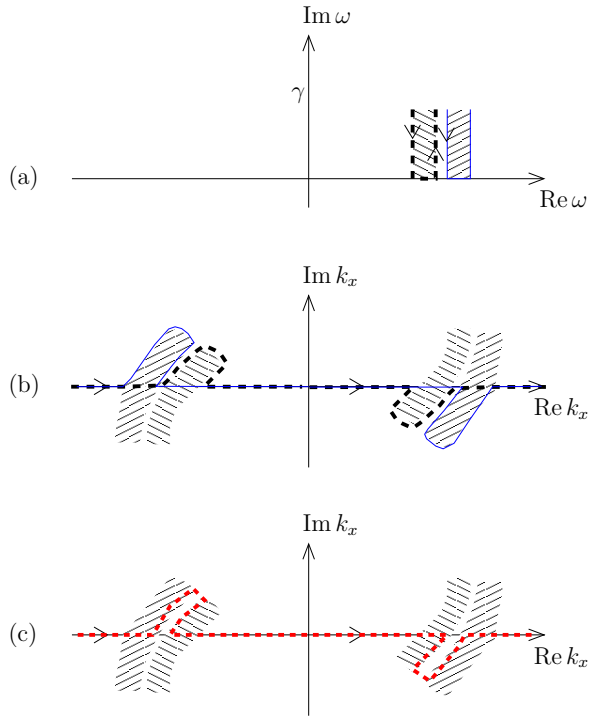

FIG. 4. Deformation of two neighboring pieces of the ω-integration curve (dashed black and solid blue) (a) and the associated k_x-integration curves (b). For ω-values along the vertical integration curves between the neighboring domains in (a), one can use a common k_x-integration curve (c).

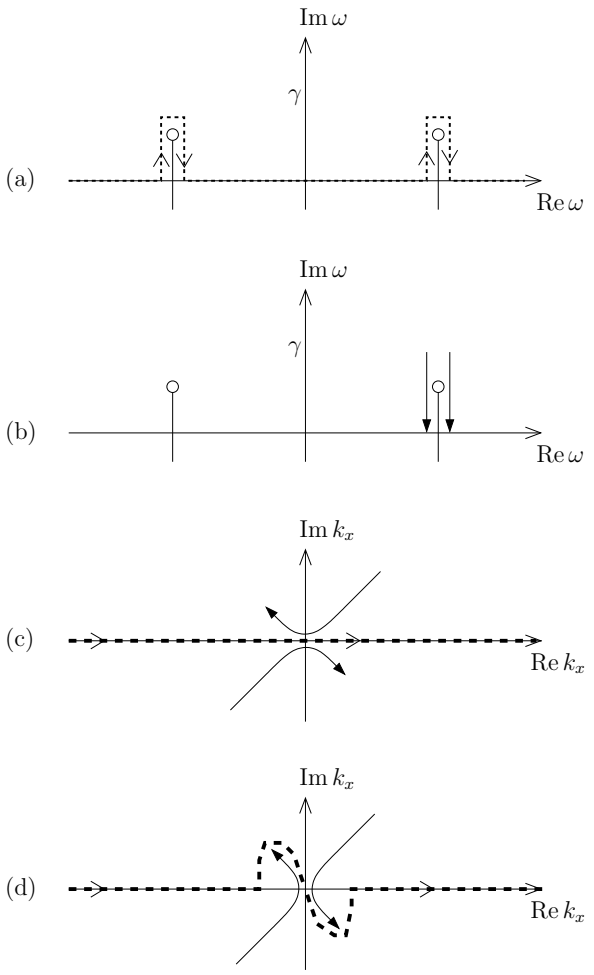

FIG. 5. Deformed integration paths (dashed) when $\sqrt{\epsilon\mu}$ has branch cuts in the upper half-plane. The branch points of $\sqrt{\epsilon\mu}$ are shown by open circles in (a); the cuts go vertically towards $-i\infty$. As $\mathrm{Im}\,\omega$ is reduced from γ to zero along the left and right arrows in (b), the corresponding trajectories of $k_x = \pm\sqrt{\epsilon\mu}\omega/c$ are shown by solid lines in (c) and (d), respectively.

and will decay exponentially. For later use, we define the monochromatic limit $\lim_{\omega_1} \mathcal{E}(x,z,t)$ as the field when the excitation is given by (18), and for sufficiently large t such that the transients can be ignored:

$$\lim_{\omega_1} \mathcal{E}(x,z,t) = \mathcal{E}(x,z,t) - \text{transients}(t). \qquad (21)$$

For the case where $\epsilon\mu$ is analytic and zero-free for $\mathrm{Im}\,\omega \geq 0$, the monochromatic limit $\lim_{\omega_1} \mathcal{E}(x,z,t)$ exists, and is given by the first line in (20). Even though the monochromatic limit exists in principle, in some situations (media with large gain and large x or z) the transients may be extremely strong, which means it may take very long time before they have died out.

We now consider the more complicated situation where $\epsilon\mu$ is not analytic or zero-free everywhere in the upper half-plane $\mathrm{Im}\,\omega > 0$. For concreteness we assume $\epsilon\mu$ has two simple zeros but is analytic otherwise. Then $\sqrt{\epsilon\mu}$ has branch cuts, which we take to be vertical towards $-i\infty$. Since $\sqrt{\epsilon\mu}$ is analytic everywhere in the upper half-plane except at the branch cuts, we can use the procedure above to deform the integration paths, leading to the ω-integration curve depicted in Fig. 5a. It is natural to try to deform also the remaining detours, to reach the real ω-axis everywhere. To this end we let $\mathrm{Im}\,\omega$ be reduced from γ to zero, on the left-hand side and right-hand side of $\sqrt{\epsilon\mu}$'s branch cut (Fig 5b). The corresponding trajectories of $k_x = \pm\sqrt{\epsilon\mu}\omega/c$ are shown in Figs. 5c and 5d, respectively. Apparently, the result of the integration in Fig. 5c differ from that of Fig. 5d, so the integrations up and down in Fig. 5a generally do not cancel. As a result the detours cannot be omitted. The presence of complex frequencies $\exp(-i\omega t)$ with $\mathrm{Im}\,\omega > 0$ means that the field will diverge with time, even at a fixed point in space. This means that the field cannot be interpreted at real frequencies as in (20); we have an absolute instability.

IV. PLANE WAVE LIMIT

We have seen that when there are no absolute instabilities, it is possible to move the inverse Laplace transform path down to the real axis, enabling the interpretation

of the fields (5) and (6) for real frequencies. However, this has come at a price: The integration curve in k_x must be deformed to include complex values of k_x. As will be demonstrated shortly, this means that it is not necessarily possible to approach the plane wave limit any longer.

Consider an excitation in the form $u(x)v(t)$, with transform $U(k_x)V(\omega)$. This excitation corresponds to, e.g., a current source $J(k_x,\omega)$, or an incident wave $A(k_x,\omega)$, as defined in Sec. II. The function $v(t)$ could be given by (18), while $u(x)$ could be e.g. one of the following alternatives:

$$u_1(x) = \mathrm{tri}(x/\sigma)\exp(iK_x x), \tag{22a}$$

$$u_2(x) = \exp(-x^2/2\sigma^2)\exp(iK_x x). \tag{22b}$$

Here $\mathrm{tri}(x/\sigma) = \max(1-|x/\sigma|,0)$ stands for the triangular function. Both alternatives represent a beam of thickness $\sim\sigma$ and a bundle of k_x's around the central transversal wavenumber K_x. The wavenumber spectra of the excitations are given by

$$U_1(k_x) = \sigma\,\mathrm{sinc}^2[\sigma(k_x-K_x)/2], \tag{23a}$$

$$U_2(k_x) = \sqrt{2\pi}\sigma\exp[-\sigma^2(k_x-K_x)^2/2]. \tag{23b}$$

Both spectra are entire functions in k_x. However, the two of them are fundamentally different in the sense that the first goes slowly to zero compared to the second. For real k_x and K_x both functions approach $2\pi\cdot\delta(k_x-K_x)$ in the limit $\sigma\to\infty$.

To approach plane waves, it is natural to consider the limit $\sigma\to\infty$ in (15)-(16). Here the field is expressed using real frequencies (assuming no absolute instabilities), and deformed paths in the complex k_x-plane such as that in Fig. 3b. Surprisingly, the limit $\sigma\to\infty$ does not necessarily exist, as $U_1(k_x)$ diverges for complex k_x. Perhaps even more surprisingly, even though the limit does not exist when using $U_1(k_x)$, it may exist when using $U_2(k_x)$, since the gaussian does not diverge provided $|\mathrm{Im}\,k_x| \le |\mathrm{Re}\,k_x - K_x|$. Thus, when the detours of the k_x-integration curve are not too far away from the real axis, or too close to the excitation wavenumber K_x, we can take the plane wave limit using a gaussian excitation, but not a triangular excitation. When the limit exists, we can write

$$\mathcal{E}(x,z,t) = \frac{1}{2\pi}\int_{-\infty}^{\infty}\frac{E(K_x,z,\omega)}{U(K_x)}\exp(iK_x x - i\omega t)\mathrm{d}\omega, \tag{24}$$

expressing the field with a single wavenumber K_x. Note that $U(K_x)$ is a factor in $E(K_x,z,\omega)$ so the ratio is independent of $U(K_x)$.

The peculiar divergence discussed above, can be interpreted as follows. For certain frequencies ω and wavenumbers $\pm k_x$, the longitudinal wavenumber k_z becomes zero. These modes correspond to side waves, which propagate in the $\pm x$-direction. If the medium is gainy, and the excitation extends over all x's, the field at an observation point x may diverge since the side waves propagate an unlimited distance before reaching the point. For the triangular excitation $u_1(x)$ (or more generally, for any excitation of finite support), as σ increases, side waves will have the chance to propagate a larger distance before reaching the observation point; thus we expect an exponential growth. At the same time, the excitation $U_1(k_x)$ at the particular k_x associated with the side wave becomes weaker, but only as $\propto\sigma^{-1}$. For the gaussian excitation $u_2(x)$, an increased σ will again give rise to an exponential growth as a result of the increased distance; however, the excitation itself at the particular k_x associated with the side wave, may be much weaker due to the factor $\exp[-\sigma^2(k_x-K_x)^2/2]$.

So far we have expressed the field using real frequencies (when there are no absolute instabilities), before we tried to take the plane wave limit. We can also do this procedure the other way around: First we can take the plane wave limit, while keeping the Bromwich path at $\mathrm{Im}\,\omega=\gamma$. Since only real k_x's are involved in (4), the plane wave limit $\sigma\to\infty$ always exists, which leads to

$$\mathcal{E}(x,z,t) = \frac{1}{2\pi}\int_{i\gamma-\infty}^{i\gamma+\infty}\frac{E(K_x,z,\omega)}{U(K_x)}\exp(iK_x x - i\omega t)\mathrm{d}\omega. \tag{25}$$

Equation (25) has the disadvantage that it is expressed using complex frequencies. We would like to be able to set $\gamma=0$ in (25) for interpretation at real frequencies. If the integrand is analytic for $\omega\ge 0$, we can move the integration path to the real axis. However, as we will see below, this is not always the case, not even for media with analytic and zero-free $\epsilon\mu$ for $\mathrm{Im}\,\omega\ge 0$. Since K_x is fixed, we must require that $\sqrt{\epsilon\mu\omega^2/c^2-K_x^2}$ is analytic in the upper half-plane $\mathrm{Im}\,\omega\ge 0$, to avoid absolute instabilities. Although this can happen, it is not very common; it is not even the case for conventional, weak gain media [5, 8]: For such media, there is a branch point slightly above the real ω-axis, corresponding to a side wave with $K_z=0$. For plane wave excitations, this side wave propagates an infinite distance along the x-axis, thus picking up an infinite amount of gain.

This type of absolute instability is somewhat artificial, since it is induced by the excitation of infinite width. For the case with finite σ we have seen that the instability is only convective, as long as the medium has analytic and zero-free $\epsilon\mu$ for $\mathrm{Im}\,\omega\ge 0$. This makes sense intuitively, since for finite σ, the side wave has only propagated a finite distance from the excitation to a fixed observation point.

In other words, let $\lim_{\omega_1}$ denote the monochromatic limit, as defined in Section III. If $\epsilon\mu$ is analytic and zero-free for $\mathrm{Im}\,\omega\ge 0$, but $\sqrt{\epsilon\mu\omega^2/c^2-K_x^2}$ is not analytic there,

$$\lim_{\omega_1}\mathcal{E}(x,z,t) = \text{finite} \tag{26}$$

for any finite σ, while

$$\lim_{\omega_1}\lim_{\sigma\to\infty}\mathcal{E}(x,z,t) = \infty. \tag{27}$$

However,

$$\lim_{\sigma\to\infty}\lim_{\omega_1}\mathcal{E}(x,z,t), \tag{28}$$

on the other hand, is dependent on the manner in which the plane wave limit is taken. If it is taken using an excitation $U_1(k_x)$ of finite support, it is infinite, but if it is taken using a gaussian $U_2(k_x)$, it is finite provided $|\mathrm{Im}\, k_x| \le |\mathrm{Re}\, k_x - K_x|$ along the integration detour. The gaussian excitation $u_2(x)$ is somewhat unphysical, as it requires an infinite wide source even for finite σ. Even though the gaussian excitation is unphysical, the fact that it makes it possible to take the plane wave limit is very interesting. It tells us that the growing side waves in a gain medium may be limited by making the source sufficiently smooth, and will disappear in the limit of a perfectly smooth source (gaussian).

Remarkably, and less intuitively, for certain media with absolute instabilities for finite σ (meaning that $\epsilon\mu$ is not analytic and zero-free everywhere in the upper half-plane), it is possible to eliminate the absolute instabilities by letting $\sigma\to\infty$. Indeed, if $\sqrt{\epsilon\mu\omega^2/c^2 - K_x^2}$ is analytic for $\mathrm{Im}\,\omega > 0$ while $\epsilon\mu$ is not analytic and zero-free,

$$\lim_{\omega_1}\mathcal{E}(x,z,t) = \infty, \tag{29}$$

for any σ, while

$$\lim_{\omega_1}\lim_{\sigma\to\infty}\mathcal{E}(x,z,t) = \text{finite}. \tag{30}$$

For example, this happens for media for which $\epsilon\mu\omega^2/c^2 - K_x^2$ has no zeros in the upper half-plane $\mathrm{Im}\,\omega > 0$, while $\epsilon\mu$ has two simple zeros there. Such a medium is suggested in Ref. [5]. Equations (29) and (30) can be interpreted as follows. Consider the field $\mathcal{E}(x,z,t)$ when σ and t are finite. As σ is made larger, the unstable mode with $k_z = 0$ is excited more weakly. Thus a larger t can be tolerated before $\mathcal{E}(x,z,t)$ gets large. If $\sigma\to\infty$ first, we can let t be infinite as well, without getting an infinite field. Thus the monochromatic limit exists.

We conclude this section by noting that the monochromatic and plane wave limits are far from trivial in gain media. Although it can be argued that these limits are unphysical, since infinite experiment durations or infinite beam thicknesses cannot exist, they provide valuable intuition for experiments with wide beam excitations, or long duration. Apparently, different results may be obtained dependent on the wideness of the excitation and the duration of the experiment.

V. MEDIA

The general method from the previous sections is now applied to analyze a wide range of media of interest, starting with simple passive and active media, and ending with novel classes of active media.

A. Passive media

Passive media are simple to analyze, due to the absence of instabilities. Fourier analysis is therefore sufficient, and the Fourier components wrt. k_x and ω can be interpreted straightforwardly. Although these facts are well known, it is useful to demonstrate the formalism before moving on to more complex cases.

A passive medium has $\mathrm{Im}\,\epsilon(\omega) > 0$, $\mathrm{Im}\,\mu(\omega) > 0$, and $\mathrm{Im}\, n(\omega) > 0$ for $\omega > 0$. Here $n(\omega) = \sqrt{\epsilon\mu}$ is the refractive index, which is analytic in the upper half-plane [16]. Due to odd symmetry of these functions, $\mathrm{Im}\, n\omega/c \ge 0$ for all real ω. Since $\mathrm{Im}\, n\omega/c$ is a harmonic function [17], it takes its minimum on the real axis; thus $\mathrm{Im}\, n\omega/c \ge 0$ in the closed upper half-plane. It follows that k_z's branch points, $k_x = \pm n\omega/c$, do not cross the real k_x-axis as we reduce $\mathrm{Im}\,\omega$ towards zero. In Fig. 6 we show two different possibilities; a passive medium which will turn out to show positive refraction (b), and a passive medium with negative refraction (c). Clearly, in both cases we can integrate along the real ω and k_x axes, and the monochromatic and plane wave limits may be taken, leading to fields with frequency ω_1 and wavenumber K_x. The resulting K_z shows the behavior of the wave in the medium.

We can find the sign of K_z by tracing $\arg k_z$ as k_x decreases from $+\infty$ to K_x. For $k_x\to+\infty$, $k_z\to+ik_x$ (see Appendix A). As k_x decreases, consider $k_z^2 = \epsilon(\omega_1)\mu(\omega_1)\omega_1^2/c^2 - k_x^2$, with the two zeros shown by the solid arrow ends in Figs. 6b-c. Now, k_z^2 picks up phase from the two zeros, but very little if K_x is in the regime far away from the zeros. Since $k_z(k_x,\omega)$ is continuous in k_x away from the branch cuts, it follows that $K_z = k_z(K_x,\omega_1) \approx iK_x$ in the regime to the right of the zeros, corresponding to an evanescent behavior in the total internal reflection regime of large K_x. So far, we have not invoked the properties of the medium; in other words, the result is valid for all media and situations where the monochromatic and plane wave limits exist.

As K_x becomes smaller, we must consider the two passive media separately. For the positive refractive medium (Fig. 6b), since the right-hand zero is above the real k_x-axis, as we pass it on the way from large k_x to small k_x, the phase $\arg k_z^2$ reduces from π through $\pi/2$ towards $\arg\{\epsilon(\omega_1)\mu(\omega_1)\}$. Again, since $k_z(k_x,\omega)$ is continuous in k_x away from the branch cuts, it follows that $\arg k_z(k_x,\omega_1)$ goes from $\pi/2$ through $\pi/4$ towards the small number $\arg\{\epsilon(\omega_1)\mu(\omega_1)\}/2$. Thus, as expected, we obtain a damped, propagating wave with wave vector directed away from the source.

For the negative refractive medium (Fig. 6c), the right-hand zero is below the real k_x-axis. Thus we find that $\arg k_z^2$ increases from π to almost 2π, and therefore, $\arg k_z$ increases from $\pi/2$ to almost π. In other words, K_z will be close to a negative number (negative refraction) in the regime of small K_x.

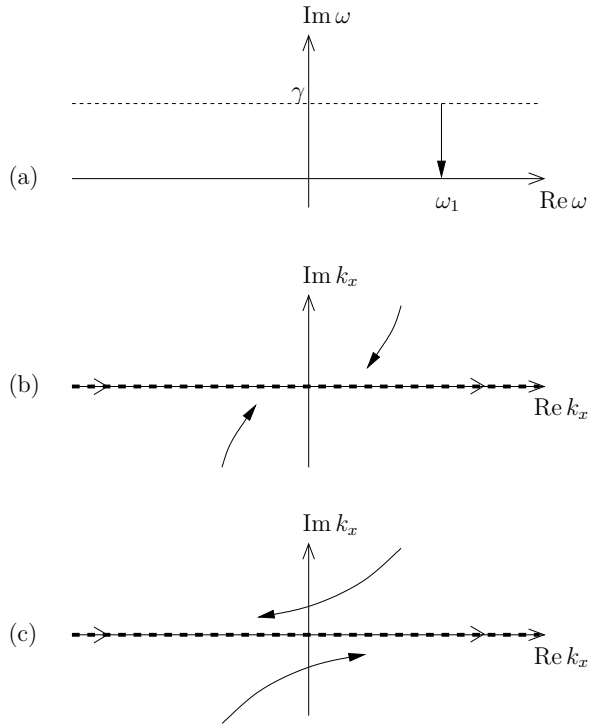

FIG. 6. As $\mathrm{Im}\,\omega$ is reduced from γ to zero (a), k_z's branch points, $k_x = \pm\sqrt{\epsilon\mu}\omega/c$, moves along the trajectories in (b) for a passive, positive refractive medium, and (c) for a passive, negative refractive medium.

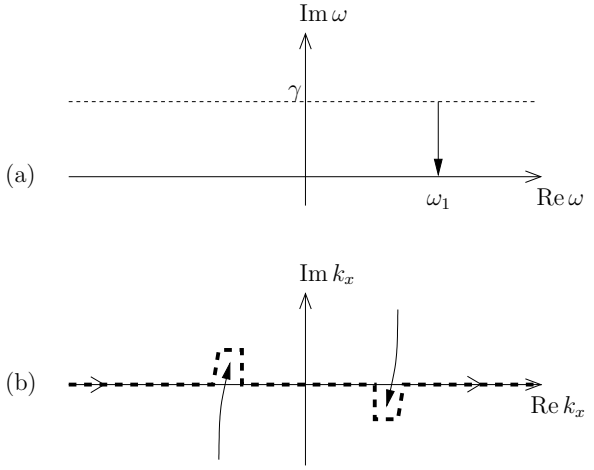

FIG. 7. As $\mathrm{Im}\,\omega$ is reduced from γ to zero (a), k_z's branch points, $k_x = \pm\sqrt{\epsilon\mu}\omega/c$, moves along the trajectories in (b) for a weak gain medium. The integration path in the k_x-domain must detour around these branch points.

B. Weak gain medium

We now consider a weak gain medium, or conventional gain medium, with $|\mathrm{Im}\,\epsilon| \ll 1$ and $|\mathrm{Im}\,\mu| \ll 1$ for all frequencies, and weak dispersion. For example, we can consider a nonmagnetic medium with $\epsilon(\omega) = 1 + \chi(\omega)$, where $\mathrm{Im}\,\chi(\omega)$ is negative at the observation frequency, and $|\chi(\omega)| \ll 1$ for all ω. When we reduce $\mathrm{Im}\,\omega$ as in Fig. 7a, the branch points $k_x = \pm\sqrt{\epsilon\mu}\omega/c$ move according to Fig. 7b. Thus, to be able to express the integral (14) with real frequencies ω, it is necessary to deform the k_x-integration with detours. These detours are result of the fact that the system supports amplifying side waves with $k_x = \pm\sqrt{\epsilon\mu}\omega/c$.

Having taken the monochromatic limit, we consider the possibility of approaching plane waves. According to the discussion in Sec. IV, the limit $\sigma \to \infty$ does not exist when using excitation profiles of finite support; then the side waves will diverge. However, for the gaussian excitation profile $u_2(x)$, and provided $|\mathrm{Im}\,\sqrt{\epsilon\mu}\omega/c| \leq |\mathrm{Re}\,\sqrt{\epsilon\mu}\omega/c - K_x|$, we can take the plane wave limit, since then the side waves are very weakly excited. By tracing $\arg k_z$ as k_x is reduced from ∞ (as in Sec. V A), we still obtain $K_z \approx iK_x$ in the total internal refraction regime of large K_x. Thus the behavior remains approximately evanescent there. For small K_x, since we have passed the zero from below, we get $\arg K_z \approx \arg\{\epsilon(\omega_1)\mu(\omega_1)\}/2$. This represents a weakly amplified wave.

As an alternative, we can take the plane wave limit while keeping the Bromwich integration path at $\mathrm{Im}\,\omega = \gamma$, leading to a single wavenumber K_x. Then we can deform the Bromwich path towards the real axis; however, there will be branch points close to $\omega = K_x c$, above the real axis. This means that the system supports absolute instabilities, and that the real frequencies is not meaningful in general. The absolute instabilities are again a result of diverging side waves, being excited infinitely far away from the observation point. However, as shown in Ref. [5], as long as the excitation frequency ω_1 is far away from $K_x c$, we can interpret the field as "quasi-monochromatic" up to a certain time, where the diverging side waves start to dominate.

C. Non-magnetic negative index medium

If the permittivity and permeability from the negative index medium in Sec. V A are denoted ϵ_p and μ_p, we let the permeability of an active, nonmagnetic medium be $\epsilon = \epsilon_\mathrm{p}\mu_\mathrm{p}$. Clearly, the behavior of the branch points and the integration paths becomes identical to that in Fig. 6c, and we get a negative refractive index at the frequency shown in the figure. This type of media was suggested in Ref. [6] and analyzed in Ref. [7]. When a plane wave is normally incident from vacuum, a backward wave is excited in the medium, drawing energy from the medium and propagating energy towards the interface [7].

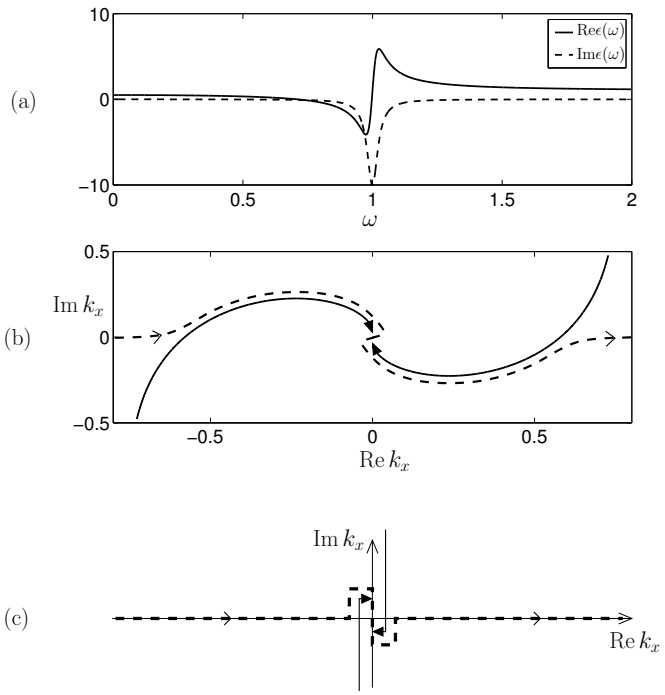

FIG. 8. Plot (a) shows $n(\omega)$ as given by (31). Plot (b) shows the trajectories of k_z's branch points, $k_x = \pm n(\omega)\omega/c$, as $\mathrm{Im}\,\omega$ is reduced from γ to zero, and $\mathrm{Re}\,\omega = \omega_1$. The values for $\omega = \omega_1$ are shown with solid arrows. The branch cuts in the k_x-domain, for $\omega = \omega_1$, can be taken along the trajectories (b, solid lines); however, it is convenient to use analytic continuation to deform them into the solid lines shown in (c). The integration path in the k_x-domain (dashed) must detour around the branch cuts.

D. Anti-evanescent medium

Having analyzed previously known media with the ω- and k_x-integration formalism, we now consider how the formalism can be used to predict novel classes of media. As we reduce $\mathrm{Im}\,\omega$ from γ to zero, the trajectories of k_z's branch points may be more complicated than in the previous examples.

Consider a nonmagnetic medium with permittivity

$$\epsilon(\omega) = (n(\omega))^2, \tag{31}$$

where

$$n(\omega) = 1 - \frac{F\omega_0^2}{\omega_0^2 - \omega^2 - i\Gamma\omega}, \tag{32}$$

and $F > 0$ (see Fig. 8a). Provided $F < 1$, the zeros of $\epsilon(\omega)$ are located in the lower half-plane, so the medium does not contain absolute instabilities. Hence we may consider the monochromatic limit. We take $F = 0.5$ and $\Gamma = 0.05\omega_0$, and consider the observation frequency $\omega_1 = 0.71\omega_0$, for which $\mathrm{Re}\,n(\omega_1) = 0$ and $\mathrm{Im}\,n(\omega_1) = -i0.072$.

The trajectories of k_z's branch points, $k_x = \pm n(\omega)\omega/c$, as $\mathrm{Im}\,\omega$ is reduced from γ to 0 while $\mathrm{Re}\,\omega = \omega_1$, are shown in Fig. 8b. For $\omega = \omega_1$ we can take the branch cuts along the solid lines in Fig. 8c, and the integration path along the dashed line. We let the two branch cuts approach each other. Considering an incident wave from vacuum, we calculate the transmitted field using the Fresnel equation (13b). For the frequency ω_1 we get

$$\begin{aligned} &2\pi\frac{E(x,z,\omega_1)}{V(\omega_1)} \\ &= \int_{-\infty}^{\infty} U(k_x)\frac{2k_{1z}e^{ik_{2z}z}}{k_{1z}+k_{2z}}e^{ik_x x}\mathrm{d}k_x \\ &+ \int_{-k_\mathrm{b}}^{k_\mathrm{b}} U(k_x)\left(\frac{2k_{1z}e^{ik_{2z}z}}{k_{1z}+k_{2z}} - \frac{2k_{1z}e^{-ik_{2z}z}}{k_{1z}-k_{2z}}\right)e^{ik_x x}\mathrm{d}k_x. \end{aligned} \tag{33}$$

Here the integration $\int_{-k_\mathrm{b}}^{k_\mathrm{b}}$ is along a vertical path from the lower to the upper branch point (indicated with solid arrows in Fig. 8c); immediately to the right of the branch cuts.

To interpret (33), we note that $k_z^2 = \epsilon\mu\omega^2/c^2 - k_x^2$ is negative for real k_x and also along the vertical integration paths in Fig. 8c. Since $k_z \to +ik_x$ for $k_x \to +\infty$, k_z must be positive imaginary for real k_x away from the branch cuts. Along the imaginary axis, however, k_z becomes negative imaginary, due to the presence of the right-hand branch cut. We choose an excitation $U(k_x) = U_1(k_x)$, with $K_x = 0$ (normal incidence). Clearly, the plane wave limit does not exist, as the second integral in (33) involves complex k_x's for which $U_1(k_x)$ diverges as $\sigma \to \infty$. For a finite, though large σ, the field is dominated by the second integral in (33). As a result of the two terms of the second integral, the field contains a superposition of modes with both signs of k_z; evanescent ($\mathrm{Im}\,k_z > 0$) and anti-evanescent ($\mathrm{Im}\,k_z < 0$).

The situation is different if we take the plane wave limit before the monochromatic limit. If we still assume $K_x = 0$, we have $K_{2z} = +n(\omega)\omega/c$. Both limits exist, and we end up with the monochromatic field amplitude

$$\mathcal{E}(x,z,t) = \frac{2K_{1z}}{K_{1z}+K_{2z}}e^{iK_x x + iK_{2z}z - i\omega_1 t}. \tag{34}$$

For the medium in this example, $n(\omega)$ is negative imaginary at the observation frequency $\omega = \omega_1$. Thus we have an anti-evanescent behavior.

In other words: Let the beam width σ be fixed and finite. Then, after sufficiently long time, the field will be a superposition of evanescent and anti-evanescent modes. On the other hand, for $\sigma \to \infty$, and after a long time the field will be purely anti-evanescent.

E. Simultaneous refractive index medium

Consider the example in Fig. 9. As ω approaches the real axis, the branch point in the first quadrant moves via the forth to the third quadrant. The integration path therefore becomes zigzag. We consider an incident wave

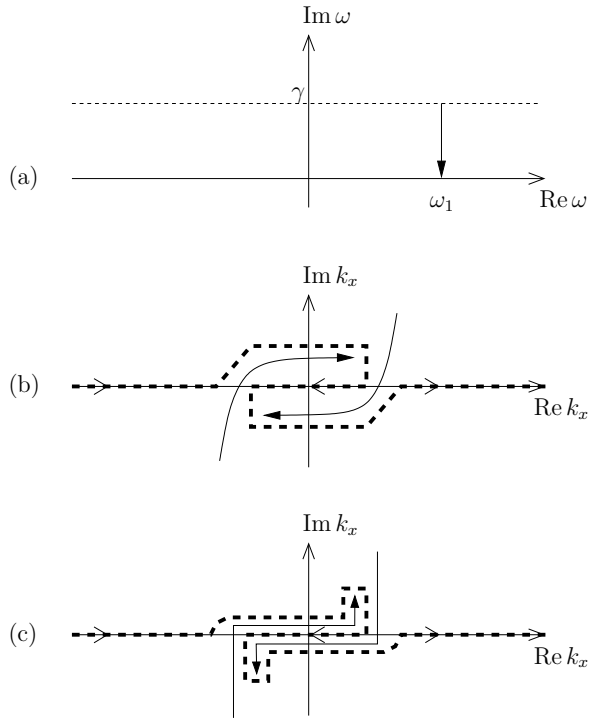

FIG. 9. As $\mathrm{Im}\,\omega$ is reduced from γ to zero (a), k_z's branch points, $k_x = \pm\sqrt{\epsilon\mu}\omega/c$, move along the trajectories (b). By deforming branch cuts and integration paths, we get situation (c). In (b) the branch cuts are taken to be along the trajectories, while in (c) they are deformed into the solid lines.

$A(k_x,\omega) = U(k_x)V(\omega)$ from a passive medium (medium 1) to the medium under investigation (medium 2), and calculate the transmitted field using (13b). Using the integration path in Fig. 9c, this leads to

$$\begin{aligned} &2\pi\frac{E(x,z,\omega_1)}{V(\omega_1)} \qquad (35)\\ &= \left(\int_{-\infty}^{-k_\mathrm{b}} + \int_{k_\mathrm{b}}^{\infty}\right) U(k_x)\frac{2\mu_2 k_{1z}e^{ik_{2z}z}}{\mu_2 k_{1z}+\mu_1 k_{2z}}e^{ik_x x}\mathrm{d}k_x\\ &+ \int_{-k_\mathrm{b}}^{k_\mathrm{b}} U(k_x)\left(\frac{4\mu_2 k_{1z}e^{ik_{2z}z}}{\mu_2 k_{1z}+\mu_1 k_{2z}} - \frac{2\mu_2 k_{1z}e^{-ik_{2z}z}}{\mu_2 k_{1z}-\mu_1 k_{2z}}\right)e^{ik_x x}\mathrm{d}k_x\\ &+ \int_{\text{vertical detours}} U(k_x)\frac{2\mu_2 k_{1z}e^{ik_{2z}z}}{\mu_2 k_{1z}+\mu_1 k_{2z}}e^{ik_x x}\mathrm{d}k_x. \end{aligned}$$

In (35) k_b is the real part of the branch point in the first quadrant, and the last integral represents all vertical integration paths in Fig. 9c, letting the up-and-down paths around a branch cut be infinitely close to each other. In the third line of (35), k_{2z} is the value along the upper integration path, above both branch cuts.

Considering the observation frequency ω_1 (monochromatic limit), we now take the plane wave limit $\sigma\to\infty$. Using the gaussian excitation $U_2(k_x)$, the limit exists provided $|\mathrm{Im}\,k_x| \le |\mathrm{Re}\,k_x - K_x|$ on the integration path. We then end up with

$$\begin{aligned} &\mathcal{E}(x,z,t) \qquad (36)\\ &= \left(\frac{4\mu_2 K_{1z}e^{iK_{2z}z}}{\mu_2 K_{1z}+\mu_1 K_{2z}} - \frac{2\mu_2 K_{1z}e^{-iK_{2z}z}}{\mu_2 K_{1z}-\mu_1 K_{2z}}\right)e^{iK_x x - i\omega_1 t}. \end{aligned}$$

With an excitation $u(x)$ of finite support, the limit would not exist; however, we may come as close as we wish to the field (36) by ensuring that the medium have branch points sufficiently close to the real k_x-axis.

On the other hand, by taking the limit $\sigma\to\infty$ without taking the monochromatic limit, we get

$$\begin{aligned} &\mathcal{E}(x,z,t) = \frac{1}{2\pi}\int_{i\gamma-\infty}^{i\gamma+\infty} V(\omega)\\ &\cdot\frac{2\mu_2 K_{1z}}{\mu_2 K_{1z}+\mu_1 K_{2z}}\exp(iK_x x + iK_{2z}z - i\omega t)\mathrm{d}\omega. \qquad (37) \end{aligned}$$

However, moving the integration path down to the real ω-axis requires K_{2z} to be analytic for $\mathrm{Im}\,\omega \ge 0$. Even for weak gain media this will not be the case [5], except for the special case $K_x = 0$.

If $K_x = 0$, and both $\sqrt{\epsilon\mu}$ and the Fresnel transmission coefficient are analytic for $\mathrm{Im}\,\omega > 0$, the integration path can in fact be moved down to the real ω-axis. In the monochromatic limit we then get

$$\mathcal{E}(x,z,t) = \frac{2\mu_2 K_{1z}}{\mu_2 K_{1z}+\mu_1 K_{2z}}e^{iK_x x + iK_{2z}z - i\omega_1 t}, \qquad (38)$$

with $K_{2z} = +n(\omega_1)\omega_1/c$, and $n(\omega)$ is given by (32). This differs from (36), and once again the two orders of the monochromatic and plane wave limits yield different results.

In other words: Consider the case $K_x = 0$, for a sufficiently large, but finite σ. In the monochromatic limit $t\to\infty$, the field will then be approximately given by (36), i.e. a superposition of waves with wavenumber $+K_{2z}$ and $-K_{2z}$ in the z-direction. However, if $\sigma\to\infty$ first, the monochromatic limit leads to a plane wave propagating in the z-direction, with wavenumber $+K_{2z}$. From this it is understood that simultaneous refraction is a two-dimensional effect. In the case of a finite σ there will always be oblique waves with $k_x \ne 0$ excited, no matter how large σ is. After a sufficiently long time t these oblique waves will somehow establish waves along the z-direction with both signs for K_{2z}. However, if $\sigma\to\infty$ is taken first, there will be no oblique waves excited. The simultaneous refracting waves can thus not be established. This latter situation is one-dimensional, as the excitation $u_2(x)$ is constant for all x, and $K_x = 0$.

Trajectories for k_z's branch points, similar to those in Fig. 9b, can be achieved using the same medium as in the previous example, but at a slightly higher observation frequency $\omega_1 = 0.853\omega_0$. At this frequency $|\mathrm{Im}\,k_x| \le |\mathrm{Re}\,k_x - K_x|$ on the integration path (Fig. 9c), so the limit $\sigma\to\infty$ exists, and we end up with (36). For

this medium both $\sqrt{\epsilon\mu}$ and the Fresnel transmission coefficient are analytic in the upper half plane. Taking the plane wave limit $K_x = 0$ before the monochromatic limit would thus lead to (38).

The time domain response of the medium with refractive index (32) was simulated using Kelley and Luebbers Finite Difference Time Domain (FDTD) method [18] for Lorentzian media [19]. In the simulation the situation with a current source in $z = 0$ was implemented. In this case the inverse Fourier transform will look the same as in (35), except that the Fresnel transmission coefficients are replaced by $\pm\mu/2k_z$. Clearly, as long as $n(\omega)$ is kept fixed (given by (32)), the response will essentially be the same if we let $\epsilon(\omega) = \mu(\omega) = n(\omega)$, rather than $\mu = 1$ and $\epsilon(\omega) = (n(\omega))^2$. For $K_x = 0$, $\omega_1 = 0.853\omega_0$, and a finite, but large σ, the simulation result should approach (36) after sufficiently long time. It turns out, however, that the time it takes to reach the monochromatic limit is much longer than what is possible to simulate.

The simulations show that the fields grow rapidly as they propagate, both in the x and z-direction. This rapid growth is explained as follows. Since the excitation vanishes for $t < 0$, it will contain other frequencies than just the observation frequency. Even though the frequency spectrum has a large peak at ω_1, the frequencies around resonance ω_0 will dominate for a very long time, due to very high gain there. Indeed, $n(\omega_0) = 1 - 10i$, so at resonance the forward propagating wave ($k_x = 0$) will grow as $\exp(20\pi z/\lambda)$, where λ is the vacuum wavelength, as it propagates in the z-directions. Also the side waves, with $k_x = \pm n(\omega_0)\omega_0/c$ and $k_z = 0$, will grow at this rate in the $\pm x$-direction. Since $|\mathrm{Im}\, k_x| > |\mathrm{Re}\, k_x|$ these side waves will be strongly excited, a fact that is also seen in the simulations. For $t \to \infty$ the excitation only contains ω_1, and the field should approach (36). However, as can be verified using frequency-domain simulations, it takes a very long time for the transients to die out, and it therefore appears impossible to see simultaneous refraction with time-domain simulations.

Due to numerical errors artificial reflections from the simulation grid may also occur. If such artificial reflections occur before the monochromatic limit is reached, the simulation will never be able to reveal simultaneous refraction: waves may be reflected back and forth, being amplified as they propagate, and the solution will eventually grow with time even at fixed points in space. This is what happened in the simulations of the medium with permittivity and permeability given by $n(\omega)$ in (32), at the expected simultaneously refracting frequency $\omega_1 = 0.853$.

Nistad and Skaar showed that negative refraction can occur with arbitrarily low loss, if there is a steep drop in $\mathrm{Im}\, n(\omega)$ just below the observation frequency ω_1 [13]. It is similarly possible to achieve a negative refractive index $n = \sqrt{\epsilon\mu}$ at arbitrarily low gain through a steep drop in $\mathrm{Im}\, n(\omega)$ just above the observation frequency. For such a medium, the trajectories of k_z's branch points will in fact be similar to those in Fig. 9b for the frequencies where $n(\omega) < 0$. One such medium, where the maximum gain was reduced to $\mathrm{Im}\, n(\omega) = -2$, was simulated, but also for this medium artificial reflections destroy the validity of the simulation solution before the transients die out. For FDTD simulations to be able to reveal simultaneous refraction, media with a significantly lower gain, while having branch point trajectories as in Fig. 9b, must be found.

VI. DISCUSSION AND CONCLUSION

Wave propagation in gain media has been considered by a Fourier–Laplace integral in space and time. How the correct monochromatic and plane wave limit can be taken is demonstrated, by deforming the integration surface in complex frequency-wavenumber space. In some cases it is possible to deform the inverse Laplace transform down to the real ω-axis, at the expense of deforming the inverse Fourier k_x-integration path. For active media where this can be done, the path will contain complex k_x, representing amplified waves as they propagate in the x-direction. If such a deformation is not possible, the inverse Laplace transform will contain complex frequencies, and the field will therefore grow exponentially with time, even at a fixe point in space: there is an absolute instability.

It is shown that the monochromatic and plane wave limits generally do not commute; for example, one order may lead to a diverging field, while the other order leads to a finite field. The plane wave limit may be dependent on whether it is realized by a gaussian excitation or a finite support excitation of infinite width. This is because amplifying side waves are less excited by the gaussian excitation.

The general path deformation theory is applied to analyze familiar passive and active media, and to predict media with novel properties. In particular it shown that certain gain media may be simultaneous refracting, i.e. they refract positively and negatively at the same time. It is argued that this is a two-dimensional effect, i.e. it will not occur if an infinitely wide source produces a wave propagating only in the z-direction. The monochromatic plane wave response of the media generally depends on which of the limits is taken first, or the width of the source relative to the duration of the experiment as both of these parameters tend to infinity.

An example of such a simultaneous refracting medium is given. For a large, but finite width of the source, this medium should be simultaneous refracting after a sufficiently long time, i.e. in the monochromatic limit. In attempt to visualize the effect, and to independently verify the theory, time domain simulations of this medium were performed. However, the simulations were not able to visualize the effect, as the monochromatic limit never was reached. The suggested medium has a very large gain at resonance, so the frequencies of the transients close to resonance will be strongly amplified as they propagate into the medium. Due to the occurrence of artificial re-

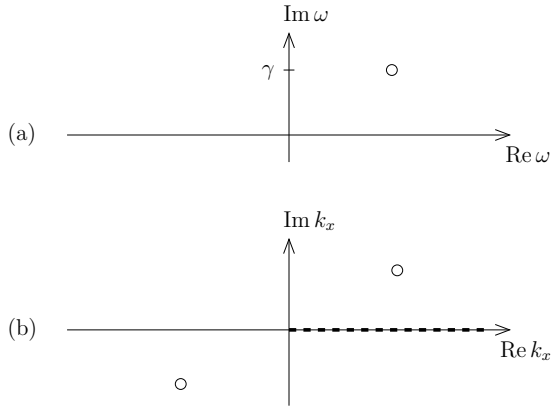

FIG. 10. For a fixed ω, with $\mathrm{Im}\,\omega > \gamma$ and $\mathrm{Re}\,\omega > 0$ (indicated by an open circle in the complex ω-plane (a)), the zeros of $k_z^2 = \epsilon\mu\omega^2/c^2 - k_x^2$ are shown in the complex k_x-plane (b). For large $\mathrm{Im}\,\omega$, the zeros $k_x = \pm\sqrt{\epsilon\mu}\omega/c$ are located away from the real axis.

flections before these transients die out, simultaneous refraction is therefore not seen in the simulations. Similar stability problems are expected for experimental realizations. It should therefore be investigated if simultaneous refracting media with significantly less gain exist.

Appendix A: Properties of $k_z(k_x, \omega)$

We here consider the properties of the function $k_z(k_x, \omega)$ along the real k_x-axis, and in a region $\mathrm{Im}\,\omega > \gamma$. We prove that $k_z(k_x, \omega)$ is zero-free and analytic in both arguments. Moreover, $k_z \to +\omega/c$ for $\omega \to \infty$ and fixed k_x, and $k_z \to +ik_x$ for $k_x \to +\infty$ and fixed ω. Initially, we require γ to be large, such that $\epsilon\mu$ is close to unity in the region. In Sec. III, we use analytic continuation to make use of the results in a larger region (i.e., reduce γ).

First, we consider the zeros of $k_z(k_x, \omega)$, given by $k_x = \pm\sqrt{\epsilon\mu}\omega/c$, see Fig. 10. None of these is located at real k_x, since ω is complex in the region $\mathrm{Im}\,\omega > \gamma$ and $\epsilon\mu$ is close to unity there: Consider first a region characterized by a bounded $\mathrm{Re}\,\omega$. If a zero existed for positive k_x, we could just increase γ (and therefore $\mathrm{Im}\,\omega$) such that $\sqrt{\epsilon\mu}$ gets closer to unity and $\arg\omega$ increases; then the zero would move away from the real k_x-axis. Next, consider $\mathrm{Re}\,\omega \to \infty$. Since $\sqrt{\epsilon\mu} = 1 + \mathcal{O}(\omega^{-2})$, the zeros are located at $k_x = \pm\omega/c + \mathcal{O}(\omega^{-1})$. Thus $k_z(k_x, \omega)$ has no zeros approaching the real k_x-axis as $\mathrm{Re}\,\omega \to \infty$.

Second, we argue that $k_z(k_x, \omega)$ is analytic in both arguments. The analyticity in ω has already been established (9), and the analyticity in k_x is immediate from (7) provided there are no sign changes. Indeed, such sign changes are impossible: If $k_z(k_x, \omega)$ were discontinuous in k_x, we could find a (k_x, ω) and a tiny δ such that $k_z(k_x + \delta, \omega) \approx -k_z(k_x, \omega)$. This leads to a contradiction since $k_z(k_x, \omega)$ is zero-free and continuous in ω in the region $\mathrm{Im}\,\omega > \gamma$, and $k_z(k_x + \delta, \omega) \to k_z(k_x, \omega)$ as $\omega \to \infty$ there.

It is interesting to examine the behavior of k_z in the limit of large k_x. The sign of k_z for active media in the total internal reflection regime has been discussed extensively in previous literature [3–5]. For $k_x = 0$, we have $k_z \approx \omega/c$ in the region $\mathrm{Im}\,\omega > \gamma$. As k_x increases along the dashed line in Fig. 10, the complex argument of k_z^2 increases according to the zero configuration in the figure. Since k_z is a continuous function of k_x it follows that as $k_x \to +\infty$, $k_z \to +ik_x$. This seems to predict an evanescent behavior in the total internal reflection regime of large k_x; however, it is important to remember that we only have considered the complex frequencies with $\mathrm{Im}\,\omega > \gamma$. Interpretation at real frequencies is possible under certain circumstances (Section V B) [4, 5]; however, for conventional, weak gain media it turns out to be an instability associated with amplified side waves.

We now prove that our solutions to Maxwell's equations are consistent with the earlier assumptions about absolute integrability wrt. k_x and ω, to enable the use of Fubini's theorem. First, consider the situation associated with the Fresnel equations (13), where the excitation takes the form of an incident wave. For $k_x = 0$ recall that $\mu_2 k_{1z} \approx \mu_1 k_{2z} \approx \omega/c$ in the region $\mathrm{Im}\,\omega > \gamma$. We let k_x increase along the dashed line in Fig. 10. Since the figure (approximately) represents the zero configuration of any of the functions $\mu_2 k_{1z}$ and $\mu_1 k_{2z}$, these functions cannot take opposite signs. Thus, from (13) we find that the reflected and transmitted fields (B and C) adopts the absolute integrability from the excitation A.

For the solution (12) associated with a current source, we define $\omega J(k_x, \omega)$ as the excitation. Since k_z has no zeros in the region of integration, not even at $\omega \to \infty$ and/or $k_x \to \infty$, it follows that both the electric and magnetic fields adopt the absolute integrability from the excitation.

Appendix B: The Titchmarsh theorem for causal diverging functions

Let $\mathcal{E}(t)$ be a causal function,

$$\mathcal{E}(t) = 0, \quad \text{for } t < 0, \tag{B1}$$

with no larger than exponential growth for large t:

$$|\mathcal{E}(t)| \le E_0 \exp(\gamma_0 t). \tag{B2}$$

Here, E_0 and γ_0 are positive constants. Let $\gamma > \gamma_0$, and write $\mathcal{F}(t) = \mathcal{E}(t)\exp(-\gamma t)$. We assume that $\mathcal{F}$ is square integrable, which is usually automatically satisfied given (B2). Consider the Laplace transform of $\mathcal{E}(t)$:

$$E(\omega) = \int_0^\infty \mathcal{E}(t)\exp(i\omega t)\mathrm{d}t, \tag{B3}$$

where $\mathrm{Im}\,\omega \ge \gamma$. The inverse Laplace transform is

$$\mathcal{E}(t) = \frac{1}{2\pi}\int_{i\gamma-\infty}^{i\gamma+\infty} E(\omega)\exp(-i\omega t)\mathrm{d}\omega. \tag{B4}$$

Making the substitution $\omega' = \omega - i\gamma$ in the integral, (B4) becomes

$$\mathcal{F}(t) = \frac{1}{2\pi}\int_{-\infty}^{+\infty} E(\omega' + i\gamma)\exp(-i\omega' t)\mathrm{d}\omega'. \qquad \text{(B5)}$$

Thus, $\mathcal{F}(t)$ and $E(\omega' + i\gamma)$ form a Fourier transform pair. Since $\mathcal{F}(t) = 0$ for $t < 0$, and $\mathcal{F}$ is square integrable, Titchmarsh' theorem tells us that

$$E(\omega) \text{ is analytic for } \mathrm{Im}\,\omega > \gamma, \qquad \text{(B6)}$$

and there is a uniform bound K such that

$$\int_{-\infty}^{\infty} |E(\omega' + i\gamma')|^2 \mathrm{d}\omega' \leq K < \infty, \quad \text{for all } \gamma' \geq \gamma. \qquad \text{(B7)}$$

By running the above argument in the reverse direction, we obtain the converse result: Let a function $E(\omega)$ satisfy (B6) and (B7) for some K. Then, the inverse transform (B4) satisfies (B1) and (B2), where we now put $\gamma_0 = \gamma$.

[1] L. Brillouin, *Wave propagation and group velocity* (Academic Press, New York and London, 1960).

[2] B. E. Saleh and M. C. Teich, *Fundamentals of photonics, 2nd ed.* (John Wiley & Sons, Inc., 2007).

[3] C. J. Koester, IEEE J. Quantum Electron. **2**, 580 (1966); G. N. Romanov and S. S. Shakhidzhanov, JETP Lett. **16**, 209 (1972); B. Y. Kogan, V. M. Volkov, and S. A. Lebedev, JETP Lett. **16**, 100 (1972); S. A. Lebedev, V. M. Volkov, and B. Y. Kogan, Opt. Spectrosc. **35**, 565 (1973); A. A. Kolokolov, JETP Lett. **21**, 312 (1975); P. R. Callary and C. K. Carniglia, J. Opt. Soc. Am. **66**, 775 (1976); W. Lukosz and P. P. Herrmann, Opt. Commun. **17**, 192 (1976); R. F. Cybulski and C. K. Carniglia, J. Opt. Soc. Am. **67**, 1620 (1977); R. F. Cybulski and M. P. Silverman, J. Opt. Soc. Am. **73**, 1732 (1983); J. Opt. Soc. Am. **73**, 1732 (1983); A. A. Kolokolov, J. Commun. Technol. Electron. **43**, 837 (1998); J. Fan, A. Dogariu, and L. J. Wang, Opt. Express **11**, 299 (2003); K. J. Willis, J. B. Schneider, and S. C. Hagness, **16**, 1903 (2008); A. Siegman, Opt. Photon. News **21**, 38 (2010).

[4] A. A. Kolokolov, Phys. Usp. **42**, 931 (1999).

[5] J. O. Grepstad and J. Skaar, Opt. Express **19**, 21404 (2011).

[6] Y.-F. Chen, P. Fischer, and F. W. Wise, Phys. Rev. Lett. **95**, 067402 (2005); T. G. Mackay and A. Lakhtakia, **96**, 159701 (2006); S. A. Ramakrishna, **98**, 059701 (2007); Y.-F. Chen, P. Fischer, and F. W. Wise, **96**, 159702 (2006); **98**, 059702 (2007); S. A. Ramakrishna and O. J. F. Martin, Opt. Lett. **30**, 2626 (2005); V. U. Nazarov and Y.-C. Chang, **32**, 2939 (2007); M. Perez-Molina and L. Carretero, **33**, 1828 (2008); V. U. Nazarov and Y.-C. Chang, **33**, 1829 (2008).

[7] J. Skaar, Phys. Rev. E **73**, 026605 (2006).

[8] J. Skaar, Opt. Lett. **31**, 3372 (2006).

[9] J. B. Geddes, III, T. G. Mackay, and A. Lakhtakia, Opt. Commun. **280**, 120 (2007).

[10] M. Premaratne and G. P. Agrawal, *Light propagation in gain media* (Cambridge University Press, 2011).

[11] S. A. Afanas′ev, D. G. Sannikov, and D. I. Sementsov, J. Comm. Tech. Electron. **58**, 1 (2013).

[12] L. D. Landau and E. M. Lifshitz, *Electrodynamics of continuous media* (Pergamon Press, New York and London, Chap. 9, 1960).

[13] B. Nistad and J. Skaar, Phys. Rev. E **78**, 036603 (2008).

[14] P. A. Sturrock, Phys. Rev. **112**, 1488 (1958).

[15] R. J. Briggs, *Electron-Stream Interactions with Plasmas* (MIT Press, 1964).

[16] H. M. Nussenzveig, *Causality and dispersion relations* (Academic Press, New York and London, Chap. 1, 1972).

[17] L. V. Ahlfors, *Complex analysis* (McGraw-Hill International Editions, 1979).

[18] K. S. Yee, IEEE Trans. Antennas Propag. **14**, 302 (1966).

[19] D. Kelley and R. Luebbers, IEEE Trans. Antennas Propag. **44**, 792 (1996).

B Matlab FDTD 2d code

```
%%Triangular passive negative refracting medium
%LorList = newMediumPassive; wc=1.06;

%%Triangular active negative refracting medium
LorList = newMedium; wc=0.97;

%%Triangular active negative refracting medium, with reduced number of Lorentzians (by varying Gamma)
%LorList = LorSuperposition3();wc = 0.96;

%%Absolute instabilities (zero in upper half-plane)
%  LorList=[ %Amplitude Resonansfrekvens Gamma
%      1.500   0.8    0.1500
%     -0.15   1.1    0.3];wc = 1.2;

%%Weak gain medium
%LorList = [-0.05 1 0.1]; wc = 1;

%%Strong passive Lorentzian for negative refraction
%LorList = [100 1 0.1]; wc=7.14;

%%Strong active Lorentzian for negative refraction
%LorList = [%Amplitud e Resonance frequency Gamma
%             -0.5 1 0.05]; wc=0.853;


%% Non-magnetic negative refracting medium
% LorList = [ 2.43811 2.638176 0.150689
%            -0.1434 3.768053 0.150692];wc=3.883;

%%Passive negative refraction medium
%  LorList = [20 1 0.2]; wc=sqrt(11);

SamplesPerPeriod = 30;                          %Number of samples per time period at observation frequency
Nperiods = 7;                                   %Number of time periods
SPeriods = 1;                                   %Number of periods being saved for videos etc

Nt = SamplesPerPeriod*Nperiods;                 %Number of time steps
Np = SamplesPerPeriod*SPeriods;                 %Save field at the time steps Nt:Nt+Np

eps_vac = 1;                                    %Epsilon for the (non-dispersive) medium to the left of the boundary
mu_vac = 1;                                     %Mu for the (non-dispersive) medium to the left of the boundary


a = 0.7;                                        % = dt/dz. Stability parameter, must be less than 1/sqrt(2) for 2D
dt = 2*pi/(wc*SamplesPerPeriod);                %Time step
dz = dt/a;                                      %Spacial step (dx = dz)


sigma = 2;
Nsigma=round(sigma/dz);
Nz = round((Nt+Np)*a);
W=3;


Nx = 2*W*Nsigma+1+round(2*Nz);

Npsi_e = length(LorList(:,1));
Npsi_m = Npsi_e;

%Current source in z=0 situation
%The electric and mangetic fields
Hx = zeros(2,Nx,Nz+1);
```

```
Hz = zeros(2,Nx+1,Nz);
E = zeros(2,Nx,Nz);

%The convolution summation variables
psi_e = zeros(Npsi_e,Nx,Nz);
psi_mx = zeros(Npsi_m,Nx,Nz-1);
psi_mz = zeros(Npsi_m,Nx-1,Nz);

%Fresnel situation
% %The electric and mangetic fields
% Nz0 = round(Nz/3);
%
%
% Hx = zeros(2,Nx,Nz+1);
% Hz = zeros(2,Nx+1,Nz);
% E = zeros(2,Nx,Nz);
%
% %The convolution summation variables
% psi_e = zeros(Npsi_e,Nx,Nz-Nz0);
% psi_mx = zeros(Npsi_m,Nx,Nz-Nz0);
% psi_mz = zeros(Npsi_m,Nx-1,Nz-Nz0);


%Lists of the Lorentzian parameters
F = LorList(:,1);                       %F
Gamma = LorList(:,3);                   %Gamma
w0 = LorList(:,2);                      %omega_0
w1 = sqrt(w0.^2-Gamma.^2 /4);           %Omega_1


%Assign variables to some frequently used expressions
D = exp((-1i*w1 - Gamma./2).*dt);
C = (1-D);

%Electric chi^0 and xi^0
chi0 = F.*w0.^2.*C./(w1.*(w1-1i*Gamma./2));
xi0 = -F.*w0.^2.*(1i*C./(w1-1i*Gamma./2)+dt*D)./(dt*w1.*(w1-1i*Gamma./2));

%Electric Delta chi^0 and Delta xi^0
Dchi0 = C.*chi0;
Dxi0 = C.*xi0;
Dchixi = Dchi0-Dxi0;   %frequently used
A = (1+real(sum(chi0)) - real(sum(xi0)));
B = (1-real(sum(xi0)));

%Magnetic Chi^0, xi^0 Delta chi^0, Delta xi^0, A and B
%mu = epsilon
chi0m = chi0;
xi0m = xi0;
Dchi0m = Dchi0;
Dxi0m = Dxi0;
Dchixim = Dchi0m - Dxi0m;
Dm = D;

%mu = 1
% chi0m = 0;
% xi0m = 0;
% Dchi0m = 0;
% Dxi0m = 0;
% Dchixim = 0;
% Dm = 0;

Am = (1 + real(sum(chi0m)) - real(sum(xi0m)));
Bm = (1-real(sum(xi0m)));


%The source
source_center = floor(Nx/2)+1;
source_start = source_center-W*Nsigma;
source_end = source_center+W*Nsigma;
```

```
source = source_start:source_end;%source_center-round(sigma/dx):source_center+round(sigma/dx);
Tri = exp(-(source-source_center).^2 /(2*Nsigma^2));%triangularPulse(source(1),source(length(
    source)),source);%

%Parameters for gaussian excitation in time
duration = 0.5*Nt;
width = 0.5*duration;

Tsteps = 1:(Nt+Np);
gauss = 0.5*(1 + erf((Tsteps-duration)/(sqrt(2)*width)));
gauss(:) = 1; %Abrubt onset of source

%Kx!=0
Kx = 0;

Hx(2,source,1) = gauss(1)*sin(Kx.*(source-source_center)*dz-wc*(0.5).*dt).*Tri; %-exp(-(0.5-
    duration).^2 *width).*

E(1,:,1) = (a/eps_vac)*(-Hx(2,:,1))/A;
psi_e(:,:,1) = (Dchi0 - Dxi0)*E(1,:,1);

%Iterate through time steps
for n=2:Nt
%   tstart = tic; %Measure how long time each time step takes

   %Hx(2,source,1) = Hx_source(n)*Tri;

   %Kx!=0
   Hx(2,source,1) = gauss(n).*sin(Kx.*(source-source_center)*dz-wc*(n-0.5).*dt).*Tri;%-exp(-((
       n-0.5)-duration).^2 *width).*

   %Current source in z=0 situation

%    %Update electric and magnetic fields
   Hx(2,:,2:Nz) = (Bm*Hx(1,:,2:Nz) + a*(E(1,:,2:Nz) - E(1,:,1:Nz-1)) + real(sum(psi_mx,1)))/Am
       ;
   Hz(2,2:Nx,1:Nz) = (Bm*Hz(1,2:Nx,1:Nz) - a*(E(1,2:Nx,1:Nz)-E(1,1:Nx-1,1:Nz)) + real(sum(
       psi_mz,1)))/Am;
   E(2,:,1:Nz) = (B*E(1,:,1:Nz) + a*((Hx(2,:,2:Nz+1)-Hx(2,:,1:Nz) - Hz(2,2:Nx+1,:) + Hz(2,1:Nx
       ,:))) + real(sum(psi_e,1)))/A;

   %Update convolution summation variables
   psi_e = bsxfun(@times,E(2,:,1:Nz),Dchixi) + bsxfun(@times,E(1,:,1:Nz),Dxi0) + bsxfun(@times
       ,D,psi_e);
   psi_mx = bsxfun(@times,Hx(2,:,2:Nz),Dchixim) + bsxfun(@times,Hx(1,:,2:Nz),Dxi0m) + bsxfun(
       @times,Dm,psi_mx);
   psi_mz = bsxfun(@times,Hz(2,2:Nx,1:Nz),Dchixim) + bsxfun(@times,Hz(1,2:Nx,1:Nz),Dxi0m) +
       bsxfun(@times,Dm,psi_mz);

%
   %%Fresnel situation
%    Hx(2,:,2:Nz0) = Hx(1,:,2:Nz0) + (a/mu_vac)*(E(1,:,2:Nz0) - E(1,:,1:Nz0-1));
%    Hx(2,:,Nz0+1:Nz) = (Bm*Hx(1,:,Nz0+1:Nz) + a*(E(1,:,Nz0+1:Nz) - E(1,:,Nz0:Nz-1)) + real(
    sum(psi_mx,1)))/Am;
%
%
%    Hz(2,2:Nx,1:Nz0) = Hz(1,2:Nx,1:Nz0) - (a/mu_vac)*(E(1,2:Nx,1:Nz0) - E(1,1:Nx-1,1:Nz0));
%    Hz(2,2:Nx,Nz0+1:Nz) = (Bm*Hz(1,2:Nx,Nz0+1:Nz) - a*(E(1,2:Nx,Nz0+1:Nz)-E(1,1:Nx-1,Nz0+1:Nz
    )) + real(sum(psi_mz,1)))/Am;
%
%    E(2,:,1:Nz0) = E(1,:,1:Nz0) + (a/eps_vac)*(Hx(2,:,2:Nz0+1)-Hx(2,:,1:Nz0) - Hz(2,2:Nx+1,1:
    Nz0) + Hz(2,1:Nx,1:Nz0));
%    E(2,:,Nz0+1:Nz) = (B*E(1,:,Nz0+1:Nz) + a*(Hx(2,:,Nz0+2:Nz+1) - Hx(2,:,Nz0+1:Nz) - Hz(2,2:
    Nx+1,Nz0+1:Nz) + Hz(2,1:Nx,Nz0+1:Nz)) + real(sum(psi_e,1)))/A;
%
%    %Update convolution summation variables
%    psi_e = bsxfun(@times,E(2,:,Nz0+1:Nz),Dchixi) + bsxfun(@times,E(1,:,Nz0+1:Nz),Dxi0) +
    bsxfun(@times,D,psi_e);
%    %psi_mx = bsxfun(@times,Hx(2,:,Nz0+1:Nz),Dchixim) + bsxfun(@times,Hx(1,:,Nz0+1:Nz),Dxi0m)
     + bsxfun(@times,Dm,psi_mx);
```

```
%    %psi_mz = bsxfun(@times,Hz(2,2:Nx,Nz0+1:Nz),Dchixim) + bsxfun(@times,Hz(1,2:Nx,Nz0+1:Nz),Dxi0m) + bsxfun(@times,Dm,psi_mz);

   Hx(1,:,:) = Hx(2,:,:);
   Hz(1,:,:) = Hz(2,:,:);
   E(1,:,:) = E(2,:,:);
   disp(n/(Nt+Np));%Output how far we have gotten
end


%Start saving the electric field for the time period Np*dt
Ep = zeros(Np,Nx,Nz);
Ep (1,:,:) = E(2,:,:);

for n=2:Np
   Hx(2,source,1) = gauss(n+Nt-1).*sin(Kx.*(source-source_center)*dz-wc*((n+Nt-1)-0.5).*dt).*Tri;
%
%    %Current source in z=0 situation

   %Update electric and magnetic fields
   Hx(2,:,2:Nz) = (Bm*Hx(1,:,2:Nz) + a*(Ep(n-1,:,2:Nz) - Ep(n-1,:,1:Nz-1)) + real(sum(psi_mx,1)))/Am;
   Hz(2,2:Nx,1:Nz) = (Bm*Hz(1,2:Nx,1:Nz) - a*(Ep(n-1,2:Nx,1:Nz)-Ep(n-1,1:Nx-1,1:Nz)) + real(sum(psi_mz,1)))/Am;
   Ep(n,:,1:Nz) = (B*Ep(n-1,:,1:Nz) + a*((Hx(2,:,2:Nz+1)-Hx(2,:,1:Nz) - Hz(2,2:Nx+1,:) + Hz(2,1:Nx,:))) + real(sum(psi_e,1)))/A;

   %Update convolution summation variables
   psi_e = bsxfun(@times,Ep(n,:,1:Nz),Dchixi) + bsxfun(@times,Ep(n-1,:,1:Nz),Dxi0) + bsxfun(@times,D,psi_e);
   psi_mx = bsxfun(@times,Hx(2,:,2:Nz),Dchixim) + bsxfun(@times,Hx(1,:,2:Nz),Dxi0m) + bsxfun(@times,Dm,psi_mx);
   psi_mz = bsxfun(@times,Hz(2,2:Nx,1:Nz),Dchixim) + bsxfun(@times,Hz(1,2:Nx,1:Nz),Dxi0m) + bsxfun(@times,Dm,psi_mz);




   %Fresnel
   %Update magnetic and electric fields
%    Hx(2,:,2:Nz0) = Hx(1,:,2:Nz0) + (a/mu_vac)*(Ep(n-1,:,2:Nz0) - Ep(n-1,:,1:Nz0-1));
%    Hx(2,:,Nz0+1:Nz) = (Bm*Hx(1,:,Nz0+1:Nz) + a*(Ep(n-1,:,Nz0+1:Nz) - Ep(n-1,:,Nz0:Nz-1)) + real(sum(psi_mx,1)))/Am;
%
%    Hz(2,2:Nx,1:Nz0) = Hz(1,2:Nx,1:Nz0) - (a/mu_vac)*(Ep(n-1,2:Nx,1:Nz0) - Ep(n-1,1:Nx-1,1:Nz0));
%    Hz(2,2:Nx,Nz0+1:Nz) = (Bm*Hz(1,2:Nx,Nz0+1:Nz) - a*(Ep(n-1,2:Nx,Nz0+1:Nz)-Ep(n-1,1:Nx-1,Nz0+1:Nz)) + real(sum(psi_mz,1)))/Am;
%
%    Ep(n,:,1:Nz0) = Ep(n-1,:,1:Nz0) + (a/eps_vac)*(Hx(2,:,2:Nz0+1)-Hx(2,:,1:Nz0) - Hz(2,2:Nx+1,1:Nz0) + Hz(2,1:Nx,1:Nz0));
%    Ep(n,:,Nz0+1:Nz) = (B*Ep(n-1,:,Nz0+1:Nz) + a*(Hx(2,:,Nz0+2:Nz+1) - Hx(2,:,Nz0+1:Nz) - Hz(2,2:Nx+1,Nz0+1:Nz) + Hz(2,1:Nx,Nz0+1:Nz)) + real(sum(psi_e,1)))/A;
%
%    %Update convolution summation variables
%    psi_e = bsxfun(@times,Ep(n,:,Nz0+1:Nz),Dchixi) + bsxfun(@times,Ep(n-1,:,Nz0+1:Nz),Dxi0) + bsxfun(@times,D,psi_e);
%    %psi_mx = bsxfun(@times,Hx(2,:,Nz0+1:Nz),Dchixim) + bsxfun(@times,Hx(1,:,Nz0+1:Nz),Dxi0m) + bsxfun(@times,Dm,psi_mx);
%    %psi_mz = bsxfun(@times,Hz(2,2:Nx,Nz0+1:Nz),Dchixim) + bsxfun(@times,Hz(1,2:Nx,Nz0+1:Nz),Dxi0m) + bsxfun(@times,Dm,psi_mz);

   Hx(1,:,:) = Hx(2,:,:);
   Hz(1,:,:) = Hz(2,:,:);

   disp((Nt+n)/(Nt+Np));%Output how far we have gotten
end
```

```
242
243 %Plot parameters
244
245 K=1;
246 L=round(50/dz);
247 m=1; %Movie counter
248 plot_width = round(50/dz);
249 source_plot = source_center-round(plot_width):source_center+plot_width;
250 %source_plot = 1:Nx;
251 Q = 1;
252
253
254 for n = 1:Np;
255     P=1;
256     frame = imagesc(((0:L-1))*dz,(source_plot-source_center)*dz,squeeze(Ep(n,source_plot,K:L))
          ,[-P P]);
257
258
259     %frame = imagesc(((0:L-1)-Nz0)*dz,(source_plot-source_center)*dz,squeeze(Ep(n,source_plot,
          K:L)),[-P P]);
260     colorbar;
261     set(frame,'AlphaData',100);
262     set(gca,'fontsize',14);
263     set(gca,'dataAspectRatio',[1 1 1]);
264     xlabel('z','fontsize',20,'Interpret','latex');
265     ylabel('x','rot',0,'fontsize',20,'Interpret','latex');
266     (Nt+n)*dt
267     pause(0.01);
268
269 %       %plot(((0:L-1)-Nz0)*dz,squeeze(Ep(n,source_center+round(0/dz),K:L)));
270 %     plot(((0:L-1))*dz,squeeze(Ep(n,source_center+round(0/dz),K:L)));
271 %     P=1e2;
272 %
273 %     %set(gca,'XLim',[-Nz0*dz (L-1-Nz0)*dz]);
274 %     set(gca,'XLim',[0 (L-1)*dz]);
275 %     set(gca,'YLim',[-P P]);
276 %     set(gca,'fontsize',14);
277 %     xlabel('z','fontsize',20,'Interpret','latex');
278 %     ylabel('E(z)','fontsize',20,'Interpret','latex');
279 %     pause(0.01);
280 %     (Nt+n)*dt
281 end
282
283 % %Save movie to file
284 %   filename = 'evanescent_gain_k1.avi';
285 %   movie2avi(M,filename);
```

References

[1] V. G. Veselago. The electrodynamics of substances with simultaneously negative ϵ and μ. *Sov. Phys. Usp.*, 10:509–514, 1968.

[2] J. B. Pendry. Negative refraction makes a perfect lens. *Phys. Rev. Lett.*, 85:3966–3969, 2000.

[3] J. B. Pendry, D. Schurig, and D. R. Smith. Controlling electromagnetic fields. *Science*, 312:1780–1782, 2006.

[4] M. Fox. *Optical properties of Solids, 2nd ed.* Oxford University Press, 2010.

[5] Bahaa E.A. Saleh and Malvin Carl Teich. *Fundamentals of photonics, 2nd ed.* John Wiley & Sons, Inc., 2007.

[6] J. B. Pendry, A. J. Holden, D. J. Robbins, and W. J. Stewart. Magnetism from conductors and enhanced nonlinear phenomena. *IEEE Trans. Microwave Theory and Tech.*, 47(11):2075–2084, November 1999.

[7] Johannes Skaar. Negative refraction: A tutorial. *arXiv:1008.3223*.

[8] Yi-Fan Chen, Peer Fischer, and Frank W. Wise. Negative refraction at optical frequencies in nonmagnetic two-component molecular media. *Phys. Rev. Lett.*, 95(6):067402, 2005.

[9] Johannes Skaar. Fresnel equations and the refractive index of active media. *Phys. Rev. E*, 73:026605, 2006.

[10] Joseph B. Geddes, III, Tom G. Mackay, and Akhlesh Lakhtakia. On the refractive index for a nonmagnetic two-component medium: Resolution of a controversy. *Opt. Commun.*, 280(1):120–125, 2007.

[11] Yi S. Ding and Ruo-Peng Wang. Possible realization of negative refraction in bose-einstein condensates. *Phys. Rev. B*, 84:045107, Jul 2011.

[12] L. Brillouin. *Wave propagation and group velocity.* Academic Press, New York and London, 1960.

[13] Christopher A. Dirdal and Johannes Skaar. Negative refraction in causal media by evaluating polar paths for rational functions. *J. Opt. Soc. Am. B*, 30(2):370–376, Feb 2013.

[14] Christopher A. Dirdal and Johannes Skaar. Superpositions of lorentzians as the class of causal functions. *Phys. Rev. A*, 88:033834, Sep 2013.

[15] B. Nistad and J. Skaar. Causality and electromagnetic properties of active media. *Phys. Rev. E*, 78:036603, 2008.

[16] H. Lewy R. Courant, K. Friedrichs. Über die partiellen differenzengleichungen der mathematischen physik. *Mathematische Annalen*, 100:32–74, 1928.

[17] Kane S. Yee. Numerical solution of initial boundary value problems involving Maxwell's equations in isotropic media. *IEEE Trans. Antennas and Propagation*, pages 302–307, 1966.

[18] K.S. Kunz R.B. Standler M. Schneider R. Luebbers, F.P. Hunsberger. A frequency-dependent finite-difference time-domain formulation for dispersive materials. *IEEE Transactions on Electromagnetic Compatibility*, 32(3):222–227, 1990.

[19] Hunsberger F.P. Luebbers, R. Fdtd for nth-order dispersive media. *IEEE Transactions on Antennas and Propagation*, 40(11):1297–1301, 1992.

[20] A. Taflove and M. E. Brodwin. Numerical Solution of Steady-State Electromagnetic Scattering Problems Using the Time-Dependent Maxwell's Equations. *IEEE Transactions on Microwave Theory Techniques*, 23:623–630, August 1975.

[21] John B. Schneider. *Understanding the Finite-Difference Time-Domain Method.* 2013.

[22] A. A. Kolokolov. Reflection of plane-waves from an amplifying medium. *JETP Lett.*, 21:312–313, 1975.

[23] A. A. Kolokolov. Determination of the reflection coefficient of a plane monochromatic wave. *J. Commun. Technol. Electron.*, 43:837–845, 1998.

[24] A. A. Kolokolov. Fresnel formulas and the principle of causality. *Phys. Usp.*, 42:931–940, 1999.

[25] A. Siegman. Fresnel reflection, Lenserf reflection, and evanescent gain. *Opt. Photon. News*, 21:38–45, 2010.

[26] Jon Olav Grepstad and Johannes Skaar. Total internal reflection and evanescent gain. *Opt. Express*, 19(22):21404–21418, 2011.

[27] Jean-Pierre Berenger. A perfectly matched layer for the absorption of electromagnetic waves. *Journal of Computational Physics*, 114(2):185 – 200, 1994.